EXPERIMENTAL AND CFD MODELLING OF A VORTEX-DRIVEN TURBINE

by © Gregory Walsh

A Thesis submitted to the School of Graduate Studies in partial fulfillment of the requirements for the degree of

Master of Engineering (Mechanical), Faculty of Engineering

Memorial University of Newfoundland

May 2024

St. John’s, Newfoundland and Labrador

Abstract

Much research has been conducted into fluid-structure interaction phenomena as methods of generating clean power, but there is a gap in knowledge regarding horizontal axis wind turbines directly powered by vortices attaching to or shedding from radial blades. This study provides two outputs; it examines the characteristics of a novel vortex-powered horizontal axis wind turbine with various blade configurations using both CFD and wind tunnel testing methods, and it provides information on how the CFD model performs in a turbulence-dominated flow scenario.

Analyzing the turbine blades with the ANSYS Fluent simulation package, the peak efficiency, C_p, occurred at a tip speed ratio, C_s, of approximately 0.2 for 50.44mm cross section blades, and 0.4 for 25.28mm cross section blades. These results reasonably agreed with validation trials performed in a wind tunnel where peak C_p occurred at C_s of approximately 0.22 for 50.44mm cross section blades, and 0.35 for 25.28mm cross section blades. However, the magnitude of the values returned in the CFD simulations were significantly lower than those measured in the wind tunnel trials, indicating that the CFD turbulence model may not be accurate for this turbulence-dominated simulation.

Turbine efficiency did not approach the Betz limit, being $< 1\%$ efficient in all cases. This indicates that such turbines are not a practical technology. However similar turbines may be useful in rudimentary applications, and knowledge of the effect may be applicable in similar geometry, such as radially spoked structures operating in open flows. The comparison of the CFD model output and the experimental data indicates that the CFD

closely maps the data trends observed in the experiments but differs in absolute values. A number of possible improvements in the CFD modelling are suggested tor reduce this gap in absolute values.

Acknowledgments

I would like to express my deepest gratitude and thanks to Dr. Michael Hinchey, for his continuing to provide advice and knowledge over the drawn-out process that writing this thesis became, and for providing the motivation needed to complete it. I would also like thank Dr. Bruce Colbourne for the mentorship and guidance required to bring this thesis to completion.

Finally, I would also like to thank my wife Anna who provided the encouragement and support needed to finish writing this paper amongst a global pandemic, and so many life changes, including the birth of our three children: Ava, Nora, and Logan.

Contents

Abstract ii
Acknowledgments iv
List of Tables viii
List of Figures ix
List of Abbreviations and Symbols xii
1 Introduction 1
1.1 Background 1
1.2 Aim and Scope 3
1.3 Outline 4
2 Literature Review and Background Theory 6
2.1 Bluff-body Turbines in Literature 6
2.2 Turbine Efficiency 7
2.2.1 Coefficient of Performance 10
2.2.2 Coefficient of Speed 13
2.2.3 Turbine Performance Curve 13
2.3 Power Generated 14
3 Turbine Models 16
3.1 Physical Turbine Geometry 16
3.2 Simulation Turbine Model 17
4 CFD Simulations 19
4.1 Governing Equations 20
4.1.1 Governing Equations for CFD 20
4.1.2 Rotating Reference Frame in Fluent 22
4.2 Simulation Setup 23
4.2.1 ANSYS Workbench 19.2 23
4.2.2 Geometry 23
4.2.3 Mesh 25
4.2.4 Physics Setup 25
4.3 CFD Results 32

4.3.1 Vortex Formation 32
4.3.2 Rotor with Eight 50.44mm Square Blades 34
4.3.3 Rotor with Eight 25.28mm Square Blades 36
5 Wind Tunnel Trials 38
5.1 Setup 38
5.2 Procedure 40
6 Results and Data Analysis 41
6.1 Summarized Results 41
6.1.1 Rotor with Eight 50.44mm Square Blades 41
6.1.2 Rotor with Eight 25.28mm Square Blades 42
6.2 Wind Tunnel Test Data Error Analysis 43
6.2.1 Uncertainty in Measurement and Calculated Values 43
6.2.2 Uncertainty in Torque Value 45
6.2.3 Uncertainty in Power Value 46
7 Comparison Between Numerical Predictions and Experimental Measurements. 48
7.1 Comparison of CFD Results to Wind Tunnel Results 48
8 Conclusions 56
8.1 Future Work 57
8.2 Final Remarks 58
References 59
Appendix A – CFD Mesh Details and Model Validation 62
A1. Mesh Overview 62
A2. Mesh Quality 66
A4. Quality of Mesh for 50.44 mm Cross-Section Blade Simulation 69
A4. Quality of Mesh for 25.28 mm Cross-Section Blade Simulation 71
A5. Mesh Convergence 73
A6. Validation 77
A6.1 Conservation of Mass 77
A6.2 Simulated Blade Velocity 79
Appendix B – CFD Simulation Data 81
B1. Rotor with Eight 50.44mm Square Blades 82

B2. Rotor with Eight 25.28mm Square Blades....85
Appendix C – Wind Tunnel Test Data....88
C1. Rotor with Eight 50.44mm Square Blades....89
C2. Rotor with Eight 25.28mm Square Blades....103
C3. Rotor with Four 50.44mm Square Blades....120
C4. Rotor with Four 25.28mm Square Blades....124
C5. Rotor with Two 50.44mm Square Blades....128

List of Tables

Table 1 - Test plan for simulations 19
Table 2 - Transient simulation time step values. 31
Table 3 - Uncertainty in Measured Values 44
Table 4 - Skewness value ranges with corresponding cell quality [22]. 67
Table 5 - Orthogonal value ranges with corresponding cell quality [22]. 68
Table 6 - Cell skewness values for 50.44mm blade simulation mesh. 69
Table 7 - Cell orthogonal quality for 50.44 mm blade simulation mesh. 70
Table 8 - Cell skewness for 25.28mm blade simulation mesh. 71
Table 9 - Cell orthogonal quality for 25.28 mm blade simulation mesh. 72
Table 10 - Comparison of initial and refined mesh results. 73
Table 11 - Mass flow rate balance for Rotor with Eight 50.44mm Square Blades, 5m/s windspeed. 77
Table 12 - Mass flow rate balance for Rotor with Eight 50.44mm Square Blades, 4m/s windspeed. 78
Table 13 - Mass flow rate balance for Rotor with Eight 50.44mm Square Blades, 3m/s windspeed. 78
Table 14 - Mass flow rate balance for Rotor with Eight 25.27mm Square Blades, 5m/s windspeed. 78
Table 15 - Mass flow rate balance for Rotor with Eight 25.27mm Square Blades, 4m/s windspeed. 79
Table 16 - Mass flow rate balance for Rotor with Eight 25.27mm Square Blades, 3m/s windspeed. 79
Table 17 – Frame of reference input values vs turbine rotational velocity simulated values. 80

List of Figures

Figure 1 - Image showing control volumes of Betz's open-disk actuator model [17]. 11
Figure 2 – Image showing curvilinear flow across turbine plane included in GGS model [19]. 12
Figure 3 - Cp as a function of Cs for some common turbine types [17]. 14
Figure 4 - Image depicting overall turbine dimensions with 50.44mm profile blades. 17
Figure 5 - Wind tunnel setup showing turbine construction. 17
Figure 6 – Full CAD model of turbine with 50.44mm cross section blades. 18
Figure 7 - Simplified eighth-section CAD model of turbine with 50.44mm cross section blades. 18
Figure 8 - Simplified eighth-section CAD model of turbine with 25.28mm cross section blades 18
Figure 9 - Isometric view of fluid domain showing named selections forming simulation boundaries. 50.44mm blade shown. 24
Figure 10 - Front view of fluid domain showing named selections forming simulation boundaries. 50.44mm blade shown. 24
Figure 11 - Boundary conditions for ANSYS Fluent simulations. 27
Figure 12 - Image showing apparent vortex attached to turbine blade. 32
Figure 13 - Detail of apparent vortex region at downstream side leading corner of blade. 33
Figure 14 - Low pressure region at the leading corner, downstream side of blade. 33
Figure 15 - Detail of low pressure region at the leading corner, downstream side of blade. 34
Figure 16 - Plot of turbine power vs angular velocity for 50.44mm blade cross section turbine, for all flow speeds simulated. 35
Figure 17 - Plot of C_P vs C_s for 50.44mm blade cross section turbine, for all flow speeds simulated. 35
Figure 18 - Plot of Power vs Angular Velocity for 25.28mm cross section turbine, for all flow speeds simulated 36

Figure 19 - Wind tunnel turbine setup showing 50.44mm profile blades. 39
Figure 20 - Image showing open sides of wind tunnel setup.....39
Figure 21 - Power vs Angular Velocity for eight 50.44mm blades 41
Figure 22 - Cp vs Cs for eight 50.44mm blades 42
Figure 23 - Power vs Angular Velocity for eight 25.28mm blades 42
Figure 24 - Cp vs Cs for eight 25.28mm blades 43
Figure 25 - Input current vs applied torque curves provided by Placid Industries 45
Figure 26 - CFD results showing power plotted against rotor angular velocity 48
Figure 27 - Wind tunnel test results showing power plotted against rotor angular velocity. 49
Figure 28 - Comparison of CFD and wind tunnel trials Power vs Angular Velocity curves for U of approximately 4m/s.....49
Figure 29 - CFD results showing the coefficient of performance plotted against the coefficient of power for a turbine with eight 50.44mm cross section blades. 51
Figure 30 - Wind tunnel test results showing the coefficient of performance plotted against the coefficient of power for a turbine with eight 50.44mm cross section blades. 51
Figure 31 - Comparison of CFD and wind tunnel trial Cp and Cs curves for U of approximately 4m/s. 52
Figure 32 - Detail of inflation layers around rotor blade surface.....53
Figure 33 - Detail of mesh resolution surrounding rotor blade surfaces. 53
Figure 34 - Detail of mesh resolution immediately downstream of the rotor.....53
Figure 35 - Views of mesh for 50.5mm cross-section blades with default auto-mesh: (a) overall domain, (b) lateral section view, (c) radial section view, (d) detail of blade surface. Note the absence of inflation layers in view (d). 62
Figure 36 – Section detail of mesh on face of blade after meshing surface control is applied.....63
Figure 37 - Detail of boundary layer meshing for 50.5mm cross section blades 64

Figure 38 - Views of mesh for 50.44mm cross-section blades after mesh controls applied: (a) overall domain, (b) lateral section view, (c) radial section view, (d) detail of blade surface. 64
Figure 39 - Views of mesh for 25.28mm cross-section blades after mesh controls applied: (a) overall domain, (b) lateral section view, (c) radial section view, (d) detail of blade surface. 65
Figure 40 - Graphical examples of skewness in two-dimensional elements, with ideal elements shown on the left [27]. 66
Figure 41 - Vectors used to compute orthogonal quality: Ai, the face normal vector; ci, the vector from cell centroid to adjacent cell centroid; and fi, the vector from cell centroid to each face [27]. 68
Figure 42 - Image of skewness distribution plot for 50.44mm cross-section blade mesh. 69
Figure 43 - Image of orthogonal quality distribution plot for 50.44mm cross-section blade mesh. 70
Figure 44- Image of skewness distribution plot for 25.28mm cross-section blade mesh. . 71
Figure 45 - - Image of orthogonal quality distribution plot for 25.28mm cross-section blade mesh. 72
Figure 46 - Graphical results from initial mesh. 74
Figure 47 - Graphical results from refined mesh. 74
Figure 48 - Plots of 4 m/s, 3.142 rad/s CFD trials utilizing: (a) 499,546 element mesh, and (b) 510,504 element mesh. 75

List of Abbreviations and Symbols

Symbol	Description	Units
A	$area$	m^2
$\boldsymbol{C_p}$	$coefficient\ of\ power$	$dimensionless$
$\boldsymbol{C_s}$	$coefficient\ of\ speed$	$dimensionless$
$\boldsymbol{P}$	$power$	W
$\boldsymbol{v}$	$speed$	m/s
$\boldsymbol{\vec{v}}$	$velocity$	m/s
$\boldsymbol{\omega}$	$angular\ speed$	rad/s
$\boldsymbol{\vec{\omega}}$	$angular\ velocity$	rad/s
$\boldsymbol{z}$	$height$	m
$\boldsymbol{p}$	$pressure$	Pa
$\boldsymbol{\rho}$	$density$	kg/m^3
$\boldsymbol{g}$	$gravitational\ acceleration$	m/s^2
$\boldsymbol{Q}$	$volumetric\ flow\ rate$	m^3/s
$\boldsymbol{U}$	$free\ stream\ velocity$	m/s
$\boldsymbol{r}$	$radius$	m
T	$torque$	$N \cdot m$
$\boldsymbol{t}$	$time$	s
$\boldsymbol{n_{rpm}}$	$angular\ speed\ in\ RPM$	$dimensionless$
$\boldsymbol{C}$	$Courant - Friedrichs - Lewy\ number$	$dimensionless$
FSI	$fluid - structure\ interaction$	-
CFD	$computational\ fluid\ dynamics$	-
HAWT	$horizontal\ axis\ wind\ turbine$	-
$\boldsymbol{V}$	$volume$	m^3

1 Introduction

1.1 Background

Increasingly, research in alternative energy generation is expanding past the traditional realms of pressure head-based turbines, such as the Francis turbine, and free-stream turbines, such as the Darrieus turbine, to examine other fluid-structure interaction (FSI) phenomena which may be suitable sources of mass-produced energy. Some of these studies examine phenomena such as: panel flutter [1] [2] [3] [4], galloping [5] [6], vortexes [7], vortex-induced vibration [8], and the effects of vortex generators on turbine output [9]. In many instances, these studies have progressed into full-scale prototype installations [10]. However there has been limited published research involving horizontal axis rotary turbines that are primarily powered by turbulence, or more specifically: vortex formation and shedding from rotating bluff-body blades with rectangular prism construction.

Furthermore, it has been observed during previous tests in the MUN wind tunnel, that rotor with rectangular bluff body blades will generate torque and rotation due to vortex formation. The level of this generated torque was known to be small, but was not quantified, and could not be ascertained in the public literature. Although it was recognized at the outset that this type of rotor could not compete in efficiency with conventional airfoil rotors, it was thought that the characteristics of a vortex driven turbine rotor would make an interesting and potentially useful study.

In the current case, a study of vortex-driven turbines also provides an opportunity to compare physical and numerical models of vortex dominated flow phenomena. Vortexes are generally not a desirable feature in flows or fluid-structure interactions, as they are usually a source of energy loss. Thus, models that do incorporate vortex flows are usually doing so as a lesser part of some other more dominant flow phenomena. This study requires modelling flows that are dominated by vorticity. It was unclear how well current numerical flow models would simulate a vortex dominate flow.

Identifying these two aspects as gaps in knowledge, this study was developed to investigate the performance and practicality of a novel vortex-driven horizontal axis wind turbine (HAWT) in different configurations and examine the behaviour of CFD models in the complex situation where turbulence caused by fluid-structure interactions in a rotating system is the dominant factor in producing the characteristic (power generation) under study.

It was also recognized that the utility of a low efficiency turbine was not obvious, but the unusual nature of the flow regime would make a good scientific study, and provide a challenging exercise for CFD modeling, plus the opportunity to generate some experimental validation data for vortex flow modelling. The utility of vortex turbines was left to the future as this study would provide data on which the evaluation of such utility could be based.

1.2 Aim and Scope

The overall purpose of this study was to use computational fluid dynamics (CFD) to analyse the behaviour of two cross-flow turbines with bluff body blades, and validate the CFD simulations and turbulence models through physical experiments. Each turbine had blades with different sized square cross-sections, but the same lengths, meaning the cross-sectional area of flow covered was the same for both turbines. This was done mainly to fit the largest practical rotor diameter in the available wind tunnel facility.

The scope of the study covered four phases comprising: exploratory CFD analysis, detailed CFD analysis of the turbine output, physical experiments to generate validation / comparison data, and finally a comparative analysis of the CFD output and the experimental results.

The first component of this study was to conduct a preliminary CFD analysis to determine if the turbine setup created measurable torque through the attachment or shedding of vortexes.

Since the simulations indicated that torque was consistently created, the next step was to quantify the amount of power developed in varying flow speeds. This was done through setting multiple constant rotating frame velocities for each of three different flow speeds. With the resulting data, coefficient of performance (C_p) versus coefficient of speed (C_s), and power generated (P) versus angular velocity (ω) curves were generated to determine performance characteristics and optimal operational points for each of the turbines, as well as how performance was affected by the size of the blade cross-section.

To provide validation for the CFD analysis, physical trials were then conducted with two turbines using the same geometry as the digital turbine models. The turbines were tested in a ducted wind tunnel at three flow speeds. C_p versus C_s and P versus ω curves were generated by applying constant load torque to the turbine using a magnetic particle brake, and then recording the rotational speed of the rotor.

The CFD model was then validated by evaluating the solver convergence for each of the simulations, conducting a mesh sensitivity analysis to determine mesh convergence, and finally through comparison with the physical experimental trials. The turbine performance data gathered from the physical trials was analysed and compared to the CFD results to indicate if the computer simulations were a valid predictor of real-world operational characteristics, and if the CFD models utilized could provide accurate results in situations that were predominantly turbulent flow in rotating frames.

1.3 Outline

Chapter 1 of this paper provides an overview of the thesis project. Chapter 2 provides some background theory on fluid-structure interaction relating to turbines. Chapter 3 describes the characteristics of the turbines tested. Chapter 4 details a CFD analysis of the two turbine configurations studied using the ANSYS Fluent and Workbench software package. Chapter 5 details the wind tunnel trials with a physical turbine model, and Chapter 6 provides conclusions on the outcomes of the tests and provides some commentary on the performance of the CFD model, then gives suggestions for future

work. This is followed by a section detailing references and appendices containing the bulk of data from the CFD and wind tunnel trials.

2 Literature Review and Background Theory

2.1 Bluff-body Turbines in Literature

Early attempts at creating bluff-body turbines focused on the Magnus effect created by rotating cylinders. Since Flettner's proposal in the 1920's, there were several attempts to create bluff body turbines utilizing the Magnus effect, but the first complete turbine was finished in 1984 [10]. Early studies by Bychkov [10] indicated that cut in speeds for this type turbine could occur at relatively low wind speeds of 1 to 2 $^{m}/_{s}$ [11]. Analysis by Sedaghat has indicated that the characteristics of this type turbine is not yet viable as generating turbine due to overall poor performance [11]. Additionally, the overall mechanical complexity required for external power input to the spinning cylindrical blades is much higher than lift-based turbines [12].

In 2010 Murakami patented a configuration of a Magnus-type turbine utilizing helical ribs on the spinning cylinder blades [13]. This turbine had a higher cut-in speed of 4 $^{m}/_{s}$ and produced net power of 3kW at the rated wind speed of 8 $^{m}/_{s}$, but more comprehensive results were not available [11].

Some studies have attempted to improve overall turbine performance and reduce complexity by modifying the behaviour of vortexes created by bluff body blades through the use of additional static mechanical elements. Takahashi et al. [14] proposed the "longitudinal vortex wind/water turbine: LV-WT". This turbine was created a strong periodic lift force due longitudinal vortex-induced vibration (LVIV). Once the vortex-induced fluctuating lift force exceeds the starting friction of the rotor, the turbine will

begin to rotate. After rotation starts, the lift force becomes steady and rotation stable [15] [12]. Numerical analysis by Hemsuwan et al. indicated the power coefficient of this system was about 0.004 of the C_P developed by a conventional wind turbine but noted the benefits of low complexity and investment cost [12].

Notably, all papers found during the literature review studied bluff blades with circular cross sections, indicating the novel nature of the square cross section blades examined in this study.

2.2 Turbine Efficiency

According to Bernoulli [16], the energy of a fluid flow is described by the equation:

$$z + \frac{p}{\rho g} + \frac{v^2}{2g} = constant \qquad \textit{Eq. 2.1}$$

Where:

v *is the fluid flow speed at a certain point on a streamline*

g *is acceleration due to gravity, in* $\left[{}^{m}/_{s^2}\right]$

z *is the elevation of the point above the plane of reference, in* $[m]$

p *is the pressure at the chosen point*

ρ *is the fluid density at all points in the fluid*

In this equation, $\frac{p}{\rho g}$ is the water head pressure, or the potential energy in the fluid due to elevation, and $\frac{v^2}{2g}$ is the kinetic head, or the amount of energy in the motion of the fluid. These terms are also known as "pressure head" and "kinetic head" respectively. Note that in the sign convention for positive z is in the direction opposing gravitational acceleration ("up").

Turbines function by converting this pressure and flow kinetic energy into rotating mechanical (kinetic) energy, which is well suited to generating electricity. Traditional pressure-head turbines, such as those used in hydro dams, typically generate power through slowing large amounts of fluid flowing through a tube, creating a large pressure build-up behind the turbine which is then converted to rotational mechanical energy. In these turbines, power harnessed from the kinetic head term is negligible when compared to the pressure head. Conversely turbines which utilize free stream energy, such as Darrieus or Gorlov lift-based turbines, operate where the kinetic head term is dominant. These kinetic turbines allow large amounts of fluid to pass through, generating mechanical rotational force through harnessing the kinetic energy of the fluid flow. Wind turbines can be classified as kinetic turbines, as they develop power from large flows of moving air.

An estimate of how much kinetic free-stream power can be captured by a turbine can be obtained from the following equation, showing the amount of energy contained in a fluid stream:

$$P = pQ \qquad \textit{Eq. 2.2}$$

Where:

$P\ is\ power$ in Watts

$p\ is\ the\ static\ pressure\ in\ Pa$

$Q\ is\ the\ volumetric\ flow\ rate\ in\ {}^{m^3}/_{s}$

With pressure as:

$$p = \rho\frac{U^2}{2} \qquad \textit{Eq. 2.3}$$

And volumetric flow rate being:

$$Q = UA \qquad \textit{Eq. 2.4}$$

Then the power available in a fluid stream is:

$$P = \frac{1}{2}\rho A U^3 \qquad \textit{Eq. 2.5}$$

Where:

$P\ is\ the\ available\ power\ in\ Watts$

$\rho\ is\ the\ fluid\ density, in\ {}^{kg}/_{m^3}$

$U\ is\ the\ free\ stream\ velocity, in\ {}^{m}/_{s}$

$A\ is\ the\ cross-sectional\ area\ of\ the\ stream, in\ m^2$

2.2.1 Coefficient of Performance

Considering the equation expressing the amount of energy available in a free stream flow, along with a performance factor for the turbine indicating its effectiveness at removing energy from the flow, it is possible to find the maximum amount of energy a turbine could extract from the fluid stream:

$$P = C_p \frac{1}{2} \rho A U^3 \qquad \textit{Eq. 2.6}$$

Where:

$P\ is\ the\ power\ generated, in\ watts$

$\rho\ is\ the\ fluid\ density, in\ {}^{kg}/_{m^3}$

$U\ is\ the\ free\ stream\ velocity, in\ {}^{m}/_{s}$

$A\ is\ the\ cross-sectional\ area\ of\ the\ stream, in\ m^2$

$C_p\ is\ the\ non-dimensional\ coefficient\ of\ performance\ for\ the\ turbine$

Rearranging the above equation, we can determine the coefficient of performance for the turbine through measured values:

$$C_p = \frac{2 * P}{\rho A U^3} \qquad \textit{Eq. 2.7}$$

From this resulting equation, the turbine coefficient of performance can be determined by measuring the power generated by the turbine and comparing to the amount of energy theoretically available in the free stream flow.

2.2.1.1 Betz Efficiency Limit for Turbines

A commonly referenced term in kinetic turbine theory is the Betz Limit, first proposed by Albert Betz in 1919. Betz's law states that there is an upper limit to the amount of energy a turbine can remove from a free flowing stream of fluid, independent of the design of the turbine. Betz calculated this upper bound on turbine efficiency to be approximately 16/27 or 59.3%, representing a C_p of 0.593.

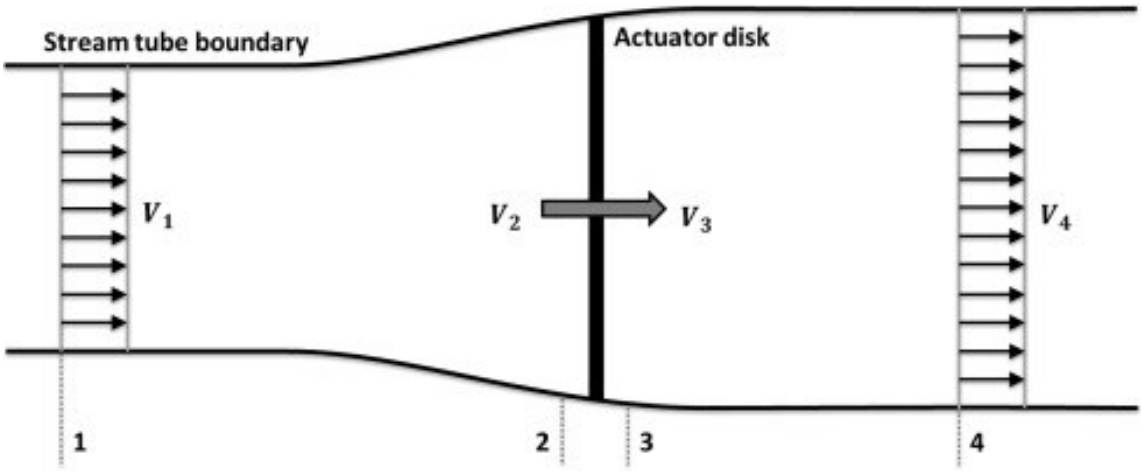

Figure 1 - Image showing control volumes of Betz's open-disk actuator model [17].

The limit is determined by deriving the energy change in a frictionless flow stream across an open-disk actuator. In this model, linear momentum theory is applied to a control volume defined by the surface and cross sections of a stream tube. As kinetic energy is extracted from the stream by the turbine, a pressure differential is developed across the turbine, and the flow exiting the turbine slows. Betz determined that the maximum power efficiency will occur at $\frac{V_4}{V_1} = \frac{1}{3}$ as shown in Figure 1, and the maximum C_p at this

point is 0.593 [17]. This limit was also independently determined by Frederick Lanchester and Nikolay Zhukowsky [18].

2.2.1.2 GGS Efficiency Limit for Turbines

More recently, Gorban, Gorlov, and Silantyev proposed a model that includes curvilinear flow and non-linear pressure distribution across the turbine, which are not accounted for in the Betz model. Similar to Betz's Law, the GGS model predicts peak efficiency to take place at an upstream to downstream flow ratio of 2/3 but determines a much lower upper limit of 0.30113 on C_p for two-dimensional propeller-type turbines [19].

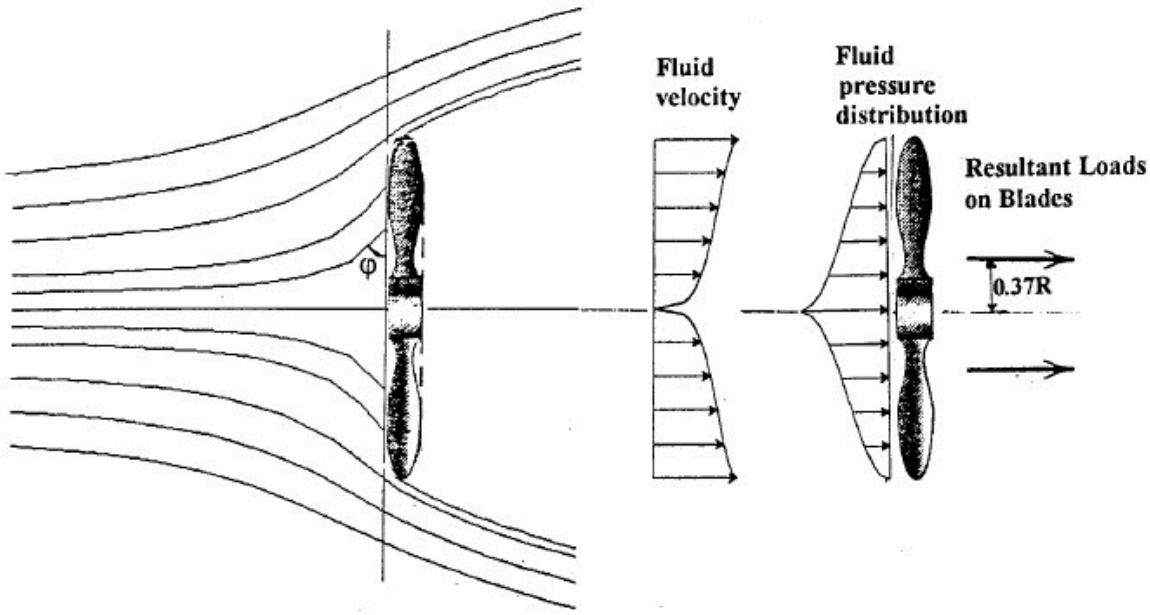

Figure 2 – Image showing curvilinear flow across turbine plane included in GGS model [19].

2.2.2 Coefficient of Speed

The turbine coefficient of speed, sometimes called the tip speed ratio, is a non-dimensional number representing the ratio of the turbine rotor tip velocity to the fluid stream speed and is used in conjunction with the coefficient of performance to determine the optimal operational point for the turbine. In other words, it can be used to find the flow speed at which the turbine can operate most effectively. The coefficient of speed is described by the equation:

$$C_s = \frac{r\omega}{U} \qquad \textit{Eq. 2.8}$$

Where:

C_s *is the turbine coefficient of speed*

ω *is the angular velocity of the turbine rotor in* $^{rad}/_{s}$

U *is the fluid stream speed in* $^{m}/_{s}$

r *is the turbine radius in* m.

2.2.3 Turbine Performance Curve

The performance curve of the turbine is obtained by plotting the non-dimensional coefficient of power against the non-dimensional coefficient of speed. The peak of this curve visually indicates the optimal operational point of the turbine, or the tip speed ratio for which the turbine is most efficient. Figure 3 illustrates the characteristic performance curves of some common wind turbine configurations. Note that in this image, even the

peak performance of these characteristic turbines is still over 10% lower than the turbine efficiency limit proposed by Betz.

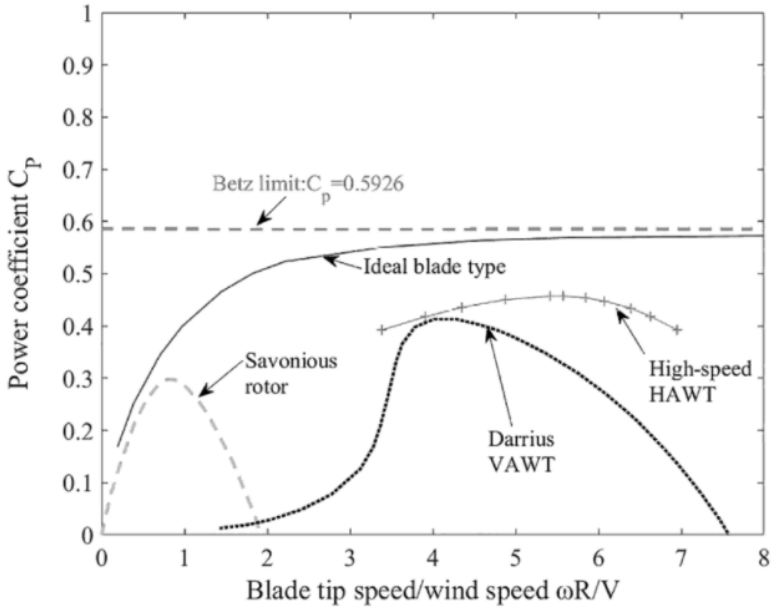

Figure 3 - C_p as a function of C_s for some common turbine types [17].

2.3 Power Generated

Turbine mechanical power generated at the shaft can be determined from first principles in terms of measured torque:

$$P = \omega \mathrm{T} \qquad \textit{Eq. 2.9}$$

Where:

$$P \textit{ is the mechanical power generated by the turbine, in Watts}$$

ω *is the rotational speed of the turbine rotor in* $^{rad}/_{s}$

T *is the mechanical torque measured at the shaft, in Nm*

Since the rotational speed of the turbine was measured in RPM, the expression for generated power becomes:

$$P = 2\pi \left(\frac{n_{rpm}}{60}\right) \mathrm{T} \qquad \textit{Eq. 2.10}$$

Where:

n_{rpm} *is the rotational speed of the turbine rotor in revolutions per minute*

3 Turbine Models

The physical turbines were designed to be a low-cost construction, using readily available off-the self materials and components. Turbine geometry was limited by availability of low-cost off-the-shelf parts for construction of the physical model. For this reason, the physical turbines were designed and built first, with the digital CAD models being developed from the as-built dimensions of the physical turbines.

3.1 Physical Turbine Geometry

The physical turbine model was composed of an ABS hub with diameter of 153mm, and 25mm square aluminum blades bolted to the hub in an equally spaced radial pattern. To form the second turbine configuration, larger 50.44mm cross section blades were made from square profile ABS and fit over the 25.44mm cross section blades with 3D printed spacers. The larger blades were then screwed in place to prevent detaching during rotation. The overall tip-to-tip turbine diameter was 768mm in both configurations.

This diameter was the largest that could reasonably be fitted in the MUN wind tunnel, the facility available for this study. A relatively large model minimized the measurement error, which was important because measured torque values were expected to be small.

The arrangement of shafts and bearings used to support the models in the wind tunnel is described in the later section covering the conduct of the experiments.

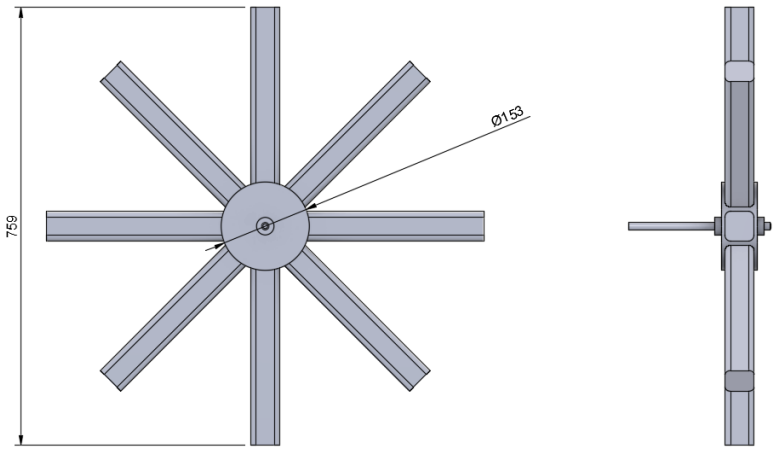

Figure 4 - Image depicting overall turbine dimensions with 50.44mm profile blades.

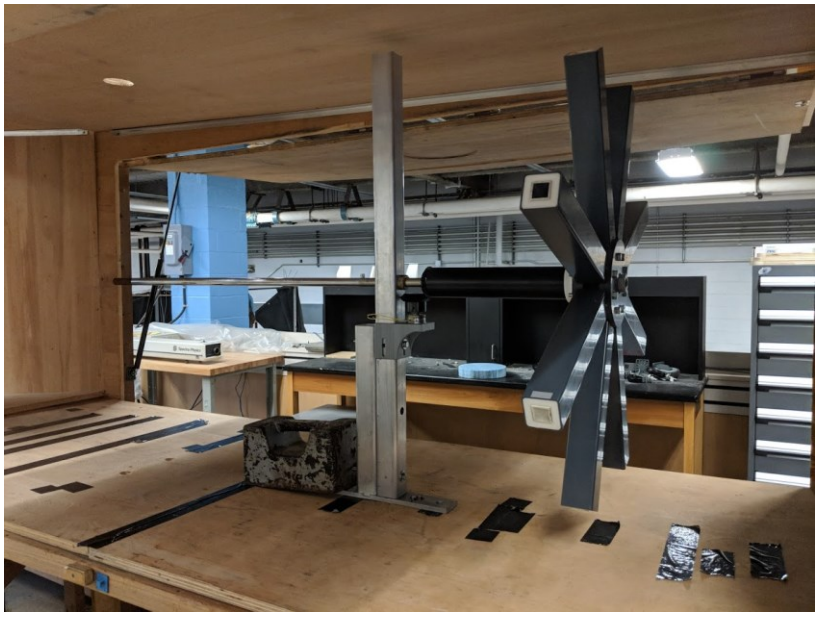

Figure 5 - Wind tunnel setup showing turbine construction.

3.2 Simulation Turbine Model

A digital model of the turbine rotor was created based on the as-built dimensions of the physical model. However, because the Fluent simulation utilized rotational symmetry to

increase mesh quality within the problem size limits, a simplified eighth-section model was used in place of a full rotor for simulation geometry.

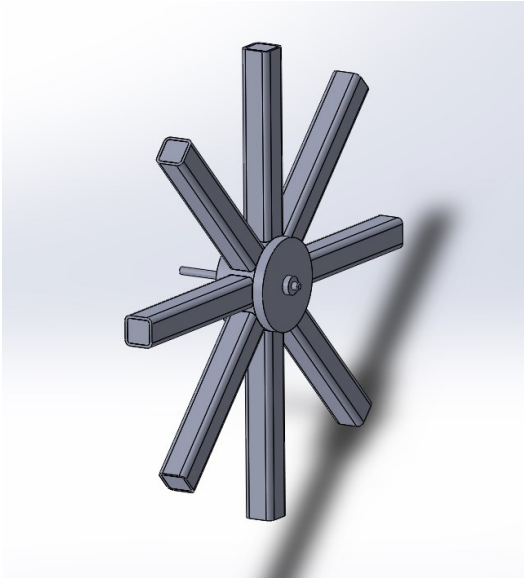

Figure 6 – Full CAD model of turbine with 50.44mm cross section blades.

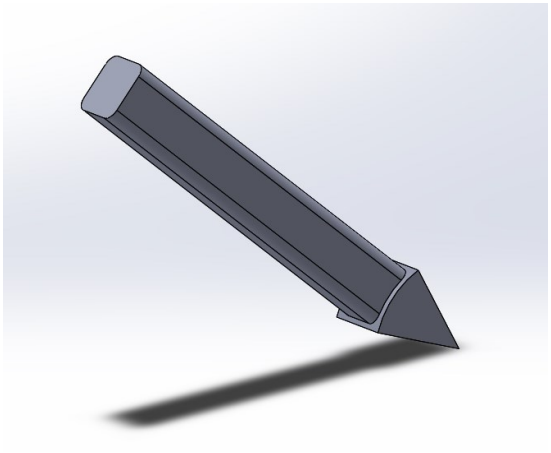

Figure 7 - Simplified eighth-section CAD model of turbine with 50.44mm cross section blades.

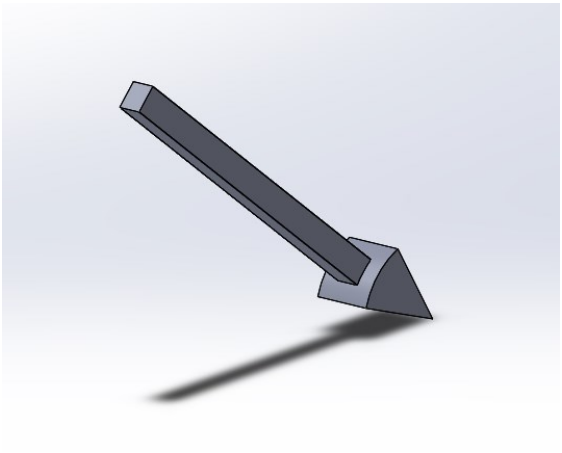

Figure 8 - Simplified eighth-section CAD model of turbine with 25.28mm cross section blades

4 CFD Simulations

Transient CFD simulations were conducted using ANSYS Fluent through the ANSYS Workbench environment. Two turbine models were tested at three flow velocities, and up to a maximum of six rotational speeds for each of the three flow velocities. From these simulations hub torque was measured, and power ($P\ vs\ \omega$), and efficiency ($C_p\ vs\ C_s$) curves were generated for each of the two turbines indicating peak power and efficiency operating points.

Table 1 - Test plan for simulations

Testing Plan for CFD Simulations			
Turbine Model	**Flow Velocity**	**RPM**	**Angular Speed**
50.5mm Blade Cross-Section	5 m/s	5 RPM	0.5236 rad/s
		10 RPM	1.047 rad/s
		20 RPM	2.094 rad/s
		30 RPM	3.142 rad/s
		40 RPM	4.189 rad/s
		50 RPM	5.236 rad/s
	4 m/s	5 RPM	0.5236 rad/s
		10 RPM	1.047 rad/s
		20 RPM	2.094 rad/s
		30 RPM	3.142 rad/s
		40 RPM	4.189 rad/s
		50 RPM	5.236 rad/s
	3 m/s	5 RPM	0.5236 rad/s
		10 RPM	1.047 rad/s
		20 RPM	2.094 rad/s
		30 RPM	3.142 rad/s
		40 RPM	4.189 rad/s
25.28mm Blade Cross Section	5 m/s	5 RPM	0.5236 rad/s
		10 RPM	1.047 rad/s
		20 RPM	2.094 rad/s
		30 RPM	3.142 rad/s
		40 RPM	4.189 rad/s
		50 RPM	5.236 rad/s
	4 m/s	5 RPM	0.5236 rad/s

		10 RPM	1.047 rad/s
		20 RPM	2.094 rad/s
		30 RPM	3.142 rad/s
		40 RPM	4.189 rad/s
		50 RPM	5.236 rad/s
	3 m/s	5 RPM	0.5236 rad/s
		10 RPM	1.047 rad/s
		20 RPM	2.094 rad/s
		30 RPM	3.142 rad/s
		40 RPM	4.189 rad/s
		50 RPM	5.236 rad/s

4.1 Governing Equations

4.1.1 Governing Equations for CFD

For simulating all flows, ANSYS Fluent solves conservation of mass, and conservation of momentum equations. The general CFD equations and solution are described below.

The conservation of mass (or continuity) equation is:

$$\frac{\partial p}{\partial t} + \rho \cdot C^2 \left(\frac{\partial U}{\partial x} + \frac{\partial V}{\partial y} + \frac{\partial W}{\partial z}\right) = 0 \qquad \textit{Eq. 4.1}$$

The conservation of momentum equations are:

$$\rho\left(\frac{\partial U}{\partial t} + \frac{U\partial U}{\partial x} + \frac{V\partial U}{\partial y} + \frac{W\partial U}{\partial z}\right) + A = -\frac{\partial p}{\partial x} + \left[\frac{\partial}{\partial x}\left(\frac{\mu\partial U}{\partial x}\right) + \frac{\partial}{\partial y}\left(\frac{\mu\partial U}{\partial y}\right) + \frac{\partial}{\partial z}\left(\frac{\mu\partial U}{\partial z}\right)\right] \qquad \textit{Eq. 4.2}$$

$$\rho\left(\frac{\partial V}{\partial t} + \frac{U\partial V}{\partial x} + \frac{V\partial V}{\partial y} + \frac{W\partial V}{dz}\right) + B = -\frac{\partial p}{\partial y} + \left[\frac{\partial}{\partial x}\left(\frac{\mu\partial V}{\partial x}\right) + \frac{\partial}{\partial y}\left(\frac{\mu\partial V}{\partial y}\right) + \frac{\partial}{\partial z}\left(\frac{\mu\partial V}{\partial z}\right)\right] \qquad \textit{Eq. 4.3}$$

$$\rho\left(\frac{\partial W}{\partial t} + \frac{U\partial W}{\partial x} + \frac{V\partial W}{\partial y} + \frac{W\partial W}{dz}\right) + C = -\frac{\partial p}{\partial Z} + \left[\frac{\partial}{\partial x}\left(\frac{\mu\partial W}{\partial x}\right) + \frac{\partial}{\partial y}\left(\frac{\mu\partial W}{\partial y}\right) + \frac{\partial}{\partial z}\left(\frac{\mu\partial W}{\partial z}\right)\right] \qquad \textit{Eq. 4.4}$$

Where:

$U, V, and\ W\ are\ fluid\ velocities$

$p\ is\ pressure$

$\rho\ is\ fluid\ density$

$\mu\ is\ the\ effective\ viscosity\ of\ the\ fluid$

$A, B, and\ C\ are\ turbulence\ source\ terms$

Effective viscosity is composed of laminar viscosity and an eddy viscosity due to turbulence. In the $k\omega$ turbulence model, k is the kinetic energy of turbulence and ω is the turbulence vorticity. The governing equations for the model are:

$$\frac{\partial k}{\partial t} + \frac{U\partial k}{\partial x} + \frac{V\partial k}{\partial y} + \frac{W\partial k}{\partial z} = T_p - T_D + \alpha\left[\frac{\partial}{\partial x}\left(\frac{\mu\partial k}{\partial x}\right) + \frac{\partial}{\partial y}\left(\frac{\mu\partial k}{\partial y}\right) + \frac{\partial}{\partial z}\left(\frac{\mu\partial k}{\partial z}\right)\right] \quad \textit{Eq. 4.5}$$

$$\frac{\partial w}{\partial t} + \frac{U\partial w}{\partial x} + \frac{V\partial w}{\partial y} + \frac{W\partial w}{\partial z} = D_p - D_D + \beta\left[\frac{\partial}{\partial x}\left(\frac{\mu\partial w}{\partial x}\right) + \frac{\partial}{\partial y}\left(\frac{\mu\partial w}{\partial y}\right) + \frac{\partial}{\partial z}\left(\frac{\mu\partial w}{\partial z}\right)\right] \quad \textit{Eq. 4.6}$$

Where:

$T\ and\ D\ are\ terms\ for\ the\ production\ and\ dissipation\ of\ turbulence.$

$Turbulence\ viscosity\ is\ \frac{\rho k}{w}.$

For rotating analysis, the governing equations are converted to a reference frame attached to the rotor. Also, each PDE is put into the form:

$$\frac{\partial M}{\partial t} = N \quad \textit{Eq. 4.7}$$

Within every cell, each governing equation is integrated numerically across a time step increment to get:

$$M(t + \Delta t) = M(t) + \Delta t N(t) \qquad \textit{Eq. 4.8}$$

Current values of the unknowns in cells are used to approximate the spatial derivatives terms in N for each cell. For each incremental time step, U , V, and W, are updated using the momentum equations, and P is updated using the mass equation. The updated U , V, and W, along with the turbulence equations are then used to update k and w.

4.1.2 Rotating Reference Frame in Fluent

The Fluent simulation uses the Conservation of Mass (or Continuity) and Navier-Stokes equations, in the frame of reference rotating with the blade, eliminating the need for a considerably more complex rotating mesh simulation. The format conservation of mass and momentum equations are provided below for reference,

Conservation of Mass:

$$\frac{\partial \rho}{\partial t} + \nabla \cdot \rho \vec{v}_r = 0 \qquad \textit{Eq. 4.9}$$

Navier-Stokes Conservation of Momentum:

$$\nabla \cdot (\rho \vec{v}_r \vec{v}_r) + \rho(2\vec{\omega} \times \vec{v}_r + \vec{\omega} \times \vec{\omega} \times \vec{r}) = -\nabla p + \nabla \cdot \bar{\bar{\tau}}_r \qquad \textit{Eq. 4.10}$$

Where:

$\vec{v}_r$ *is the relative velocity with respect to the moving frame*

$\vec{\omega}$ *is the angular velocity of the moving frame*

4.2 Simulation Setup

4.2.1 ANSYS Workbench 19.2

For each trial, a stand-alone project using the Fluent solver was created in ANSYS Workbench, allowing easy comparison of results, as well as storing data in an organized and easy to retrieve method. The workbench project breaks simulation workflow down into five categories: geometry, mesh, setup, solutions, and results.

4.2.2 Geometry

Geometry for the CFD simulation was created using ANSYS Design Modeler. Turbine blades were modeled in SOLIDWORKS parametric CAD software from Dassault Systèmes and exported in .STEP format. The blades were then imported in Design Modeler, where the fluid domain was built around the imported body. A Boolean subtraction was used to remove the blade volume from the fluid domain and create the FSI surfaces for analysis.

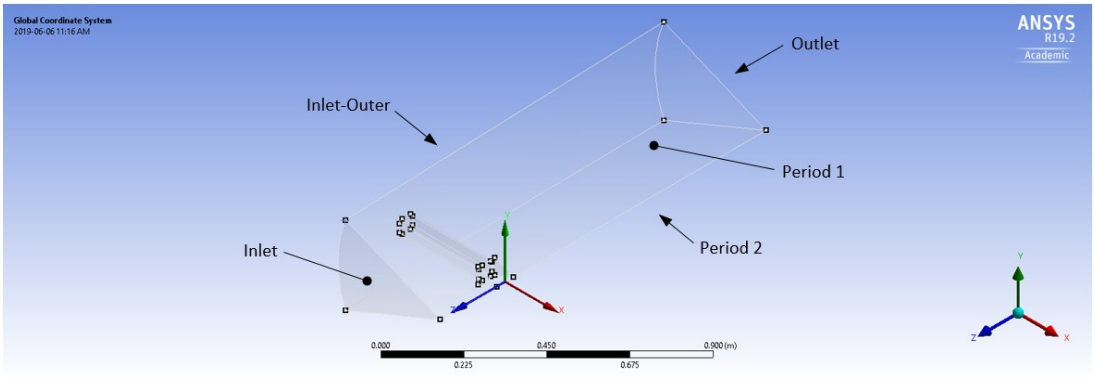

Figure 9 - Isometric view of fluid domain showing named selections forming simulation boundaries. 50.44mm blade shown.

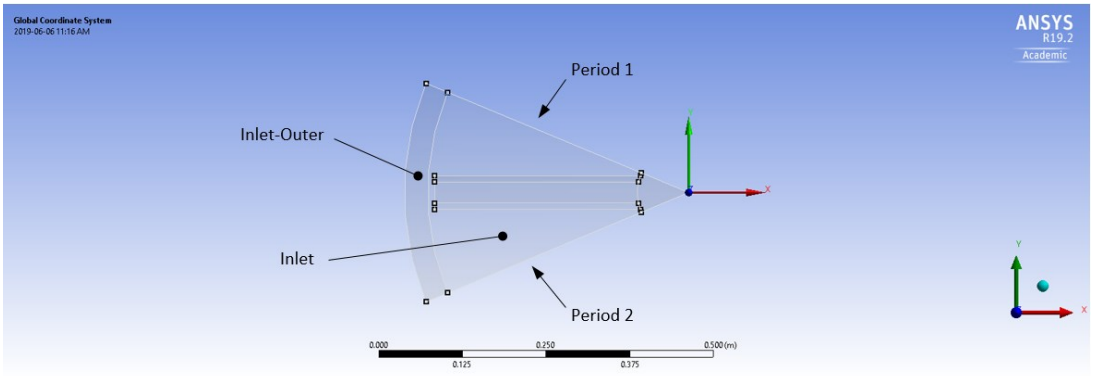

Figure 10 - Front view of fluid domain showing named selections forming simulation boundaries. 50.44mm blade shown.

Due to the 512,000 cell and node limitations imposed on the mesh by the ANSYS Academic software version, the simulation was modeled as a single blade, or 1/8th of the turbine to maximize mesh resolution in the flow domain around the blade. Periodic interfaces were used to extrapolate the single blade solution to the full eight blades.

4.2.3 Mesh

The simulation mesh was set up using localized mesh controls along the blade surface, as well as inflation layers surrounding the blade. The periodic interface boundaries also had mesh controls applied to match nodes on these boundaries, allowing rotational symmetry. Full details on the CFD mesh can be found in Appendix A – CFD Mesh Details and Model Validation.

4.2.4 Physics Setup

ANSYS Fluent was the chosen fluid flow simulation application for this project. The simulations were launched with double precision and parallel processing options enabled. The maximum of four cores for the academic license were used for the calculations.

4.2.4.1 Turbulence Model

For the simulations in this study, the κ-ω SST turbulence model was chosen for being better suited to complex flows such as eddies and vortices, than the simpler but less computationally intensive κ-ε model. According to Menter, the κ-ω SST (Shear Stress Transport) model is more accurate and reliable for a wider class of flows than the standard and BSL κ-ω models, as it also accounts for the transport of turbulence shear stress in the definition of turbulent viscosity [20] [21].

4.2.4.2 Frame Motion

Cell zone conditions for the fluid region were set to include a frame of reference motion. This accounts for the effect the rotation of the turbine blade has on the flow [22]. Frame motion was set at about the z-axis in the clockwise direction, meaning torque moments in the direction of rotation will be negative.

4.2.4.3 Environmental Conditions / Constants

The following values were used for all simulations:

Kinematic viscosity of air, ν, at 15°C = 1.48×10^{-5} [m^2/s]

Dynamic viscosity of air, μ, at 15°C = 1.81×10^{-5} [kg/(m*s)] aka [Pa*s]

4.2.4.4 Boundary Conditions

The overall shape of the fluid domain set up in design modeller was one-eighth of a truncated cone. The front face of the domain was set as a velocity inlet along with the outer radial surface. The rear face of the domain was set as a pressure outlet at atmospheric pressure. Blade and hub surfaces created by the Boolean subtraction of the imported geometry were set as no-slip walls. The surfaces dividing the cone shape into eighths were set as periodic interfaces.

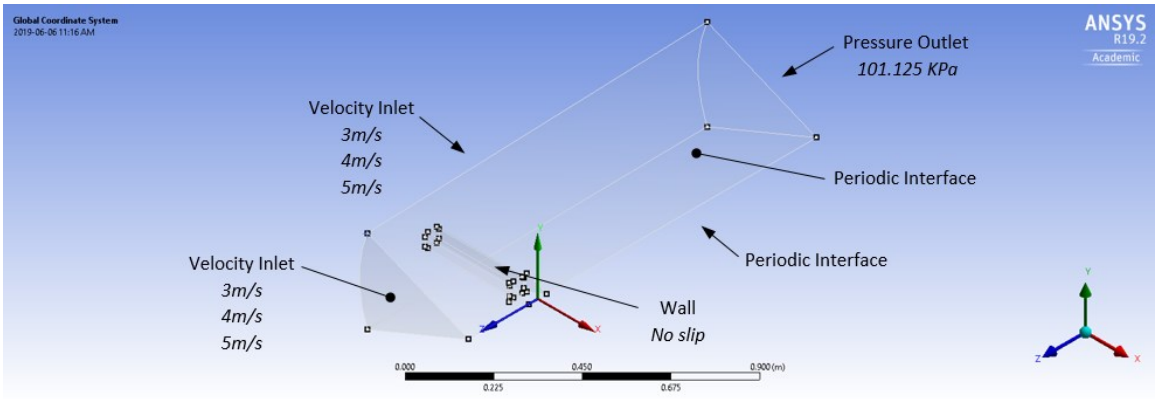

Figure 11 - Boundary conditions for ANSYS Fluent simulations.

4.2.4.4.1 Inlet

Boundary conditions for both the front face and outer conical surface were set as inlets, with velocity at -5.00 m/s, -4.00m/, or -3.00 m/s in the z-direction, depending on the trial run. Turbulent intensity is set to 5% and turbulent viscosity ratio is 10.

4.2.4.4.2 Outlet

Outlet pressure is set to ambient, which is the default value of one atmosphere.

4.2.4.4.3 Blade

Blade wall boundaries are set to no-slip.

4.2.4.5 Periodicity

The interface boundary conditions, used for sliding mesh and multiple reference frame calculations, was chosen for periodic symmetry faces. Following this, through the mesh interfaces menu, a periodic interface was set up using the two periodic symmetry faces. Options for a matching, rotational interface with an automatically computed offset were selected.

4.2.4.6 Convergence Conditions

Residual monitors were set with absolute time step convergence criteria to determine when a time step calculation had converged enough to be considered solved. "Absolute" criteria requires the residuals to drop below some fixed-value threshold. ANSYS suggests accepting the solution when residual values for continuity drop below $1e^{-3}$, and residuals for all other equations drop below $1e^{-4}$ [23], however the criteria used for convergence in this study was more stringent, with residual levels for solution acceptance set at $1e^{-4}$for continuity, and $1e^{-6}$ for all other equations. It should be noted that these are relative residuals, so a residual value of $1e^{-4}$ would indicate a magnitude of four orders less than the equation solution value [23].

4.2.4.7 Solver Selection

For these simulations, the pressure-based coupled solver with high order term relaxation was selected. While more computationally expensive than SIMPLE methods, the coupled

solver (along with PISO) is preferred for transient simulations due to its more aggressive convergence behaviour, and is less affected by lower mesh quality and poor initial time-step guesses [24].

4.2.4.8 Time Step Selection

Time step selection criteria for transient simulations involve weighing accuracy, convergence, and computing power criteria, then making acceptable trade-offs between the three to get a converged solution with an acceptable accuracy and within a reasonable timeframe considering the computing power available.

A popular method for setting time steps is known as the Courant- Friedrichs-Lewy condition [25], commonly called the CFL number, C. This condition requires that:

$$C = \frac{U\,\Delta t}{\Delta x} \geq C_{max} \qquad \textit{Eq. 4.11}$$

Where:

$C = Courant - Friedrichs - Lewy\ (CFL)\ number$ (non-dimensional)

$\Delta t = time\ step\ size$ (s)

$\Delta x = minimum\ mesh\ cell\ characteristic\ dimension$ (m)

$C_{max} =\ limiting\ CFL\ number\ for\ particular\ flow\ and\ mesh\ conditions$

Essentially, the CFL number is a measure of how many grid cells the flow will pass through in any given time step. For explicit solvers, the maximum CFL number should be less than or equal to one for unconditional stability of the calculation. For implicit solvers, the maximum CFL number may be considerably higher, with the ANSYS Fluent default setting for density-based implicit formulation being a $C_{max} = 5$ [23]. For the implicit solver, depending on complexity of the problem, the CFL can often be increased to 100 or higher [23]. Note that the simulations examined in this study utilized the implicit pressure-based solver, so there is no available option to control time stepping by setting a limiting CFL. However, the CFL still provides and excellent estimate for selecting a time step size that will converge and provide reasonable results.

To determine time step size for a CFL number, $C_{max} = 1$, we solve:

$$\frac{U\,\Delta t}{\Delta x} \geq 1 \qquad \textit{Eq. 4.12}$$

$$\Delta t = \frac{\Delta x}{U} \qquad \textit{Eq. 4.13}$$

For tetrahedral cells, the minimum characteristic mesh dimension, Δx, is estimated by taking the third root of the minimum cell volume:

$$\Delta x = \sqrt[3]{V_{cell,min}} \qquad \textit{Eq. 4.14}$$

Where:

$\Delta x = minimum\ mesh\ cell\ characteristic\ dimension$ (m)

$V_{cell,min} = minimum\ mesh\ cell\ volume\ (m^3)$

The minimum cell volume for the mesh, as well as minimum face areas, were determined using Fluent's mesh check tool.

Table 2 - Transient simulation time step values.

Transient Time Step by Simulation Flow Velocity and Element Size						
Blade Cross-Section	Minimum Element Volume	Minimum Element Dim., Δx	Flow Velocity, U	Δt		
				$C_{max} = 1$	$C_{max} = 5$	First Implement
50.44 mm	0.2656 mm^3	0.6428 mm	5,000 mm/s	0.000129 s	0.000645 s	0.0005 s
			4,000 mm/s	0.000161 s	0.000805 s	0.0005 s
			3,000 mm/s	0.000214 s	0.00107 s	0.001 s
25.28 mm	0.00391 mm^3	0.1575 mm	5,000 mm/s	0.0000315 s	0.000158 s	0.0001 s
			4,000 mm/s	0.0000394 s	0.000197 s	0.0001 s
			3,000 mm/s	0.0000525 s	0.000263 s	0.0001 s

After monitoring initial convergence, adjustments were made to the time step size for the 50.50mm, 4m/s, 50 RPM trial, as well as the 50.50mm, 5 m/s, 50 RPM trial. It was noticed the time steps were often using a full 150 iterations without meeting convergence conditions, so the step size was reduced to 0.00025s, after which steps were resolved in an acceptable number of iterations. This is likely due to the increased apparent flow speed at the turbine blade tip, caused by the increased rotational speed.

Maximum iterations per time step was set to 150. Combined with the convergence criteria, this allows the first few time steps to converge well with a large number of iterations, setting up the problem in a stable, well-converged manner. For most simulations, after the initial ten time steps, the number of iterations required for the solver to reach convergence at each step was typically between five and twenty-five, depending on the flow and rotor speeds.

4.3 CFD Results

4.3.1 Vortex Formation

Inspecting particle velocity and pressure plots of the CFD trials indicate that vortex formation did occur. In Figure 12 and Figure 13, the particle velocity plots indicate a vortex formation on the leading downstream corner of the blade, which would agree with a low-pressure vortex region "pulling" the blade along, such as the one indicated in Figure 14 and Figure 15. Note that the apparent vortex does not extend the full length of the blade but affects only a short portion of the overall blade length. The results in these figures are typical of both blade sizes and all flow speeds.

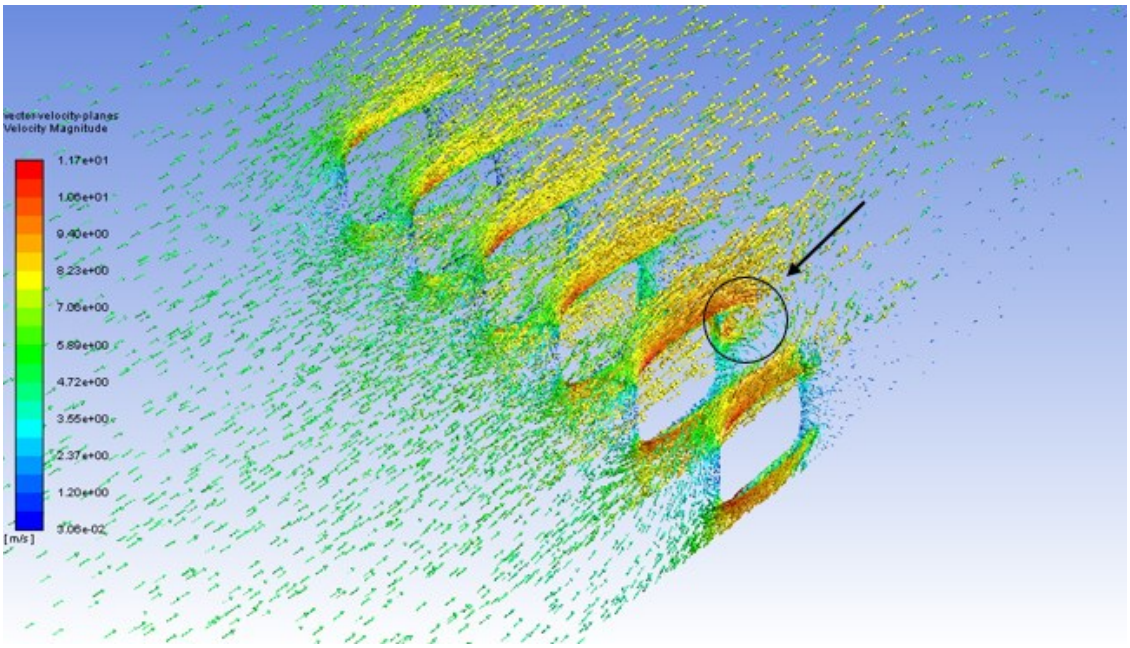

Figure 12 - Image showing apparent vortex attached to turbine blade.

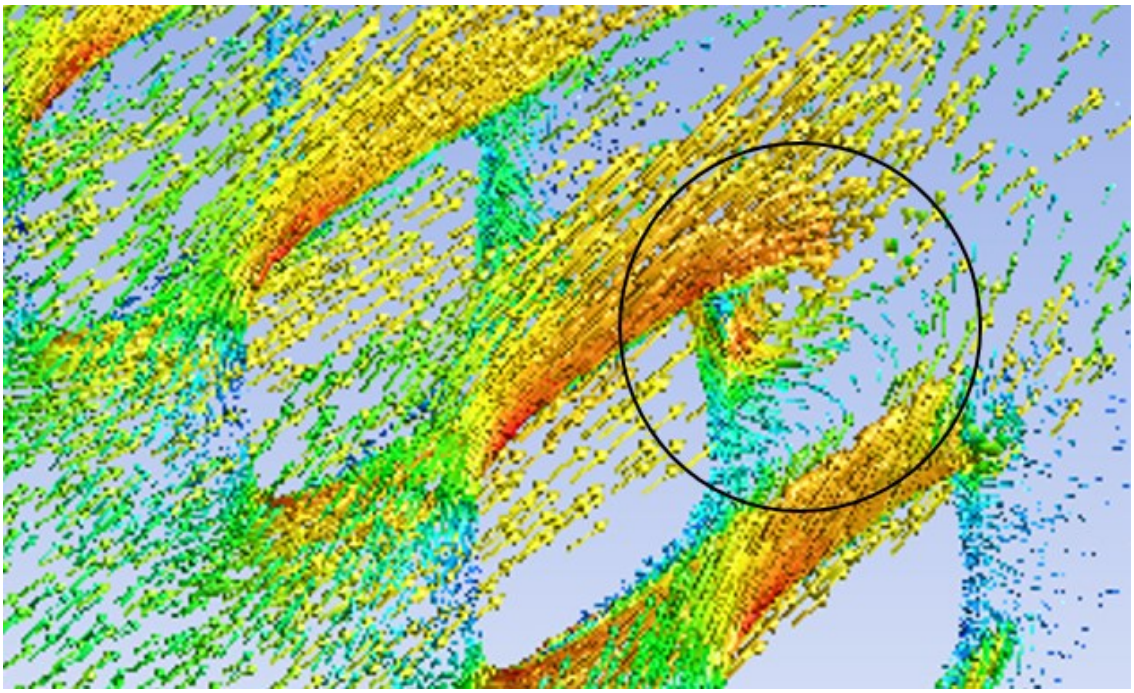

Figure 13 - Detail of apparent vortex region at downstream side leading corner of blade.

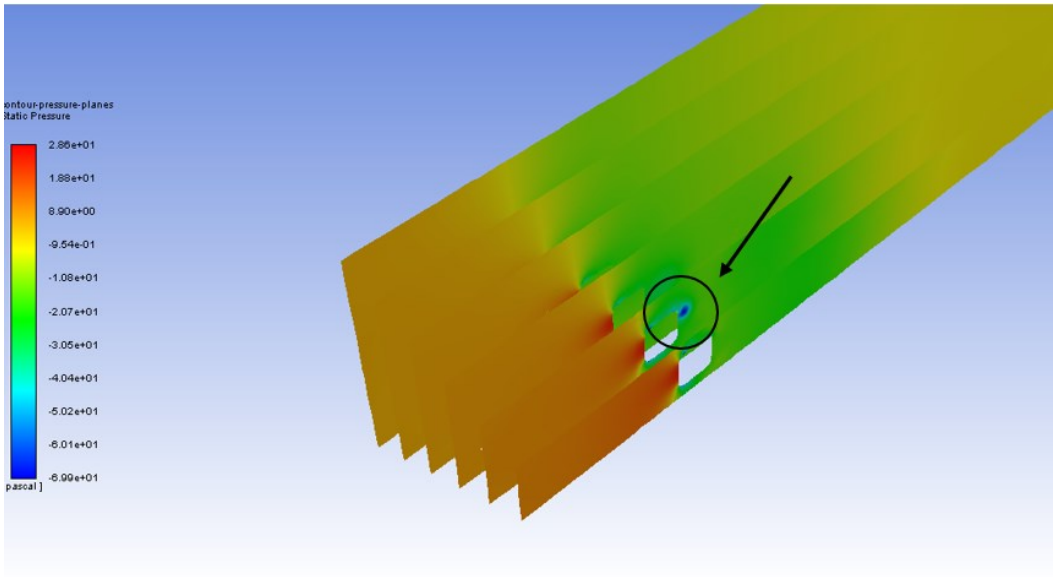

Figure 14 - Low pressure region at the leading corner, downstream side of blade.

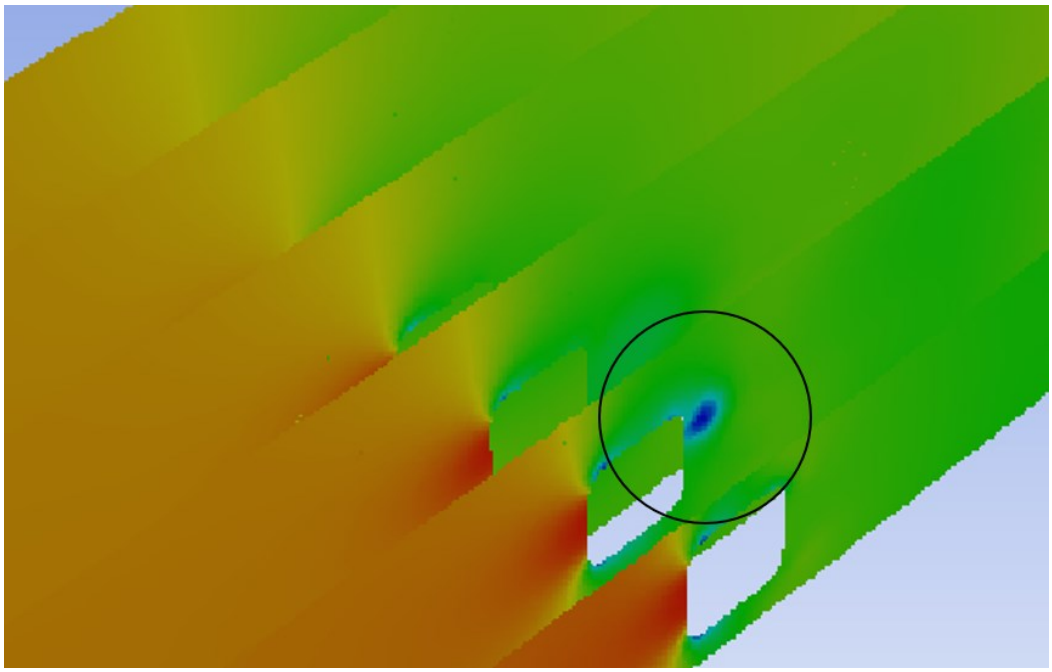

Figure 15 - Detail of low pressure region at the leading corner, downstream side of blade.

4.3.2 Rotor with Eight 50.44mm Square Blades

Overall results from all flow speeds for the CFD simulations were tabulated and plotted. For absolute power generated, the simulations predict that increasing flow speed will increase the maximum power generated. Additionally, the angular velocity of the turbine which corresponds with peak power generation increases with flow speed. This is congruent with the Cp vs Cs peak remaining at a constant value for all flow speeds. Note that these simulations prescribed turbine rotational speed and measured the resulting torque generated at the rotor axis, so negative power values indicate rotational speeds which could only be reached with external power input.

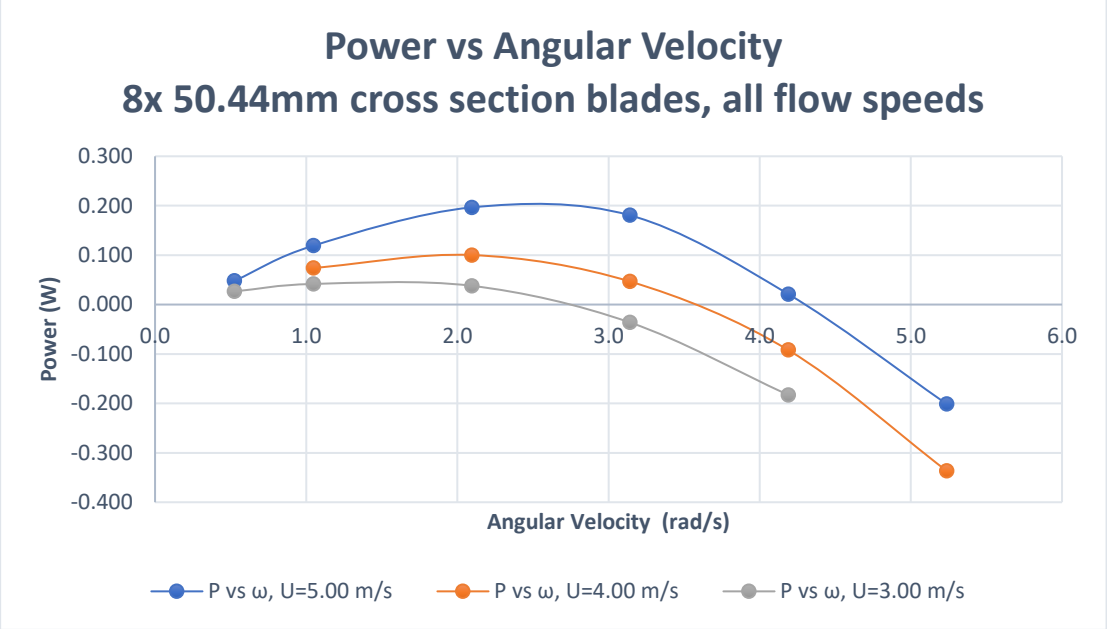

Figure 16 - Plot of turbine power vs angular velocity for 50.44mm blade cross section turbine, for all flow speeds simulated.

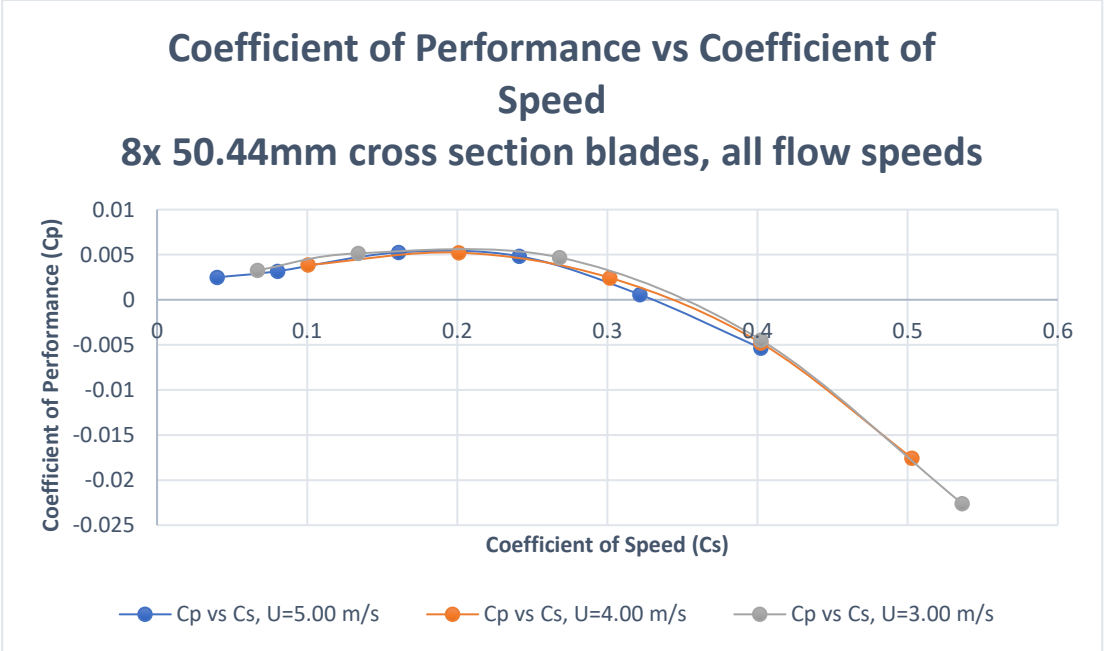

Figure 17 - Plot of C_P vs C_S for 50.44mm blade cross section turbine, for all flow speeds simulated.

The data also clearly indicates a peak efficiency for the turbine across all three simulated flows, with Cp peaking at a Cs value of just over 0.2 for all speeds.

4.3.3 Rotor with Eight 25.28mm Square Blades

As with the 50.44mm cross section blades, the smaller 25.28mm cross section blades showed that the angular velocity corresponding to the peak power generation increased as the flow speed increased. Notably, the angular velocity of the 25.28mm blade cross section turbine corresponding with peak power generation was greater than that of the 50.44mm blade cross section turbine for each flow speed simulated. The peak for the 25.28mm blade cross section turbine power vs. angular velocity curve appears to be just past the highest angular velocity simulated of 5.236 rad/s (50 RPM).

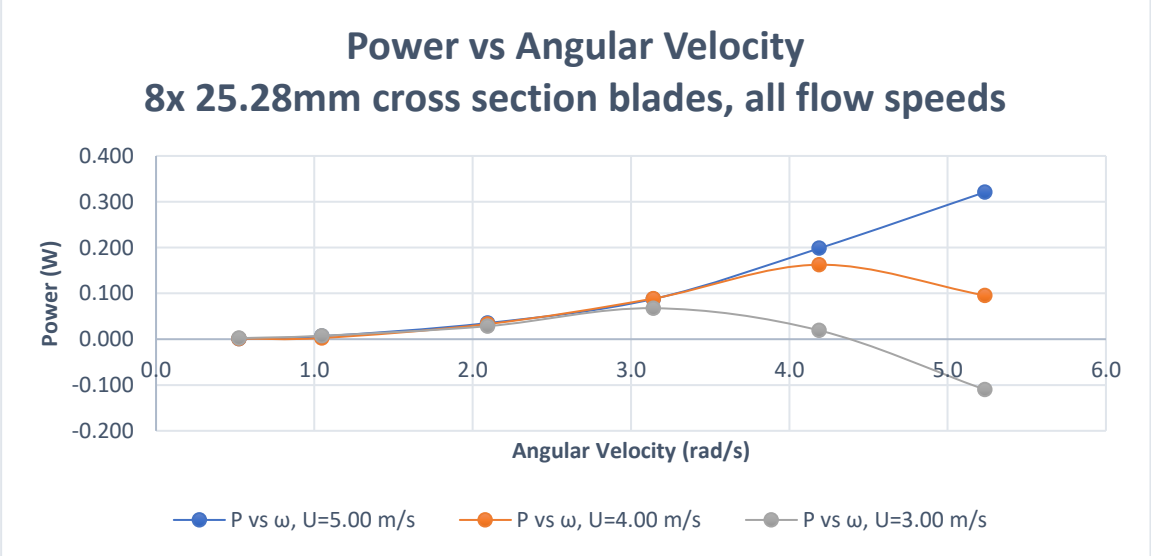

Figure 18 - Plot of Power vs Angular Velocity for 25.28mm cross section turbine, for all flow speeds simulated

Like the 50.44mm cross section blade turbine, the peak C_P for the 25.28mm cross section blade turbine was constant across all flow speeds simulated at approximately $C_s = 0.4$. Meaning the peak at occurs at approximately twice the C_s of the 50.44mm cross section blade turbine.

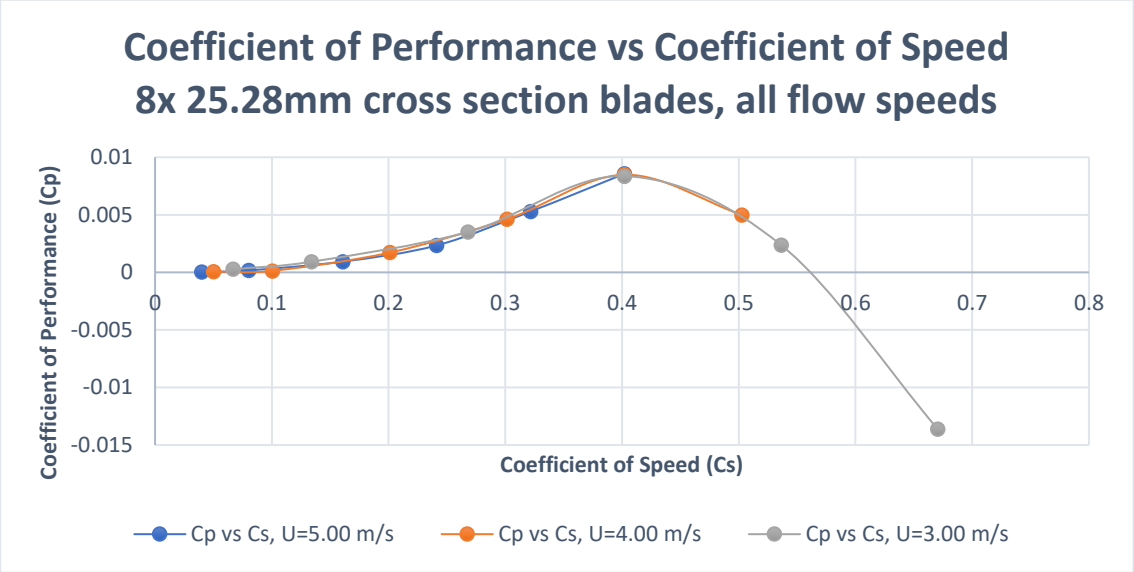

5 Wind Tunnel Trials

To provide physical validation to the CFD models, two turbine models were tested in the Memorial University Faculty of Engineering wind tunnel.

5.1 Setup

Turbines were set in the wind tunnel on a horizontal shaft fixed to vertical post. The turbines were cantilevered from the post by 475mm to minimize the effect of flow disturbances caused by the vertical post on the turbine action. The turbines were mounted to the shaft with a bearing interface to allow rotation. Bearings were held in place using keeper plates on the turbine hub and friction collars on the shaft. A rotating sleeve with a 30 tooth, 12 pitch mitre gear was fixed to the rear of the turbine. The sleeve was set on bearings, rotating around the shaft.

A Placid Industries B1-6-1FRM magnetic particle brake was mounted to the vertical shaft using 3D printed brackets. The brake was connected to the rotating sleeve via an interfacing mitre gear. The magnetic particle brake was wired to a BK Precision 1627A DC regulated power supply to provide control of the brake's resistive torque.

Figure 19 - Wind tunnel turbine setup showing 50.44mm profile blades.

The sides of the wind tunnel in the region where the turbine was located were left open to better simulate open-stream flow, and to prevent a large pressure buildup on the upstream side of the turbine by allowing an escape path for air.

Figure 20 - Image showing open sides of wind tunnel setup.

5.2 Procedure

For each trial run, the tunnel wind speed started from zero and was gradually increased. An EXTECH 451104 anemometer was used to take measurements for increasing wind speed in approximately 0.5 m/s increments. At each step, a TSI 9565-P mechanical multi-meter with hot-wire wind speed sensor was used to measure the air flow profile across the cross-section of the tunnel, 600mm in front of the turbine face. The average wind speed across this profile was used for calculations of power and efficiency.

At each constant wind speed, the BK Precision 1627A DC regulated power supply output voltage was set to limit at 6V, the maximum brake voltage. Output current was set to zero, and increased in increments of 0.010A. As brake torque dynamic torque resistance differs depending on if the input current set point is approached from above or below, each step in current was approached from below. If the set point was overshot, or digital meter wavered on current output value, then the output was reduced to zero, and the set point was approached from below again. Once the current set point was reached, current and voltage values were recorded, and a Tenma digital photo tachometer was used to read turbine rotational speed until it settled. Then the rotational speed was recorded, and the measurement procedure was repeated for the next current step.

6 Results and Data Analysis

6.1 Summarized Results

Below are plots of summarized results presented in the same order as the CFD results.

Detailed results are reported in Appendix C – Wind Tunnel Test Data.

6.1.1 Rotor with Eight 50.44mm Square Blades

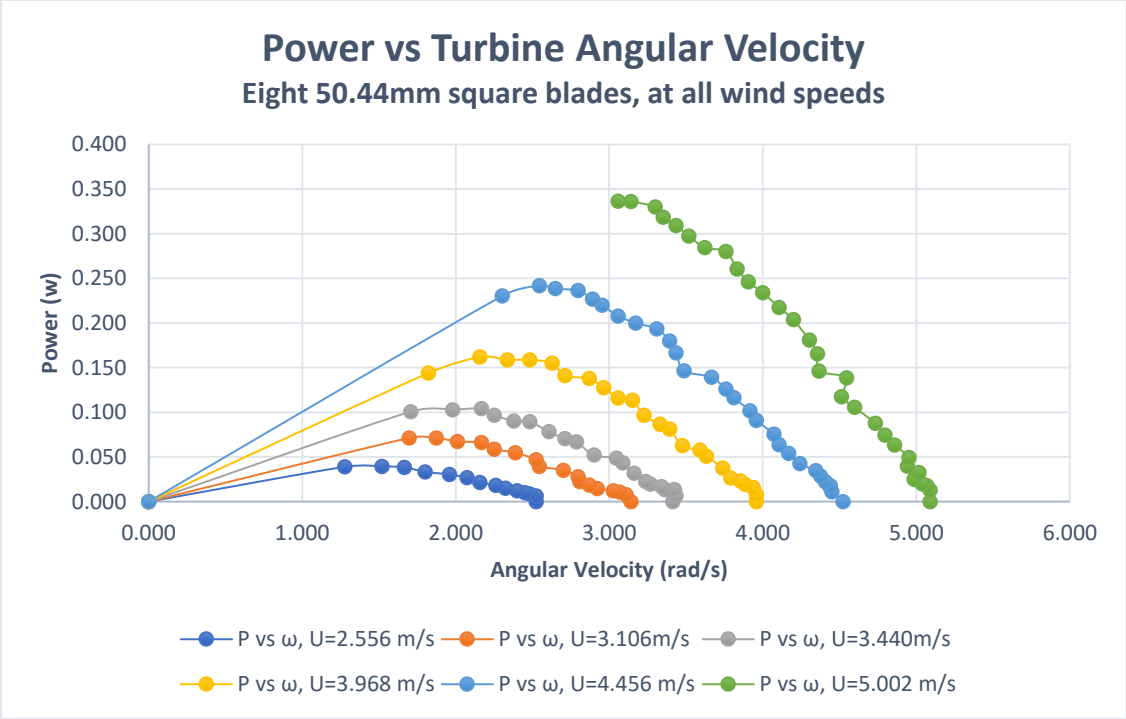

Figure 21 - Power vs Angular Velocity for eight 50.44mm blades

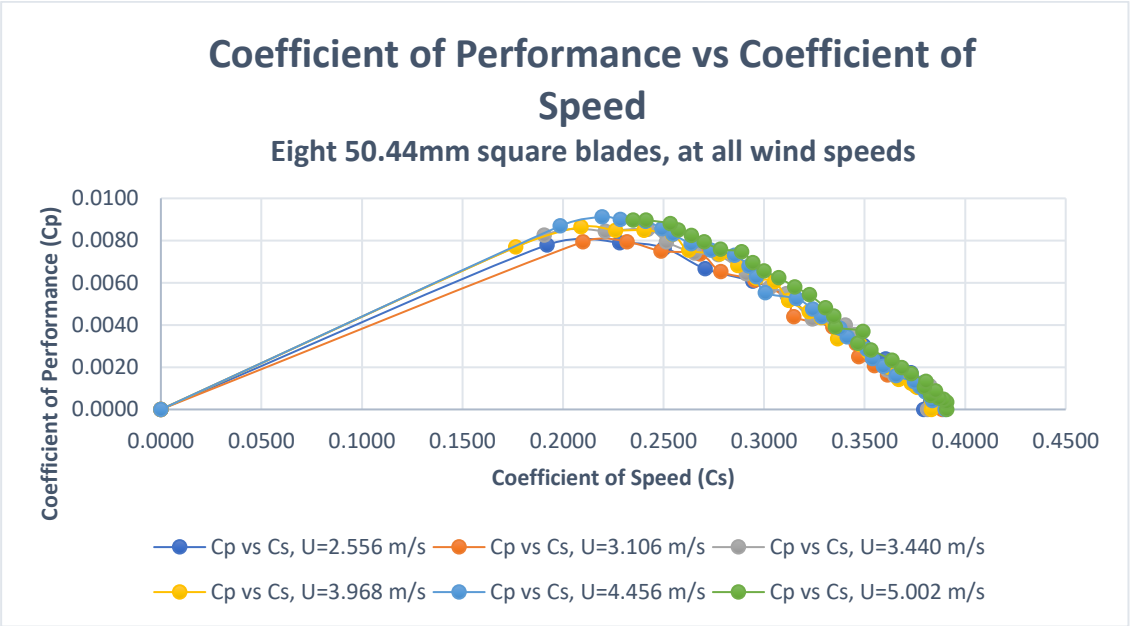

Figure 22 - Cp vs Cs for eight 50.44mm blades

6.1.2 Rotor with Eight 25.28mm Square Blades

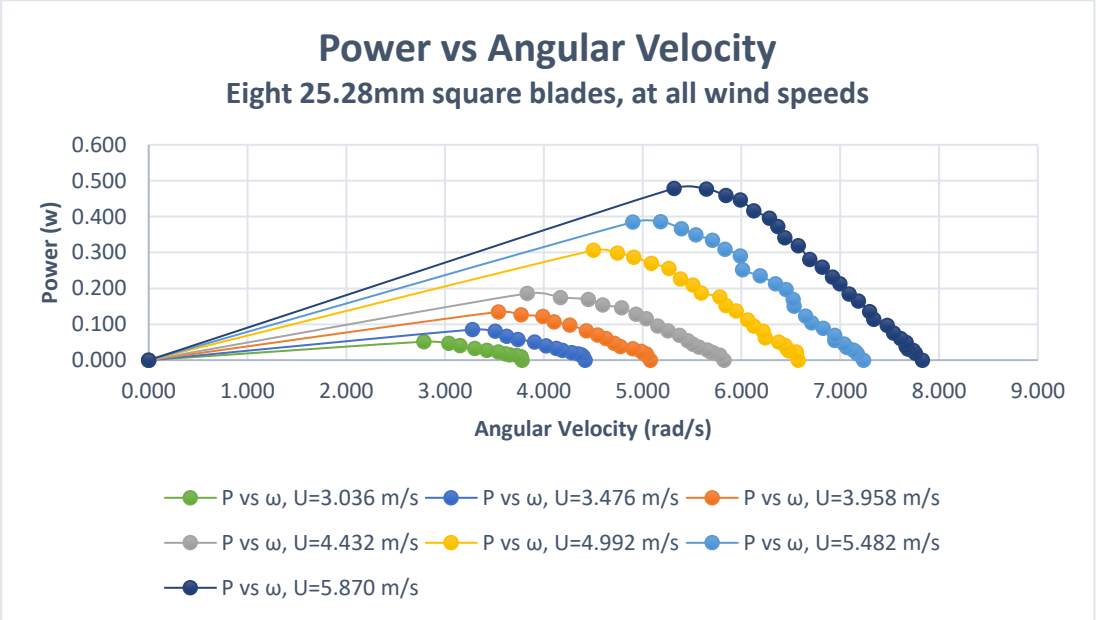

Figure 23 - Power vs Angular Velocity for eight 25.28mm blades

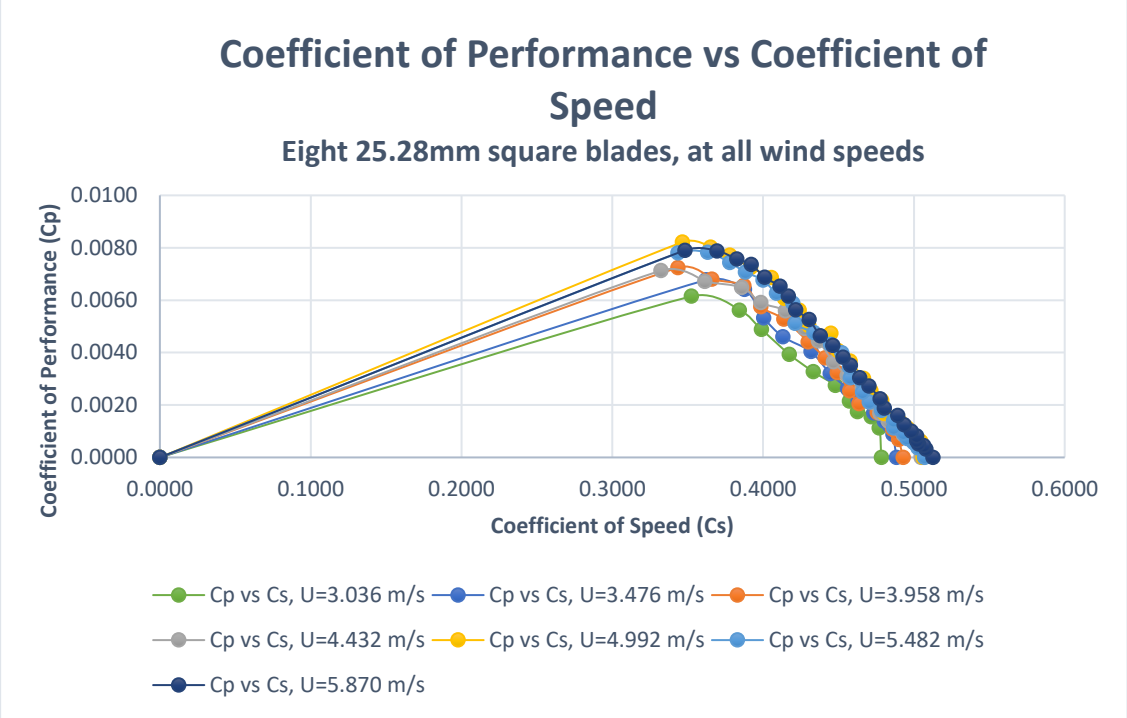

Figure 24 - Cp vs Cs for eight 25.28mm blades

6.2 Wind Tunnel Test Data Error Analysis

6.2.1 Uncertainty in Measurement and Calculated Values

Uncertainty in measurement of wind speed, angular velocity, applied torque for the wind tunnel trials contribute to the uncertainty of the calculated values C_p and C_s. The measurement uncertainties below are determined from the equipment specification sheets.

Table 3 - Uncertainty in Measured Values

Factor	Equipment Uncertainty	Measured Value	Uncertainty (σ) in Measurement
Wind Speed, *U*	Greater of: $\pm$ 3% of reading, or $\pm$ 0.015 m/s	3 m/s 4 m/s 5 m/s	$0.09 m/s$ $0.12\ m/s$ $0.15\ m/s$
Angular Velocity in RPM	$\pm$ 0.05% + 1 digit	0 RPM 10 RPM 20 RPM 30 RPM 40 RPM 50 RPM 60 RPM	1 RPM 1.005 RPM 1.01 RPM 1.015 RPM 1.02 RPM 1.025 RPM 1.03 RMP
Amperage (DC Supply)	$\pm$ 2% + 2 $digits$	0.00 0.01 0.02 0.03 0.04 0.05 0.06 0.07 0.08 0.09 0.10 0.11 0.12 0.13 0.14 0.15	0.02 A 0.0202 A 0.0204 A 0.0206 A 0.0208 A 0.021 A 0.0212 A 0.0214 A 0.0216 A 0.0218 A 0.0220 A 0.0222 A 0.0224 A 0.0226 A 0.0228 A 0.0230 A
Amperage, DMM	$\pm$ 1.5% + 4 at 4A	0.000 0.010 0.020 0.030 0.040 0.050 0.060 0.070 0.080 0.090 0.100 0.110 0.120 0.130 0.140 0.150	0.0040 A 0.00415 A 0.0043 A 0.00445 A 0.00460 A 0.00475 A 0.00490 A 0.00505 A 0.00520 A 0.00535 A 0.00550 A 0.00565 A 0.00280 A 0.00595 A 0.00610 A 0.00625 A
Applied Torque, *T*		Maximum for all values	0.0009625 N·m

6.2.2 Uncertainty in Torque Value

In general, the relationship between uncertainty in a measured variable x, and a dependant variable y, where $y = f(x)$ is [26]:

$$\sigma_y = \sigma_x \left(\frac{dy}{dx}\right)_{x=\bar{x}} \qquad \textit{Eq. 6.1}$$

In this experiment, the torque value is dependant on the measured current value. As the brake manufacturer states they do not have a function for the applied current to torque relationship of the brake, the torque reading was determined from a manufacturer-supplied table.

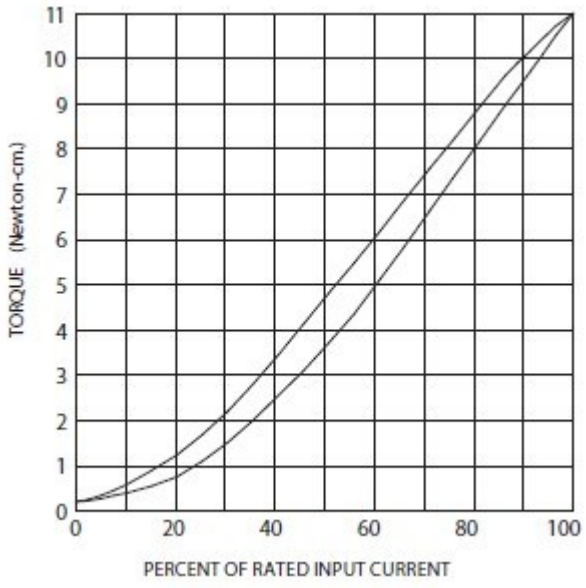

Figure 25 - Input current vs applied torque curves provided by Placid Industries

To estimate the uncertainty in the dependent variable, the steepest slope of the fit line was used. Taking the slope between 59 and 86 percent of rated input current gives:

$$m = \frac{y_2 - y_1}{x_2 - x_1} = \frac{9 - 4.85}{86 - 59} = 0.154 \qquad \textit{Eq. 6.2}$$

Meaning the uncertainty in torque is:

$$\sigma_y = \sigma_x(0.154) \qquad \textit{Eq. 6.3}$$

For the maximum uncertainty in torque measurement, at 100% of rated input current, this is:

$$\sigma_T = (0.00625\ A)\left(0.154\frac{N \cdot cm}{A}\right) = 0.0009625\ N \cdot cm \qquad \textit{Eq. 6.4}$$

When considering the range of current recorded in this experiment, the maximum uncertainty in torque is approximately 0.32% of the measured value.

6.2.3 Uncertainty in Power Value

For a function, $f = AB$, the uncertainty (variance) in the function is [26]:

$$\sigma_f{}^2 = f^2\left[\left(\frac{\sigma_A}{A}\right)^2 + \left(\frac{\sigma_B}{B}\right)^2 + \frac{2\sigma_A\sigma_B}{AB}\right] \qquad \textit{Eq. 6.5}$$

For uncorrelated terms, $\sigma_{AB} = 0$, and the equation can be reduced to:

$$\sigma_f{}^2 = f^2\left[\left(\frac{\sigma_A}{A}\right)^2 + \left(\frac{\sigma_B}{B}\right)^2\right] \qquad \textit{Eq. 6.6}$$

Using this, it is possible to determine the uncertainty in the calculated power value:

$$Power = 2\pi\left(\frac{n_{rpm}}{60}\right)\mathrm{T} \qquad \textit{Eq. 6.7}$$

Where:

$$\left(\frac{n_{rpm}}{60}\right) = \omega \qquad \textit{Eq. 6.8}$$

The uncertainty (variance) in the power function becomes:

$${\sigma_P}^2 = P^2\left[\left(\frac{\sigma_\omega}{\omega}\right)^2 + \left(\frac{\sigma_T}{T}\right)^2\right] \qquad \textit{Eq. 6.9}$$

For values of power calculated in this study, the maximum uncertainty in calculated power is 8.24%. Maximum uncertainty decreased with increasing wind speed and was overall lower for the smaller blade turbine.

In general, the calculated uncertainties in the measured values are fairly small compared to the measured levels and do not affect the conclusions arising from the data analysis.

7 Comparison Between Numerical Predictions and Experimental Measurements.

7.1 Comparison of CFD Results to Wind Tunnel Results

Comparing the summary results from the wind tunnel validation testing in Figure 27 to the CFD simulation results in Figure 26, as well as a sample direct comparison for a flow speed of approximately 4.0 m/s in Figure 28, that the peak power for wind tunnel tests measured higher for each flow speed than was predicted by the simulations.

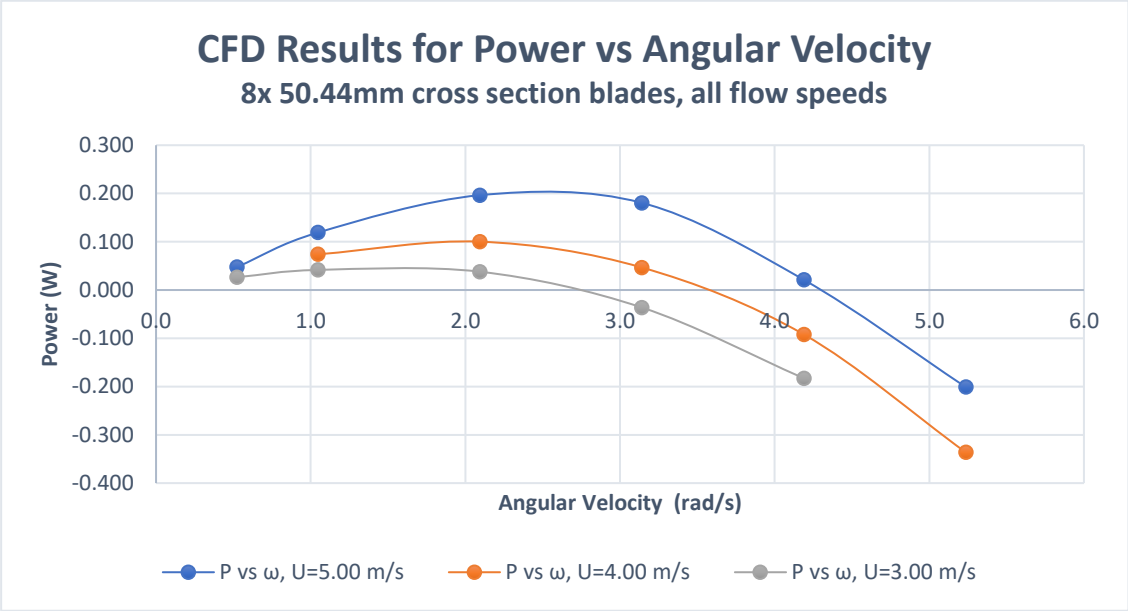

Figure 26 - CFD results showing power plotted against rotor angular velocity

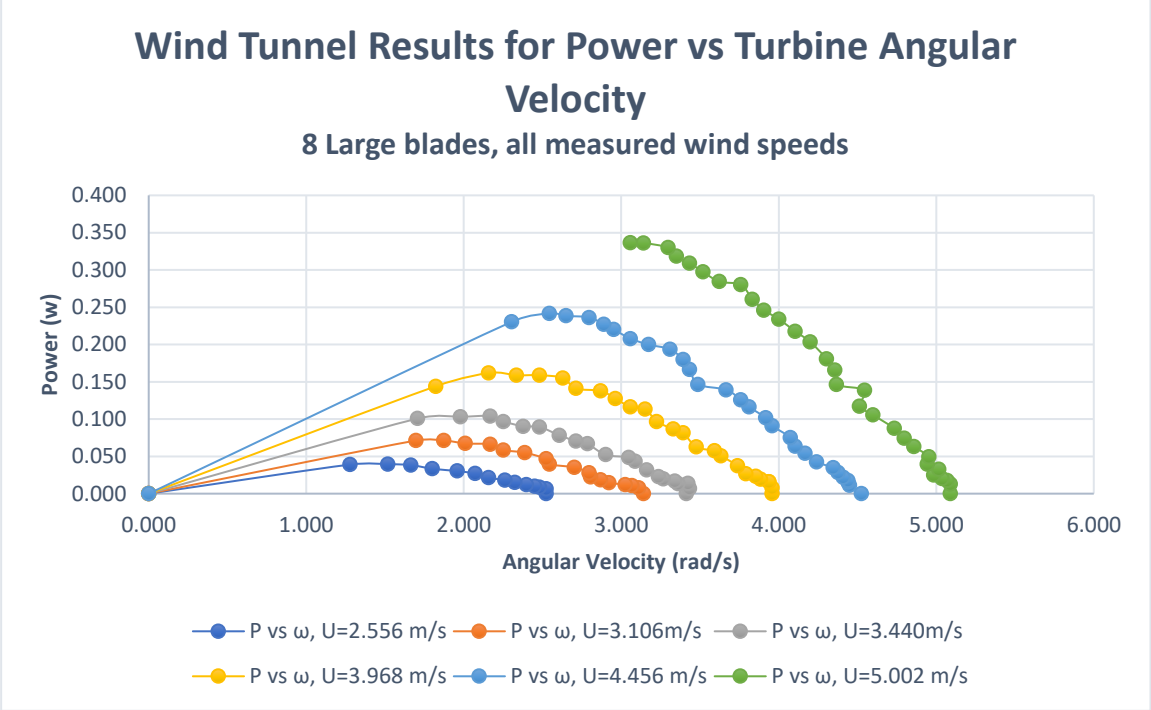

Figure 27 - Wind tunnel test results showing power plotted against rotor angular velocity.

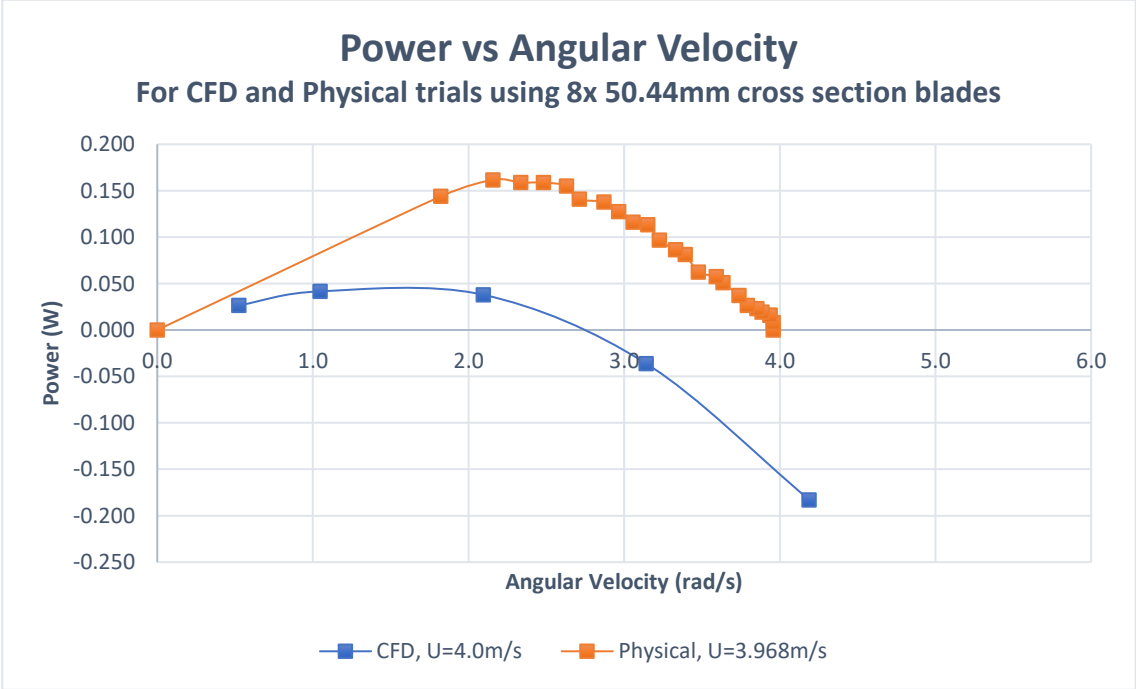

Figure 28 - Comparison of CFD and wind tunnel trials Power vs Angular Velocity curves for U of approximately 4m/s.

Though peak power results for the simulations and the wind tunnel trials do not exactly agree in magnitude, at roughly equivalent flow speeds both the simulation and the validation experiment measured similar angular velocities for peak power points. For example: at a flow speed of 4.0 m/s, the CFD simulation predicted a peak power point at an angular velocity of 2.094 rad/s. The wind tunnel result at the nearest comparable flow speed of 3.968 m/s measured peak power at 2.157 rad/s. Similarly, CFD predicts that the angular velocity at which peak power is generated increases as flow speed increases. The wind tunnel trials validate this result.

Another validating point of the CFD simulations is provided in the agreement of peak values of the $C_P \; vs \; C_s$ curves for both experiments. For both sets of data, the C_s value at which peak C_P occurs is constant, as well as close in magnitude. For example: as shown in Figure 29, at a flow speed of 4.0 m/s, CFD simulation predicted a peak C_P value at a C_s value of 0.2089. As shown in Figure 30, at a comparable flow speed of 3.968 m/s, the wind tunnel experiment measured a peak C_P at a C_s value of 0.2012. The superimposed curves for the CFD and wind tunnel trials are shown in Figure 31.

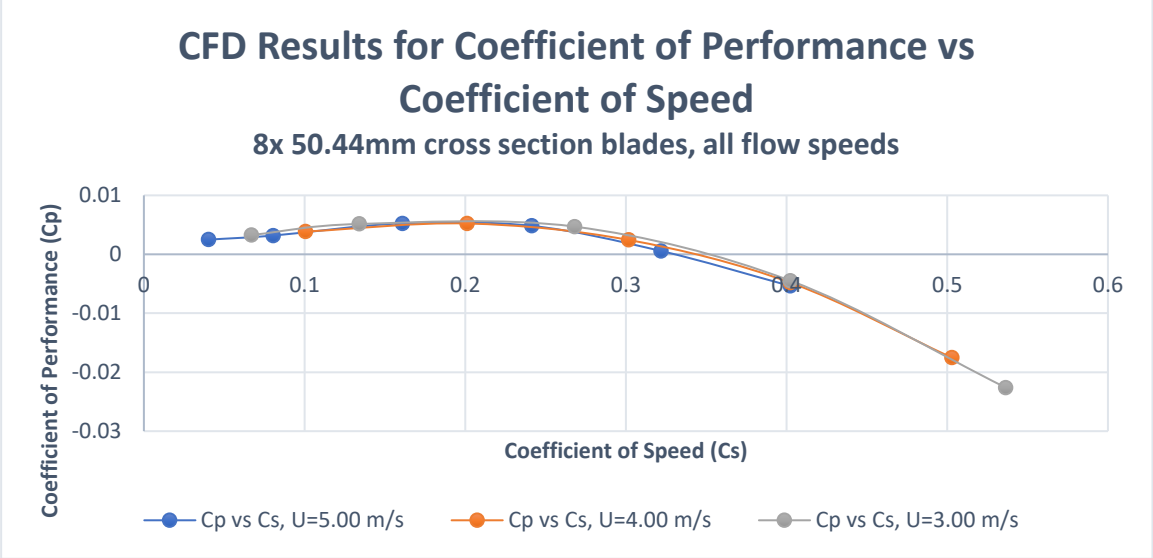

Figure 29 - CFD results showing the coefficient of performance plotted against the coefficient of power for a turbine with eight 50.44mm cross section blades.

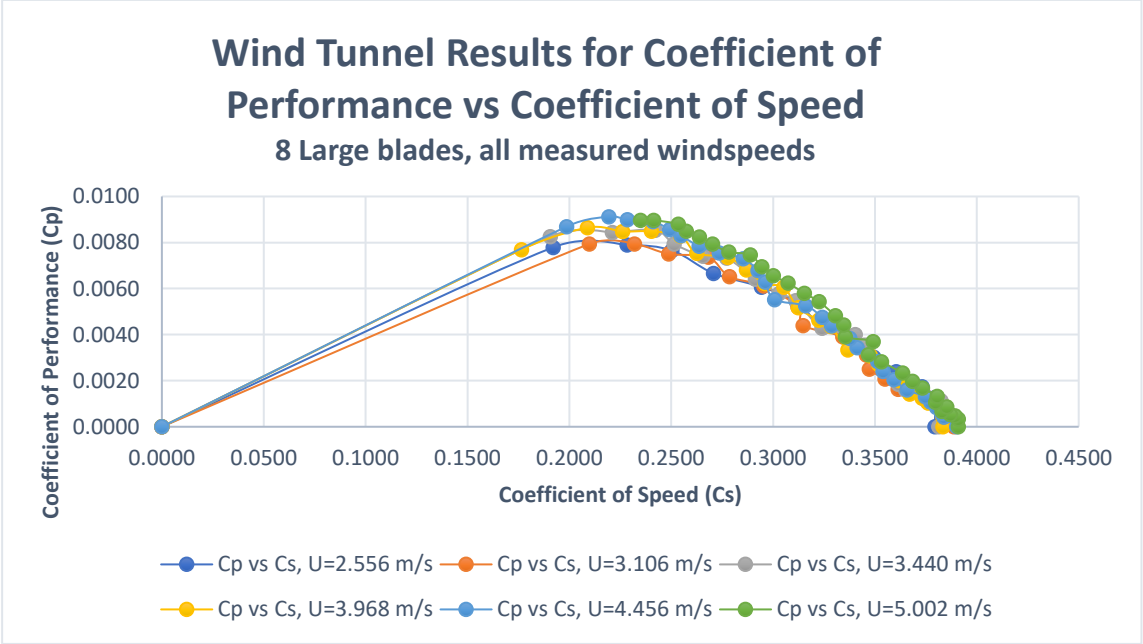

Figure 30 - Wind tunnel test results showing the coefficient of performance plotted against the coefficient of power for a turbine with eight 50.44mm cross section blades.

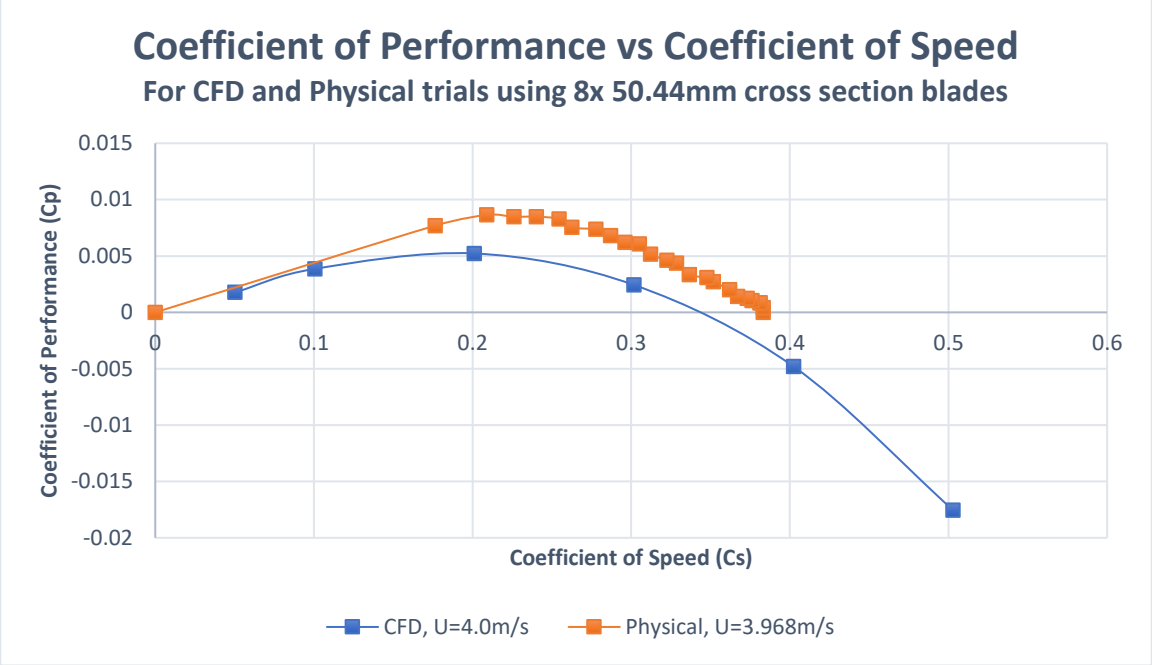

Figure 31 - Comparison of CFD and wind tunnel trial Cp and Cs curves for U of approximately 4m/s.

There could be several reasons for the difference in magnitude between the CFD and physical experiment results. Firstly, the resolution of the CFD trials was limited by software and available computational power. With reference to Figure 32, Figure 33, and Figure 34, the minimum reasonable number of inflation layers were used around the blade surfaces, and a limited number of cells were used in the flow volume surrounding the rotor blade and immediately downstream.

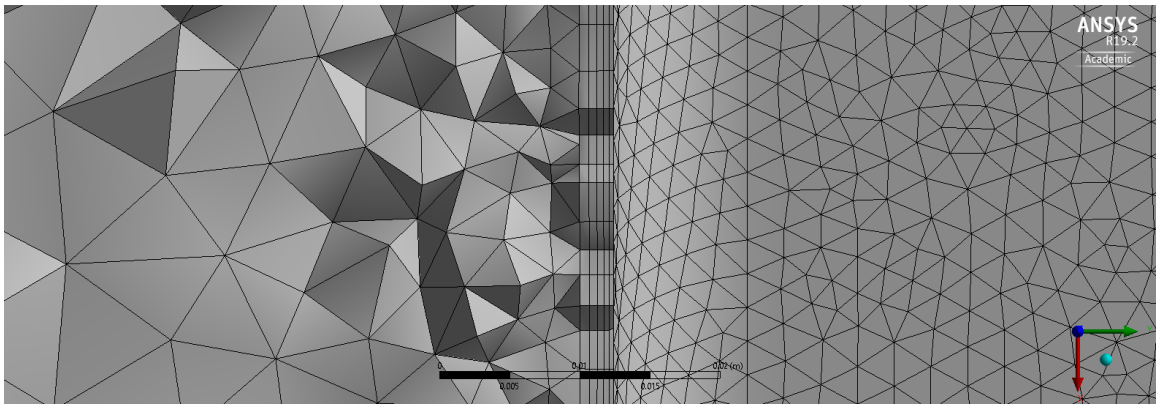

Figure 32 - Detail of inflation layers around rotor blade surface.

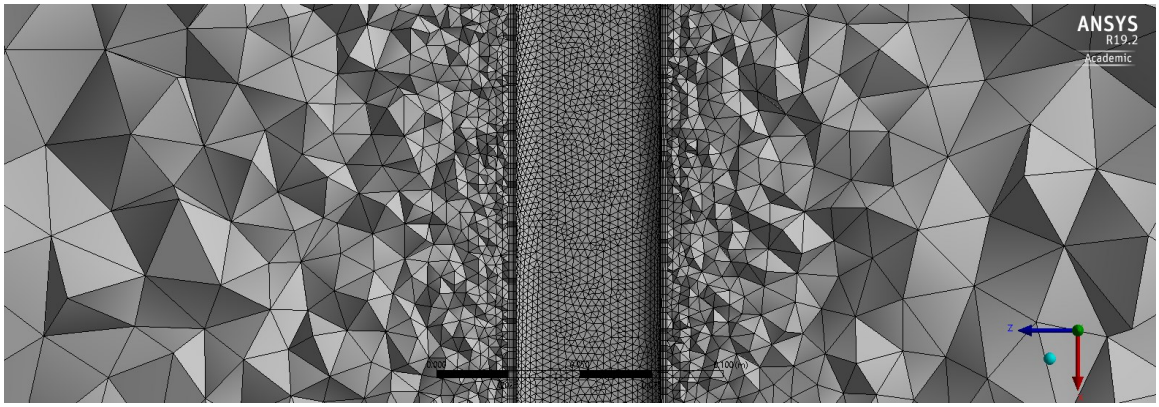

Figure 33 - Detail of mesh resolution surrounding rotor blade surfaces.

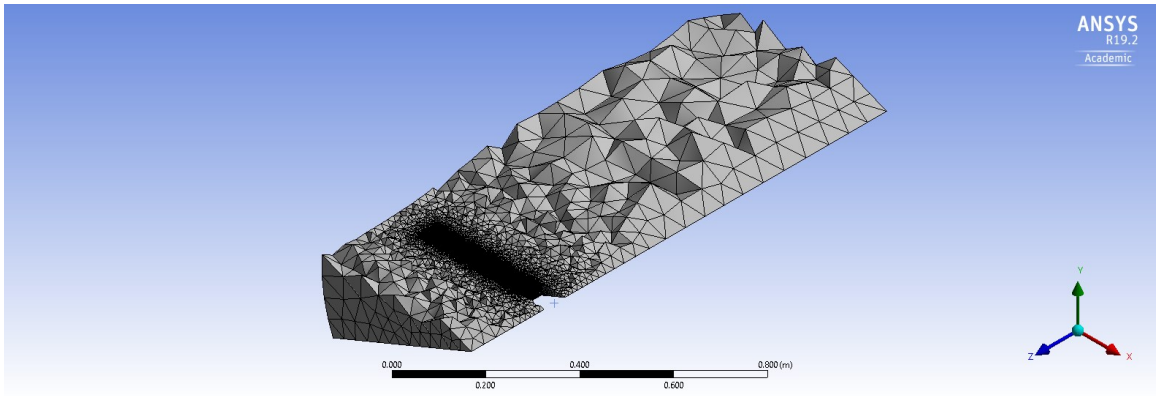

Figure 34 - Detail of mesh resolution immediately downstream of the rotor.

It is possible that the flow region containing the most complex turbulent interactions has inadequate resolution to compute the outcome with a level of accuracy approaching the physical trials. If computational power and software allowed, a greater number of inflation layers could be used surrounding the blades, and the mesh resolution in the flow region surrounding the blade and immediately downstream could be increased. This may allow the simulation to better capture the complex turbulent interactions with the blade surfaces, and where the vortices attach to the turbine blades, possibly allowing the CFD solution to converge to the physical data. Ideally, with no limitation on mesh elements and with access to adequate computational power, a full mesh convergence study could be carried out to determine if the mesh of the CFD simulation is capturing the full details of the model. This would provide some indication as to whether it is the simulation setup is not detailed enough to provide an accurate result, or if the solver and turbulence model chosen are incapable of providing an accurate result when compared with physical data.

Another factor that may have affected the accuracy of the CFD output is using rotational symmetry in a rotating flow simulation. Due to the software limitation on cell elements, the one-eighth rotor model was used to maximize the resolution around a single representative blade, with rotational symmetry implemented to provide an overall result. This setup decision may have affected the overall power estimate determined by the simulation, as the wake interactions of trailing rotor blades might not accurately be captured by the symmetry model. Again, access to an unlimited software license along with adequate computing power could allow comparison of the one-eighth model turbine simulation results to those of a one-quarter or full turbine simulation.

A third factor that may have played a role in the difference in CFD versus wind tunnel results is the semi-bounded nature of the wind tunnel experiment. Even though the sides of the wind tunnel were open to prevent the buildup of pressure upstream of the turbine, when considering the size of the turbine and the size of the tunnel, the bounding wall top and bottom of the tunnel may have had some effect on the results by forcing air that would flow around a turbine in a fully open flow through the turbine instead.

Finally, it is possible that the selection of solver, combined with the chosen turbulence model is inadequate for accurately solving this problem in which the simulation is predominantly turbulent flow, and in a rotating frame.

8 Conclusions

With reference to the stated objectives of this study, the proposed novel vortex-driven turbine was studied in two configurations, both theoretically through computational fluid dynamics, and experimentally in wind tunnel tests. Both investigations indicate the turbine format has low power output and beak efficiency of less than 1%, meaning that this particular turbine configuration is neither an efficient nor practical method of harnessing wind energy when compared to other turbines of similar complexity.

Thus, although the bluff body turbine does generate a certain level of torque, and will induce a level of rotation, the magnitude of the output renders it an impractical device. A further possible limitation is that the direction of the rotation is arbitrary in the simple symmetrical configuration studied here. Thus, it is difficult to recommend any further study or development of this technology.

Regarding the second aim of the study, the overall results indicate that while the CFD simulations provided an approximately correlated C_P vs C_S curve shape and prediction of flow speed for peak power, the computational model returned values for generated power that were considerably lower than what was measured during the wind tunnel trials.

While it is evident that the CFD results do not fully agree with the results of the wind tunnel tests in this set of experiments, there is a general agreement in the data trends, indicating that the CFD models are providing a reasonable simulation for flows that are dominated by vorticity effects. This study was somewhat resource limited, and some further investigation would be required to verify which, if any, of the previously

identified possibilities for observed differences had a significant effect on outcomes. Some strategies for further investigation are highlighted in the section following.

8.1 Future Work

The results of this research provide information on the behaviour of rotating square cross-section turbine blades in flow. This information does not really support further development of the concept as a practical energy generating device. However, as a theoretical study of vortex modelling, the experiment does identify areas where future work could provide additional information on the modelling of vortex flows. Some areas that have been identified for future study are:

- The effect of blade and turbine configuration on vortex characteristics in comparison with CFD models. While the study examined two different turbine blade configurations, an expanded study could set more variables such as: blade length, width, thickness, spacing, asymmetry, and corner radius to determine primary effects on results, or interactions between blade characteristics though the use of surface response methods in experiments. Physical models of turbines might be rapidly iterated using AM (additive manufacturing) methods. Model size could be limited to minimize possibility of flow interaction with walls of wind tunnel, and data from this set of experiment could be used to specify a magnetic particle brake that would work for a larger range of flow speeds.
- Further refinement of the mesh and model. Due to the computational power and license available for this study, the mesh resolution and time-step increments were

limited. Use of an unrestricted license, as well as a workstation built for simulation would allow the completion of a full mesh convergence study, and likely provide additional accuracy in results. Alternatively, use of an open-source CFD package such as OpenFOAM could provide the additional detail desired.

8.2 Final Remarks

With both CFD and physical experiment in this study indicating a turbine peak efficiency of less than 1%, the particular configurations of the turbine studied do not make good candidates for commercial power generation. However, the findings could have implications in the design of spoked rotational devices operating in fluids, particularly those with bluff-bodied spokes. Additionally, this study serves as a good baseline for a fully designed study on vortex-driven horizontal-axis turbines, and the factors affecting their performance.

References

[1] N. Khan, "Modelling, Design and Control of A Small Marine Current Energy Conversion System," St. John's.

[2] A. Aquino, J. Calautit and B. Hughes, "A Study on the Wind-Induced Flutter Energy Harvester (WIFEH) Integration into Buildings," *Energy Procedia,* vol. 142, pp. 321-327, 2017.

[3] S. Olivieri, G. Boccalero, A. Mazzino and C. Boragno, "FLuttering Energy Harvester for Autonomous Powering (FLEHAP): aeroelastic characterisation and preliminary performance evaluation," *Procedia Engineering,* vol. 199, pp. 3474-3479, 2017.

[4] J. Park, G. Morgenthal, K. Kim, S.-D. Kwon and K. Law, "Power evaluation of flutter-based electromagnetic energy harvesters using computational fluid dynamics simulations," *Journal of Intelligent Material Systems and Structures,* vol. 25, no. 14, pp. 1800-1812, 2014.

[5] A. Abdelkefi, Z. Yan and M. Hajj, "Power Generation from Galloping-based Piezoaeroelastic Energy Harvesters for Different Cross-Section Geometries," in *54th AIAA/ASME/ASCE/AHS/ASC Structures, Structural Dynamics, and Materials Conference*, 2013.

[6] G. Hu, J. Wang, H. Qiao, L. Zhao, Z. Li and L. Tang, "An experimental study of a two-degree-of-freedom galloping energy harvester," *International Journal of Energy Research,* 2020.

[7] A. Venukumar, "Artificial Vortex (ArVo) power generation — An innovative micro hydroelectric power generation scheme," in *2013 IEEE Global Humanitarian Technology Conference: South Asia Satellite*, 2013.

[8] C. M. Asre, V. K. Kurkute and N. J. Kanu, "Power generation with the application of vortex wind turbine," in *Materials Today: Proceedings*, 2021.

[9] H. M. Lee and O. J. Kwan, "Numerical Simulation of Horizontal Axis Wind Turbines with Vortex Generators," *Int. J. Aeronaut. Space Sci.,* vol. 20, p. 325–334, 2019.

[10] N. M. Bychkov, A. Dovgal and K. V. V, "Magnus wind turbines as an alternative to the blade ones," *Journal of Physics: Conference Series,* no. 012004, 2007.

[11] A. Sedaghat, "Magnus type wind turbines: Prospectus and challenges in design and modelling," *Renewable Energy,* vol. 62, pp. 619-628, 2014.

[12] W. Hemsuwan, K. Sakamoto, S. Nakada and T. Takahashi, "A longitudinal vortex wind turbine: Numerical Study," *Journal of Wind Engineering & Industrial Aerodynamics,* vol. 180, pp. 213-230, 2018.

[13] N. Murakami, J. Akita and J. Ito, "Magnus type wind power generator". US Patent 0038915:A1, 2010.

[14] T. Takahashi, Y. Yoshitake, K. Sakamoto and W. Hemsuwan, "An Innovative Wind/Water Turbine with Circular Cylinder Propeller Driven by Longitudinal Vortex," in *Proceeding of 15th World Wind Energy Conference and Exhibition*, Tokyo, 2016.

[15] W. Hemsuwan, K. Sakamoto and T. Takahashi, "Numerical investigation of lift-force generation on a moving circular cylinder in a uniform flow driven by longitudinal vortex," *Journal of Fluids and Structures,* vol. 83, pp. 448-470, 2018.

[16] M. C. Potter, D. C. Wiggert and B. H. Ramadan, Mechanics of Fluids 4th Edition, SI, Nelson Education, 2016.

[17] D. Zhao, N. Han, E. Goh, J. Cater and A. Reinecke, "Chapter 1 - General Introduction To Wind Turbines," in *Wind Turbines and Aerodynamics Energy Harvesters*, Academic Press, 2019, pp. 1-20.

[18] G. A. van Kuik, "The Lanchester–Betz–Joukowsky limit," *Wind Energy,* vol. 10, no. 3, pp. 289-291, 2007.

[19] A. N. Gorban, A. M. Gorlov and M. V. Silantyev, "Limits of the Turbine Efficiency for Free Fluid Flow," *Journal of Energy Resources Technology,* vol. 123, no. 4, pp. 311-317, 2001.

[20] F. R. Menter, "Two-Equation Eddy-Viscosity Turbulence Models for Engineering Applications," *AIAA Journal,* vol. 32, no. 8, pp. 1598-1605, 1994.

[21] ANSYS, "Fluent Theory Guide (19.2)," ANSYS, 2018.

[22] S. Lachance-Barret, E. Corona, S. Harvey, G. Wu and R. Bhaskaran, "A Hands-on Introduction to Engineering Simulations," Cornell University, 2018. [Online]. Available: https://courses.edx.org/courses/course-v1:CornellX+ENGR2000X+1T2018/course/. [Accessed January 2019].

[23] ANSYS, "Fluent User's Guide (19.2)," ANSYS, 2018.

[24] "CFD-Online," 06 03 2020. [Online]. Available: https://www.cfd-online.com/Forums/fluent/184470-simple-question-simple-vs-coupled-solver.html. [Accessed 24 01 2021].

[25] R. Courant, K. Friedrichs and H. Lewy, "On the partial difference equations of mathematical physics (c. 1928)," *IBM Journal of Research and Development,* pp. 215-234, 1967.

[26] R. S. Figliola and D. E. Beasley, Theory and Design for Mechanical Measurements, Hoboken: Wiley, 2014.

[27] ANSYS, "Meshing User's Guide (19.2)," 2018.

[28] Cornell University, "Sim Cafe," 18 12 2018. [Online]. Available: https://confluence.cornell.edu/pages/viewpage.action?pageId=262013005. [Accessed 02 10 2018].

[29] J. Dudley, "Selecting a Target Transient Time Step in a CFD Analysis," CAE Associates, 27 March 2015. [Online]. Available: https://caeai.com/blog/selecting-target-transient-time-step-cfd-analysis. [Accessed 07 May 2019].

[30] M. C. Potter, D. C. Wiggert and B. H. Ramadan, Mechanics of Fluids, Nelson Education, 2016.

Appendix A – CFD Mesh Details and Model Validation

A1. Mesh Overview

ANSYS Meshing was used to performing meshing for the CFD simulations. Initially the flow domain was automeshed to give an overall indication of the meshing requirements for the simulation. After examining the automatically-generated mesh, both global and local controls were put in place to refine the mesh in critical areas, as well as increase the overall combined number of mesh elements from 189,195 to 499,546 elements, near the resolution limit of 512,000 cells and nodes combined.

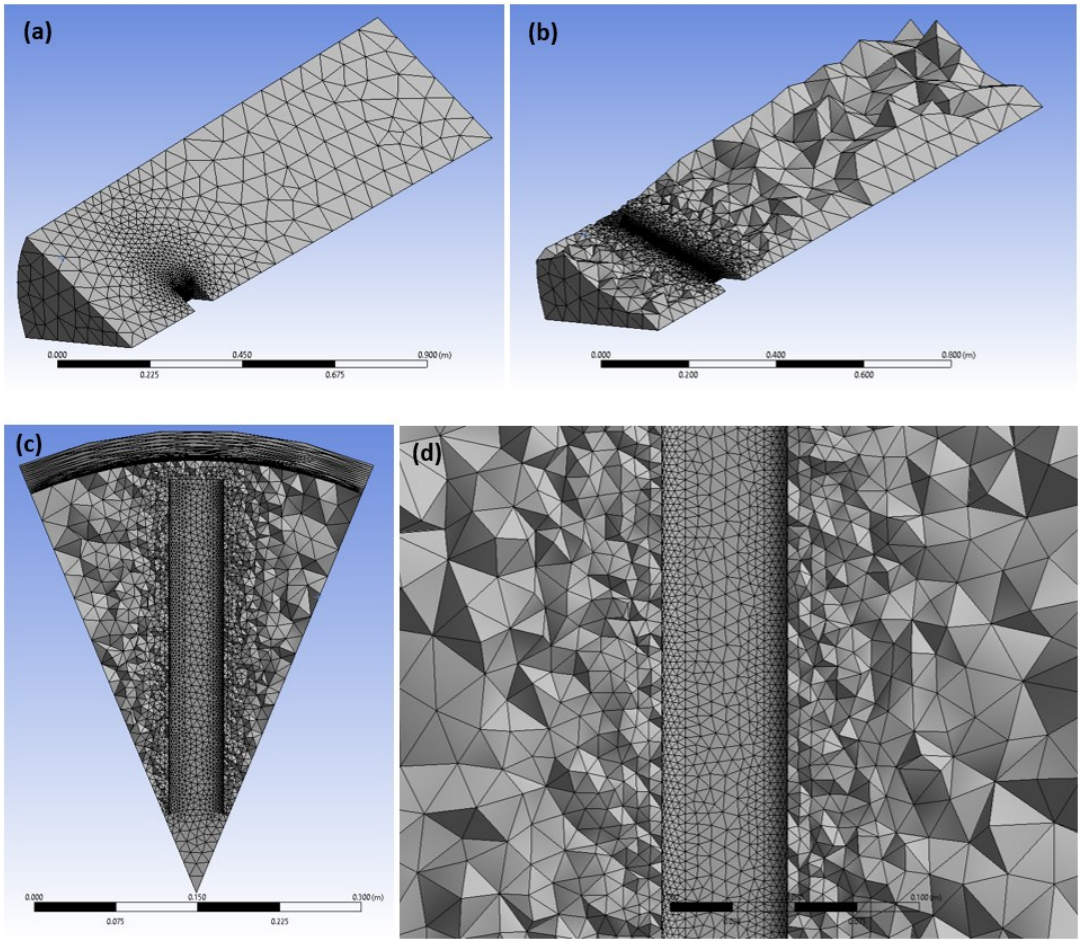

Figure 35 - Views of mesh for 50.5mm cross-section blades with default auto-mesh: (a) overall domain, (b) lateral section view, (c) radial section view, (d) detail of blade surface. Note the absence of inflation layers in view (d).

Global mesh physics preference was set to CFD, with Fluent as the solver. This optimizes the generated cells for the fluent solving package. Smoothing was set to high to improve mesh quality.

Several local mesh controls were defined, the first being a match control between the periodic faces of the fluid domain. This symmetrically aligns the nodes and cells on the periodic faces, allowing the interpolation of the 1/8 turbine result to a full turbine.

Following the periodic interfaces, a surface sizing control was applied to the blade. This allowed for manual refinement of cells around the blade, increasing the resolution of the mesh in the area expected to have the most complicated flow. For the 50.5 mm blade cross section, the element size value was set to 0.0024 mm, and behaviour was set to "hard", meaning each face element had a maximum size of 0.0024 mm.

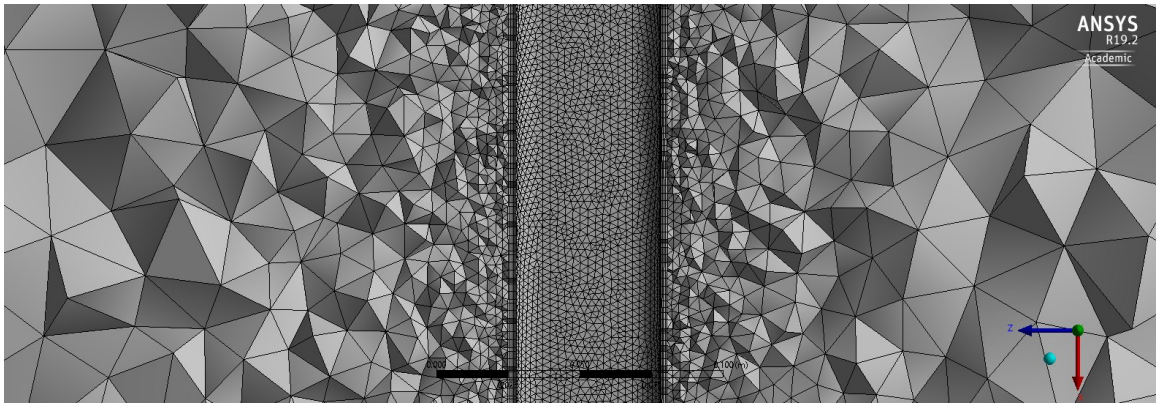

Figure 36 – Section detail of mesh on face of blade after meshing surface control is applied.

Finally, after the surface sizing control, inflation layers were added to the mesh surrounding the blade. These layers are formed of prism-shaped cells and are helpful in capturing the complex boundary layer behaviour in external flows while connecting the

blade surface mesh to the larger cells in the flow field [22]. Inflation layers were unchanged from the default value of five, with an expansion rate of 1.2. Inflation algorithm was left at default "pre" to use the TGrid algorithm for creating the inflation layers before the tetrahedral volume is filled, preventing the applied match control from being overwritten with the "post" ICEM algorithm [23].

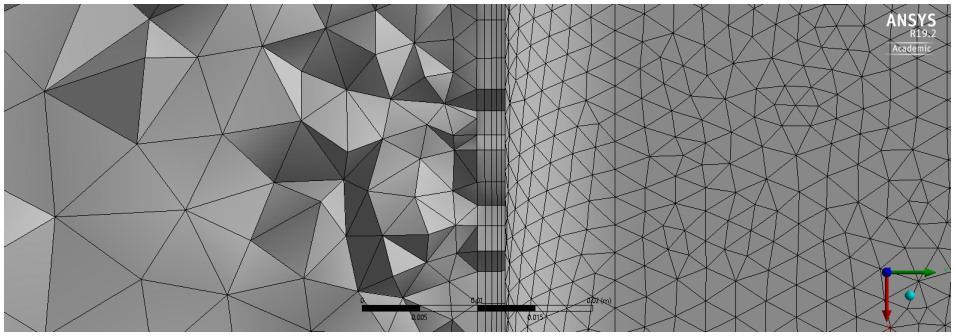

Figure 37 - Detail of boundary layer meshing for 50.5mm cross section blades

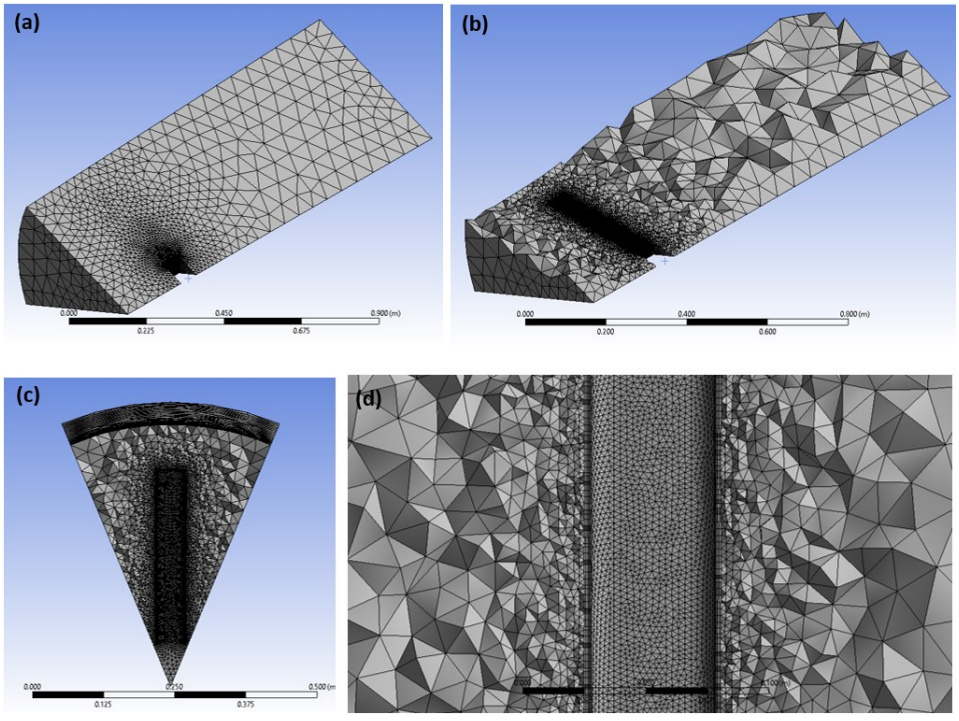

Figure 38 - Views of mesh for 50.44mm cross-section blades after mesh controls applied: (a) overall domain, (b) lateral section view, (c) radial section view, (d) detail of blade surface.

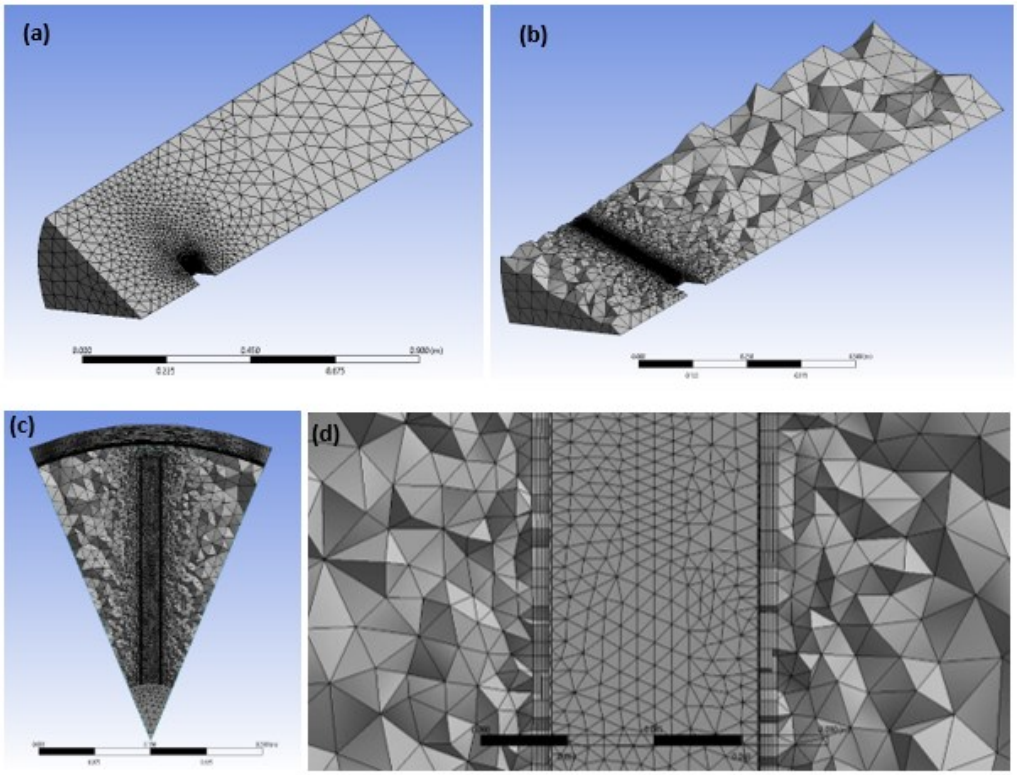

Figure 39 - Views of mesh for 25.28mm cross-section blades after mesh controls applied: (a) overall domain, (b) lateral section view, (c) radial section view, (d) detail of blade surface.

A2. Mesh Quality

Several metrics define mesh quality, with skewness and orthogonal quality being two of the important values used to determine if a mesh is adequate.

Skewness values indicate how close an element or face is to the ideal, equilateral, version of that shape. Skewness values range from 0 to 1, with 0 being the best (equilateral), and 1 being the worst (degenerate) [27].

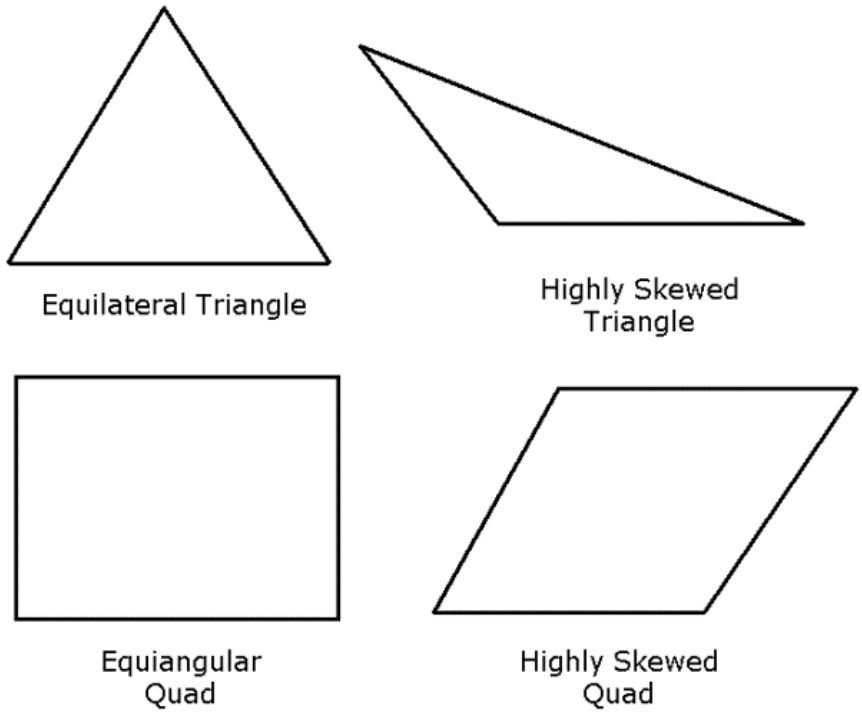

Figure 40 - Graphical examples of skewness in two-dimensional elements, with ideal elements shown on the left [27].

Table 4 - Skewness value ranges with corresponding cell quality [22].

Skewness Value	Cell Quality
0 to 0.25	Outstanding
0.25 to 0.50	Very Good
0.50 to 0.80	Good
0.80 to 0.95	Sufficient
0.95 to 0.98	Bad
0.98 to 1.00	Inappropriate

Orthogonal quality for three dimensional cells also ranges from 0 to 1, but for this metric 0 is the worst, and 1 is the best quality cell. Orthogonal quality is computed using face normal vectors for each face, vectors from the cell centroid to each of the faces, and vectors from the cell centroid to the centroids of each adjacent cell. For each of the cell faces, cosines of the angles between the vectors are computed, and the smallest value is the orthogonality of the cell. For tetrahedral and pyramid cells, the orthogonal quality is lesser of the orthogonality and (1 - cell skewness). For hexahedral and polyhedral cells, it is equal to the orthogonality. Note that orthogonal quality in the ANSYS Meshing application is equivalent to inverse orthogonal quality in ANSYS Fluent meshing, but with reversed scales [27].

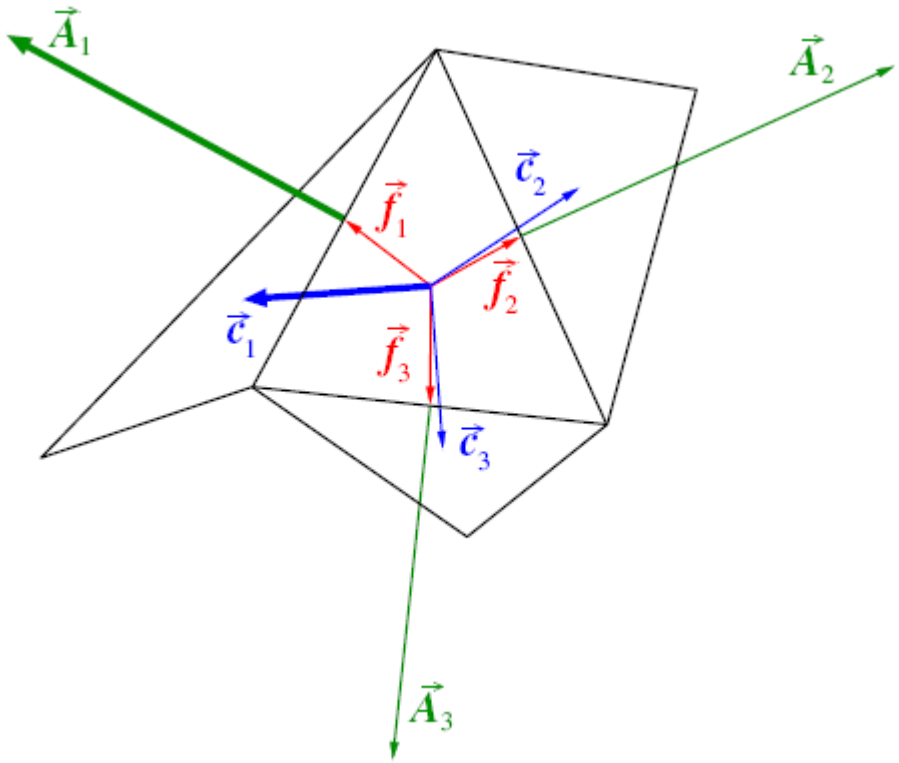

Figure 41 - Vectors used to compute orthogonal quality: $\vec{A_i}$, the face normal vector; $\vec{c_i}$, the vector from cell centroid to adjacent cell centroid; and $\vec{f_i}$, the vector from cell centroid to each face [27].

Table 5 - Orthogonal value ranges with corresponding cell quality [22].

Cell Quality Acceptability as Determined by Orthogonal Quality Value	
Orthogonal Quality Value	**Cell Quality**
0.95 to 1	Outstanding
0.70 to 0.95	Very Good
0.20 to 0.70	Good
0.15 to 0.20	Sufficient
0.001 to 0.15	Bad
0 to 0.001	Inappropriate

A4. Quality of Mesh for 50.44 mm Cross-Section Blade Simulation

From the mesh statistics for cell skewness, as reported by ANSYS Meshing, indicate that overall, the mesh is of quite good quality, with the average cell skewness value falling into the "Outstanding" quality bracket. The maximum cell skewness still falls within the "Sufficient" quality bracket, meaning there are no mesh cell elements considered to be of "Bad" or "Inappropriate" quality. From the standard deviation and distribution plot, it is evident that the vast majority of cells have skewness of 0.50 or lower, categorizing them as "Very Good" quality.

Table 6 - Cell skewness values for 50.44mm blade simulation mesh.

Reported Statistics for Cell Skewness, 50.44mm Cross-section Blade Mesh	
Statistic	**Value**
Minimum	0.000027179
Maximum	0.84174
Average	0.2212
Standard Deviation	0.11964

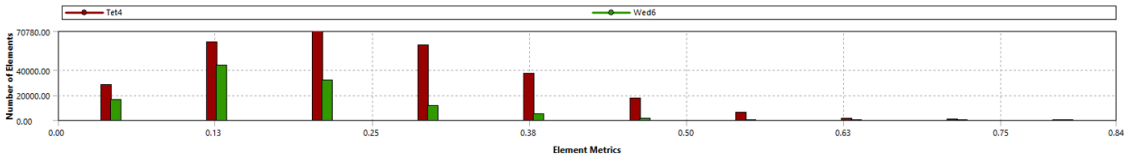

Figure 42 - Image of skewness distribution plot for 50.44mm cross-section blade mesh.

Examining the mesh statistics for cell orthogonal quality, it is again evident that according to this metric, the mesh is of quite good quality overall. The maximum cell orthogonal quality value falls within the "Outstanding" quality bracket, and the average

cell orthogonal quality falls in the “Very Good” cell quality bracket. From the standard deviation and distribution plot, it is apparent that nearly all cells have orthogonal quality of 0.50 or better, meaning they are considered to be of anywhere from “Good” to “Outstanding” quality.

Table 7 - Cell orthogonal quality for 50.44 mm blade simulation mesh.

Reported Statistics for Cell Orthogonal Quality, 50.44mm Cross-section Blade Mesh	
Statistic	**Value**
Minimum	0.15826
Maximum	0.99637
Average	0.7777
Standard Deviation	0.11828

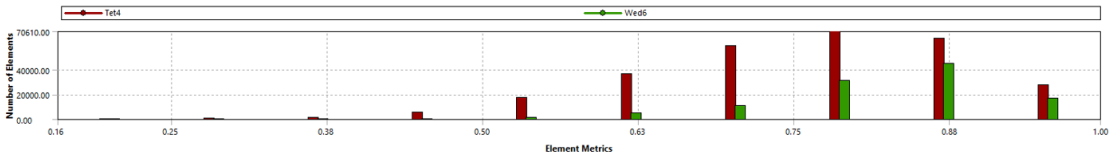

Figure 43 - Image of orthogonal quality distribution plot for 50.44mm cross-section blade mesh.

Taking both cell quality metrics into account, it is evident that the overall mesh can be considered of good to very good quality, and should not adversely affect calculation stability, or ability for solution equations to converge.

A4. Quality of Mesh for 25.28 mm Cross-Section Blade Simulation

For the 25.28mm blade simulation mesh, the average cell skewness value falls in the "Very Good" and as with the mesh for the 50.44mm blade simulation, the majority of cells have a skewness value of less than 0.50, meaning they are of "Very Good" to "Outstanding" quality.

Table 8 - Cell skewness for 25.28mm blade simulation mesh.

Reported Statistics for Cell Skewness, 25.28mm Cross-section Blade Mesh	
Statistic	**Value**
Minimum	0.00030564
Maximum	0.94858
Average	0.26396
Standard Deviation	0.14964

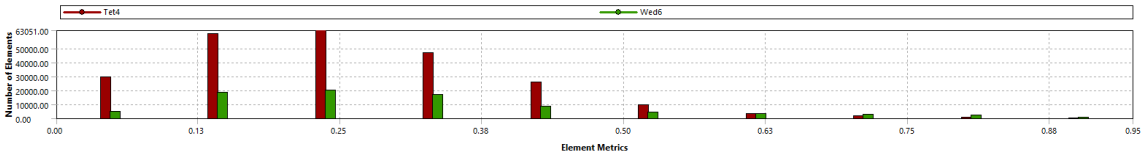

Figure 44- Image of skewness distribution plot for 25.28mm cross-section blade mesh.

The cell orthogonal quality for the 25.28mm blade simulation mesh indicate that the majority of cells have an orthogonal quality value of over 0.55 and fall within the "Good" to "Outstanding" quality range. Additionally, over 70% (by volume) of the mesh is of "Very Good" to "Outstanding" quality.

Table 9 - Cell orthogonal quality for 25.28 mm blade simulation mesh.

Reported Statistics for Cell Orthogonal Quality, 25.28mm Cross-section Blade Mesh	
Statistic	**Value**
Minimum	0.051416
Maximum	0.99349
Average	0.73498
Standard Deviation	0.14833

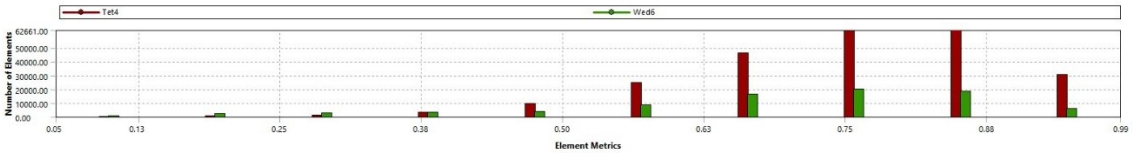

Figure 45 - - Image of orthogonal quality distribution plot for 25.28mm cross-section blade mesh.

Considering both these metrics, the overall mesh can be considered of good to very good quality, and should not adversely affect calculation stability, or ability for solution equations to converge.

A5. Mesh Convergence

Mesh convergence has been defined as occurring when a fourfold increase in the number of mesh cells does not have a significant effect on the simulation solution [22]. Since the academic license restrictions prevented increasing the cell count by a multiple of four, a 50.44mm blade simulation with flow at 4m/s, and angular velocity of ω=3.142 rad/s trial, was copied, and mesh element count was increased by 10,958 to 510,504. To accomplish this, the face sizing control was modified from having a maximum size of 0.0024m to a maximum size of 0.002365m. The results of the two simulations were then compared to determine if the small increase in mesh resolution had a noticeable effect on the results.

Table 10 - Comparison of initial and refined mesh results.

Comparison of Results from Initial and Refined Mesh CFD Trials		
Trial Details	499,546 mesh elements *Max cell face size = 2.4e^{-3}m* *U= 4.0 m/s* *ω=2.094 rad/s*	510,504 mesh elements *Max cell face size = 2.365e^{-3}m* *U= 4.0 m/s* *ω=2.094 rad/s*
Net Mass Flow Rate	1.0482305e^{-08} kg/s	5.9849908e^{-10} kg/s
Turbine Tip Velocity	7.958e^{-01}	7.957e^{-01}
Torque Generated	-0.0059794208 n-m	-0.0048933115 n-m

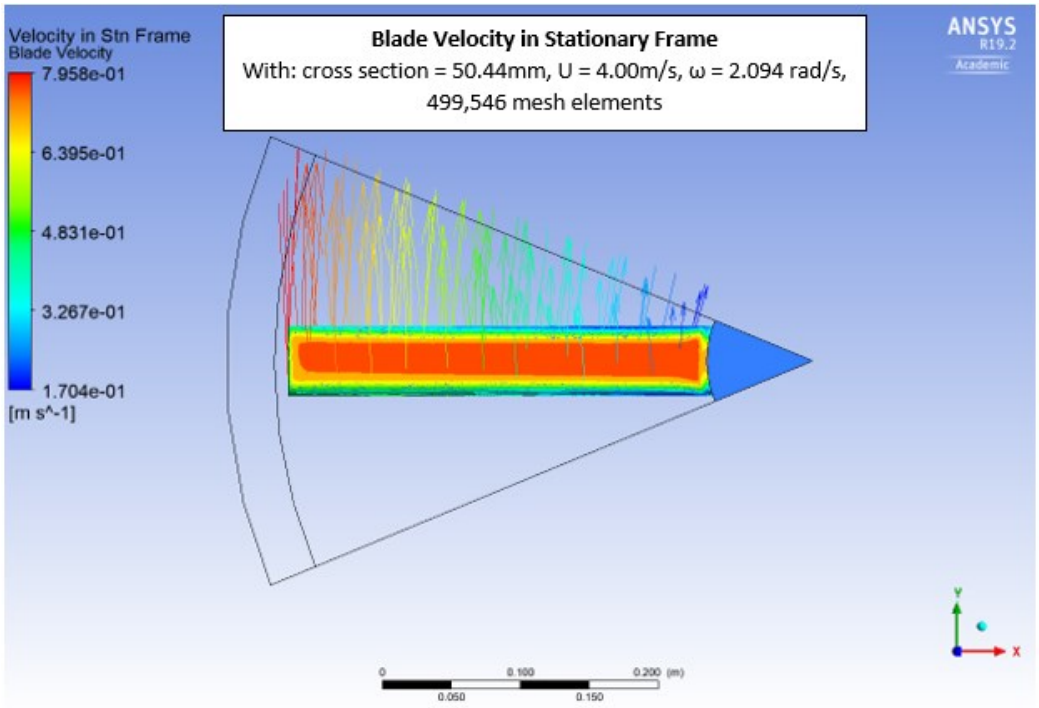

Figure 46 - Graphical results from initial mesh.

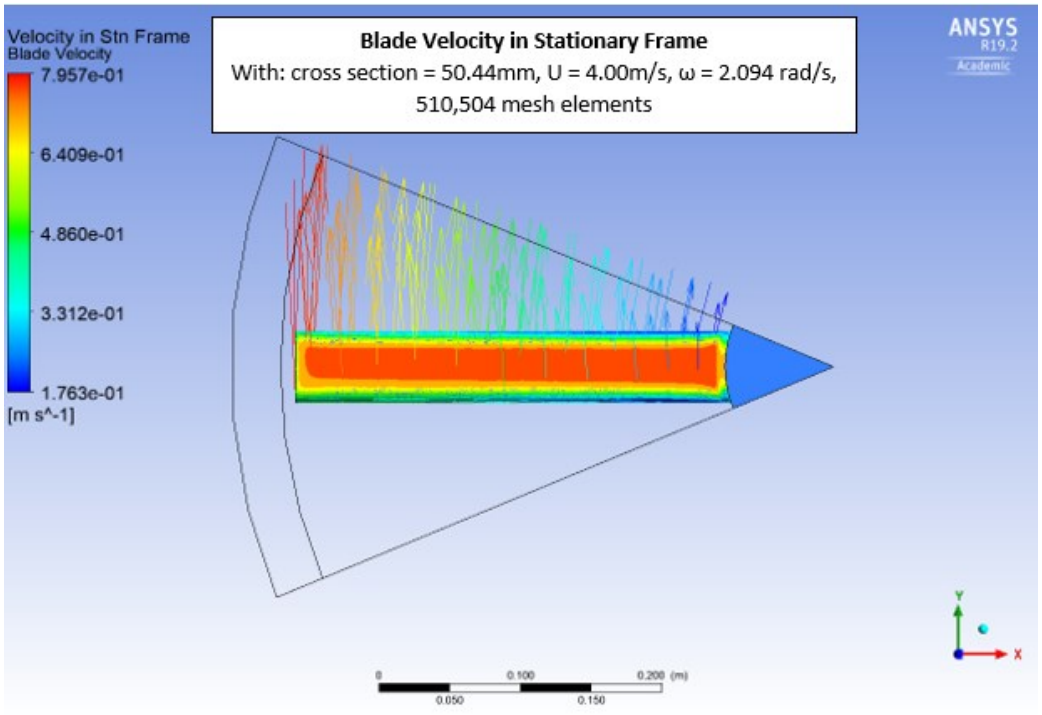

Figure 47 - Graphical results from refined mesh.

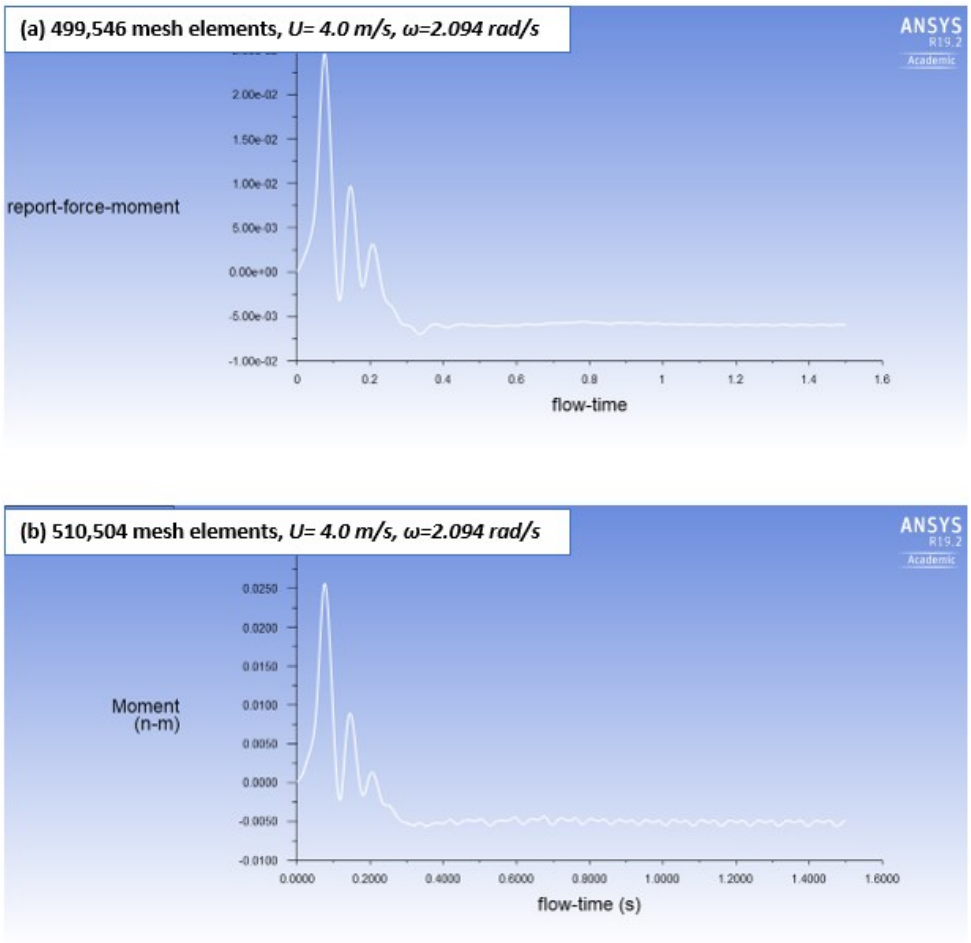

Figure 48 - Plots of 4 m/s, 3.142 rad/s CFD trials utilizing: (a) 499,546 element mesh, and (b) 510,504 element mesh.

Comparing the moment data plot from the initial 499,546 mesh element simulation with the moment data plot from a simulation with the same boundary and flow conditions, but with a slightly refined mesh (a 2% increase in elements), shows that the mesh refinement does seem to have an effect on the simulation solution. In the refined mesh simulation, the returned average moment on the turbine blade is slightly lower than that in the coarser mesh. Additionally, the solution oscillation around the average value is more prominent

in the simulation with the refined mesh, and both rotor tip velocity and mass flowrate balance are changing.

From the above factors, it can be assumed that mesh convergence has not been reached, and the simulation would likely benefit from further refinement, though it would be beneficial to use a full FLUENT license to perform another simulation with a fourfold increase in mesh elements to provide more conclusive evidence of convergence or lack thereof.

A6. Validation

A6.1 Conservation of Mass

As the first step in validating the simulations, conservation of mass was verified for each trial run in Fluent. For each trial, a flux report of the mass flow rate through the inlet, outer radial inlet, and outlet was calculated and checked for balance. The results for rotational speeds of 0.5236 rad/s to 4.189 rad/s are provided in the following tables. From the computed values, it is evident that mass is conserved through the domain of the simulation. Note the values for Inlet, Inlet-outer, and Outlet, are truncated to a length that will fit in the columns.

Table 11 - Mass flow rate balance for Rotor with Eight 50.44mm Square Blades, 5m/s windspeed.

Mass Flow Rate Balance for Rotor with Eight 50.44mm Square Blades					
Control Boundary	**Mass Flow Rate (kg/s)**				
	U= 5.0 m/s ω=0.5236 rad/s	*U= 5.0 m/s ω=1.047 rad/s*	*U= 5.0 m/s ω=2.094 rad/s*	*U= 5.0 m/s ω=3.142 rad/s*	*U= 5.0 m/s ω=4.189 rad/s*
Inlet	0.36479613	0.36479613	0.36479613	0.48621744	0.36479613
Inlet-outer	0.067863243	0.067863243	0.067863243	0.11361948	0.067863243
Outlet	-0.43265934	-0.43265939	-0.4326594	-0.59983697	-0.4326594
Net	$2.5045529e^{-08}$	$-1.9465512e^{-08}$	$-3.5445968e^{-08}$	$-5.8774095e^{-8}$	$-3.221899e^{-08}$

Table 12 - Mass flow rate balance for Rotor with Eight 50.44mm Square Blades, 4m/s windspeed.

Mass Flow Rate Balance for Rotor with Eight 50.44mm Square Blades					
Control Boundary	**Mass Flow Rate (kg/s)**				
	U= 4.0 m/s ω=0.5236 rad/s	*U= 4.0 m/s ω=1.047 rad/s*	*U= 4.0 m/s ω=2.094 rad/s*	*U= 4.0 m/s ω=3.142 rad/s*	*U= 4.0 m/s ω=4.189 rad/s*
Inlet	0.2918369	0.2918369	0.2918369	0.2918369	0.2918369
Inlet-outer	0.054290594	0.054290594	0.054290594	0.054290594	0.054290594
Outlet	-0.3461275	-0.34612749	-0.34612748	-0.34612749	-0.34612749
Net	-1.6286781e-^{09}	4.1467655e^{-09}	1.0482305e^{-08}	2.7000159e^{-09}	1.7553126e^{-09}

Table 13 - Mass flow rate balance for Rotor with Eight 50.44mm Square Blades, 3m/s windspeed.

Mass Flow Rate Balance for Rotor with Eight 50.44mm Square Blades					
Control Boundary	**Mass Flow Rate (kg/s)**				
	U= 3.0 m/s ω=0.5236 rad/s	*U= 3.0 m/s ω=1.047 rad/s*	*U= 3.0 m/s ω=2.094 rad/s*	*U= 3.0 m/s ω=3.142 rad/s*	*U= 3.0 m/s ω=4.189 rad/s*
Inlet	0.21887768	0.21887768	0.21887768	0.21887768	0.21887768
Inlet-outer	0.040717946	0.040717946	0.040717946	0.040717946	0.040717946
Outlet	-0.25959561	-0.25959556	-0.25959563	-0.25959552	-0.25959558
Net	1.5019898e^{-08}	6.0812947e^{-08}	-9.6435649e^{-09}	1.049518e^{-07}	3.6615402e-^{08}

Table 14 - Mass flow rate balance for Rotor with Eight 25.27mm Square Blades, 5m/s windspeed.

Mass Flow Rate Balance for Rotor with Eight 25.28mm Square Blades					
Control Boundary	**Mass Flow Rate (kg/s)**				
	U= 5.0 m/s ω=0.5236 rad/s	*U= 5.0 m/s ω=1.047 rad/s*	*U= 5.0 m/s ω=2.094 rad/s*	*U= 5.0 m/s ω=3.142 rad/s*	*U= 5.0 m/s ω=4.189 rad/s*
Inlet	0.36506613	0.36506613	0.36506613	0.36506613	0.36506613
Inlet-outer	0.067594095	0.067594095	0.067594095	0.067594095	0.067594095
Outlet	-0.43266023	-0.43266023	-0.43266022	-0.43266023	-0.43266023
Net	7.0895945e^{-10}	-1.6337753e^{-09}	3.5075922e^{-09}	9.1800961e^{-10}	1.2275625e^{-10}

Table 15 - Mass flow rate balance for Rotor with Eight 25.27mm Square Blades, 4m/s windspeed.

Mass Flow Rate Balance for Rotor with Eight 25.28mm Square Blades					
Control Boundary	**Mass Flow Rate (kg/s)**				
	U= 4.0 m/s ω=0.5236 rad/s	*U= 4.0 m/s ω=1.047 rad/s*	*U= 4.0 m/s ω=2.094 rad/s*	*U= 4.0 m/s ω=3.142 rad/s*	*U= 4.0 m/s ω=4.189 rad/s*
Inlet	0.29205291	0.29205291	0.29205291	0.29205291	0.29205291
Inlet-outer	0.054075276	0.054075276	0.054075276	0.054075276	0.054075276
Outlet	-0.34612817	-0.34612817	-0.34612818	-0.34612818	-0.34612818
Net	$7.7485631e^{-09}$	$7.7485631e^{-09}$	$-2.8250398e^{-09}$	$1.1859786e^{-09}$	$5.6292584e^{-09}$

Table 16 - Mass flow rate balance for Rotor with Eight 25.27mm Square Blades, 3m/s windspeed.

Mass Flow Rate Balance for Rotor with Eight 25.28mm Square Blades					
Control Boundary	**Mass Flow Rate (kg/s)**				
	U= 3.0 m/s ω=0.5236 rad/s	*U= 3.0 m/s ω=1.047 rad/s*	*U= 3.0 m/s ω=2.094 rad/s*	*U= 3.0 m/s ω=3.142 rad/s*	*U= 3.0 m/s ω=4.189 rad/s*
Inlet	0.21903968	0.21903968	0.21903968	0.21903968	0.21903968
Inlet-outer	0.040556457	0.040556457	0.040556457	0.040556457	0.040556457
Outlet	-0.25959614	-0.25959613	-0.25959614	-0.25959613	-0.25959614
Net	$-9.7432468e^{-10}$	$5.1921519e^{-09}$	$-1.9529123e^{-10}$	$4.2204925e^{-09}$	$-1.245854e^{-09}$

A6.2 Simulated Blade Velocity

The simulated blade rotation relative to the standard frame was calculated using ANSYS CFD Post. This simulated rotation should closely agree with the angular velocity set for the frame of reference motion set in the cell zone conditions (described in Section 4.2.4.2). The input values for reference frame rotation are compared to the blade rotational speed output by the simulation in Table 17.

Table 17 – Frame of reference input values vs turbine rotational velocity simulated values.

Comparison of Frame of Reference Input Angular Velocities and Simulated Blade Angular Velocities				
Blade Cross Section	Flow Speed	Frame Angular Velocity *(user input)*	Rotor Tip Speed *(calculated from user input)*	Rotor Tip Speed *(simulation output)*
50.44mm	3 m/s	0.524	0.1989	0.19915
		1.047	0.3973	0.39792
		2.094	0.7947	0.795839
		3.142	1.1924	1.19414
		4.189	1.5897	1.59206
	4 m/s	0.524	0.1989	0.198998
		1.047	0.3973	0.39792
		2.094	0.7947	0.795839
		3.142	1.1924	1.19414
		4.189	1.5897	1.59206
		5.236	1.9870	1.98998
	5 m/s	0.524	0.1989	0.198998
		1.047	0.3973	0.39792
		2.094	0.7947	0.795839
		3.142	1.1924	1.19414
		4.189	1.5897	1.59206
		5.236	1.9870	1.98998
25.28	3 m/s	0.524	0.1989	0.198786
		1.047	0.3973	0.397338
		2.094	0.7947	0.794676
		3.142	1.1924	1.19287
		4.189	1.5897	1.58973
		5.236	1.9870	1.98707
	4 m/s	0.524	0.1989	0.198707
		1.047	0.3973	0.198707*
		2.094	0.7947	0.794676
		3.142	1.1924	1.19239
		4.189	1.5897	1.58973
		5.236	1.9870	1.98707
	5 m/s	0.524	0.1989	0.198707
		1.047	0.3973	0.397338
		2.094	0.7947	0.794676
		3.142	1.1924	1.19239
		4.189	1.5897	1.58973
		5.236	1.9870	1.98707

Note: * indicates an error in the simulation identified by this validation check. The 4m/s 1.047 rad/s trial was run with a prescribed rotation of 0.524 rad/s. The data did not affect the findings of the experiment as it was far from the efficiency curve peak.

Appendix B – CFD Simulation Data

B1. Rotor with Eight 50.44mm Square Blades

CFD Data for Rotor with Eight 50.44mm Square Blades

U=3.0 m/s

	Measured Data						Calculated Data			
Run Number	U_{stream}	ω_{rotor} (RPM)	ω_{rotor} ($rad/_s$)	$\tau_{pressure}$ (N·m)	$\tau_{viscous}$ (N·m)	τ_{rotor} (N·m)	P_{blade} (W)	P_{rotor} (W)	C_p	C_s
1	3.0	5	0.524	-0.0062975718	-0.000041946005	-0.0063395178	0.0033193638	0.0265549101	0.003283314	0.067051
2	3.0	10	1.047	-0.0049575893	-0.000012327129	-0.0049699164	0.0052044843	0.0416358745	0.005147961	0.134102
3	3.0	20	2.094	-0.0023201024	0.000055291479	-0.0022648109	0.0047434089	0.0379472712	0.004691893	0.268205
4	3.0	30	3.142	0.0013084257	0.000131846550	0.0014402723	-0.0045247487	-0.0361979898	-0.004475608	0.402307
5	3.0	40	4.189	0.005245181	0.000211372370	0.0054565538	-0.0228563590	-0.1828508719	-0.022608128	0.536409

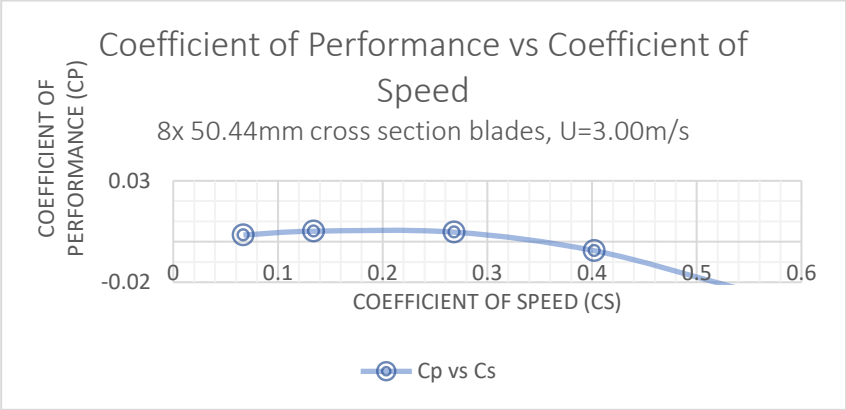

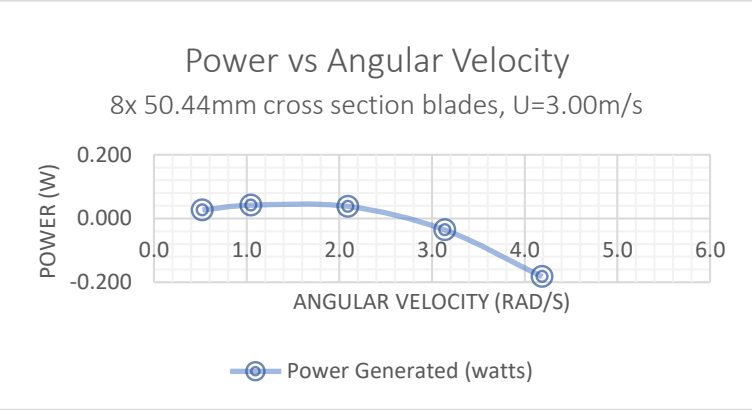

CFD Data for Rotor with Eight 50.44mm Square Blades

U=4.0 m/s

Measured Data							Calculated Data			
Run Number	U_{stream}	ω_{rotor} **(RPM)**	ω_{rotor} $\left(rad/_s\right)$	$\tau_{pressure}$ **(N·m)**	$\tau_{viscous}$ **(N·m)**	τ_{rotor} **(N·m)**	P_{blade} **(W)**	P_{rotor} **(W)**	C_p	C_s
1	4.0	5	0.524	-0.008091048200	-0.000041552248	-0.0081326004	0.0042582196	0.0340657571	0.001776926	0.05028839
2	4.0	10	1.047	-0.0088121980	-0.000020476349	-0.0088326743	0.0092495549	0.0739964396	0.003859777	0.10057678
3	4.0	20	2.094	-0.0060316120	0.000052191200	-0.0059794208	0.0125232696	0.1001861571	0.005225876	0.20115356
4	4.0	30	3.142	-0.0019953254	0.000138758590	-0.0018565668	0.0058325767	0.0466606132	0.002433895	0.301730339
5	4.0	40	4.189	0.002519200900	0.000227478930	0.0027466798	-0.0115052656	-0.0920421245	-0.004801069	0.402307119
6	4.0	50	5.236	0.007706357300	0.000323311340	0.0080296686	-0.0420432467	-0.3363459735	-0.017544362	0.502884

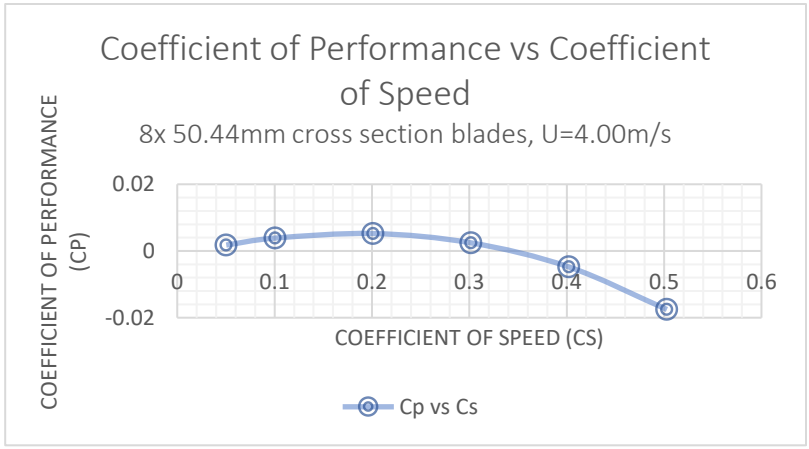

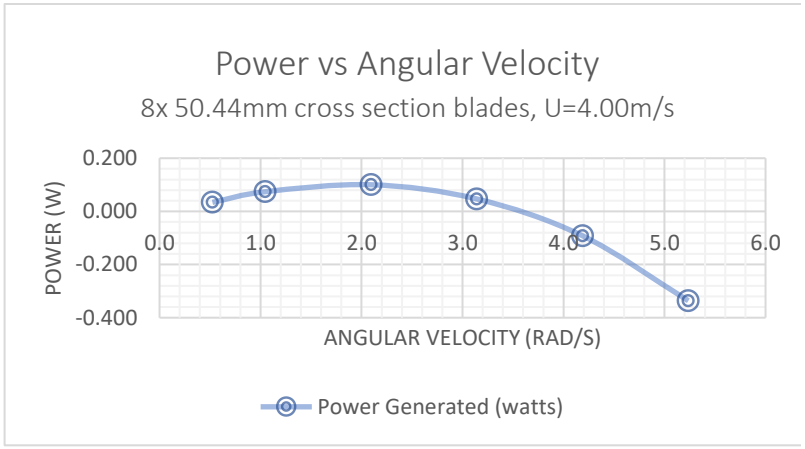

CFD Data for Rotor with Eight 50.44mm Square Blades

U=5.0 m/s

Measured Data							Calculated Data			
Run Number	U_{stream}	ω_{rotor} (RPM)	ω_{rotor} (rad/s)	$\tau_{pressure}$ (N·m)	$\tau_{viscous}$ (N·m)	τ_{rotor} (N·m)	P_{blade} (W)	P_{rotor} (W)	C_p	C_s
1	5.0	5	0.524	-0.011349612000	-0.000059929939	-0.0114095419	0.0059740222	0.0477921775	0.002492919	0.040230712
2	5.0	10	1.047	-0.014167768000	-0.000047039113	-0.0142148071	0.0148857112	0.1190856896	0.003180394	0.080461424
3	5.0	20	2.094	-0.011757056000	0.000026336128	-0.0117307199	0.0245687622	0.1965500980	0.005249218	0.160922848
4	5.0	30	3.142	-0.0073000751	0.000113576910	-0.0071864982	0.0225770499	0.1806163993	0.00482368	0.241384272
5	5.0	40	4.189	-0.000887420950	0.000255497580	-0.00063192337	0.0026469944	0.0211759554	0.000565541	0.321845695
6	5.0	50	5.236	0.004430038800	0.000370085370	0.0048001242	-0.0251333914	-0.2010671311	-0.005369853	0.402307

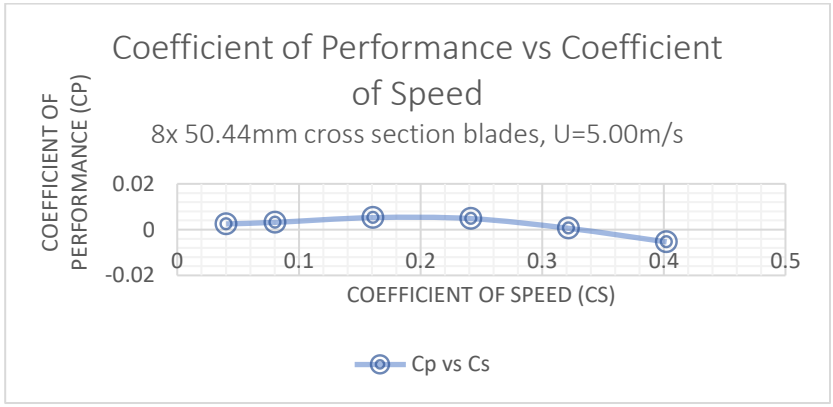

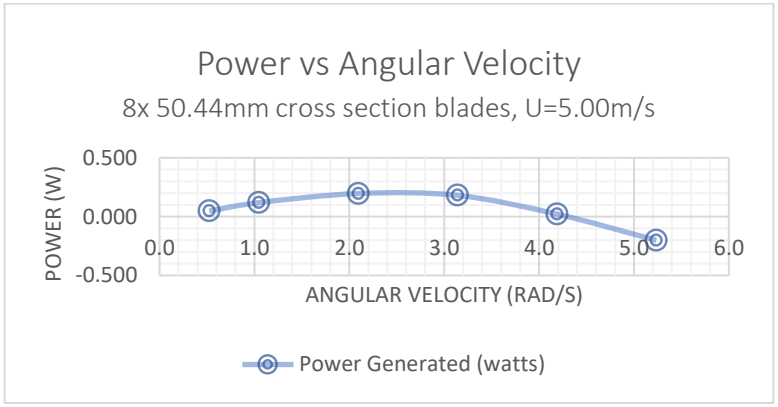

B2. Rotor with Eight 25.28mm Square Blades

CFD Data for Rotor with Eight 25.28mm Square Blades

U=3.0 m/s

	Measured Data						Calculated Data			
Run Number	U_{stream}	ω_{rotor} (RPM)	ω_{rotor} (rad/s)	$\tau_{pressure}$ (N·m)	$\tau_{viscous}$ (N·m)	τ_{rotor} (N·m)	P_{blade} (W)	P_{rotor} (W)	C_p	C_s
1	3.0	5	0.524	-0.000547084550	0.000005706997	-0.0005413776	0.0002834646	0.0022677170	0.000280386	0.067051
2	3.0	10	1.047	-0.000911450230	0.000014875888	-0.0008965743	0.0009388905	0.0075111236	0.000928694	0.134102
3	3.0	20	2.094	-0.001729837800	0.000035538675	-0.0016942991	0.0035485318	0.0283882543	0.003509993	0.268205
4	3.0	30	3.142	-0.002730616100	0.000040276201	-0.0026903399	0.0084519521	0.0676156165	0.00836016	0.402307
5	3.0	40	4.189	-0.000643968620	0.000073335300	-0.0005706333	0.0023902633	0.0191221061	0.002364304	0.536409
6	3.0	50	5.236	0.002519721	0.000110178	0.0026298991	-0.0137701196	-0.1101609567	-0.013620569	0.670512

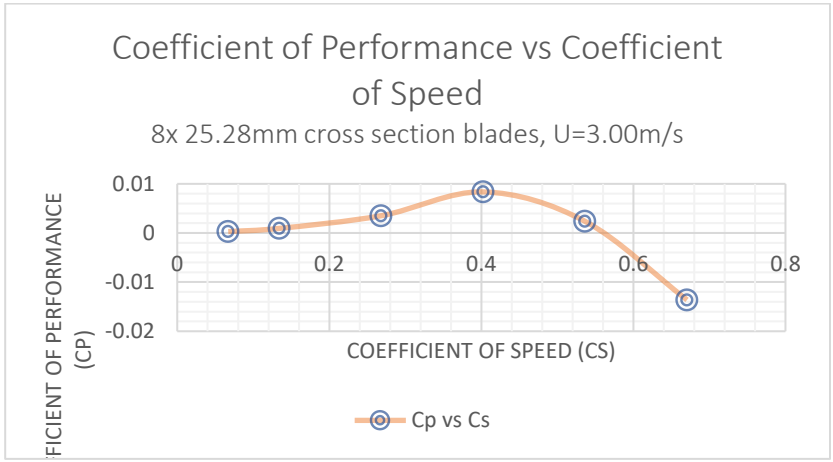

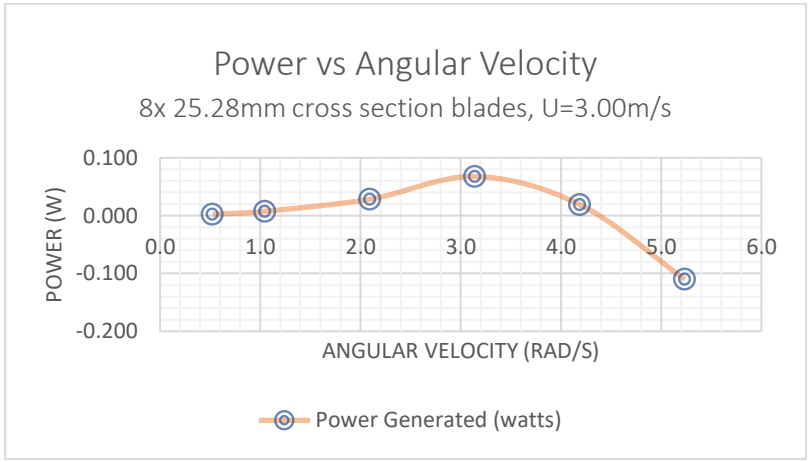

CFD Data for Rotor with Eight 25.28mm Square Blades

U=4.0 m/s

Measured Data							Calculated Data			
Run Number	U_{stream}	ω_{rotor} (RPM)	ω_{rotor} (rad/s)	$\tau_{pressure}$ (N·m)	$\tau_{viscous}$ (N·m)	τ_{rotor} (N·m)	P_{blade} (W)	P_{rotor} (W)	C_p	C_s
1	4.0	5	0.524	-0.000320852530	0.000013223889	-0.0003076286	0.0001610740	0.0012885918	0.0000672151	0.050288
2	4.0	10	1.047	-0.000320852530	0.000013223889	-0.0003076286	0.0003221480	0.0025771837	0.00013443	0.100577
3	4.0	20	2.094	-0.002010347400	0.000041524731	-0.0019688227	0.0041234926	0.0329879404	0.001720706	0.201154
4	4.0	30	3.142	-0.003595217800	0.000066738613	-0.0035284792	0.0110850443	0.0886803543	0.004625714	0.30173
5	4.0	40	4.189	-0.004911896400	0.000061586697	-0.0048503097	0.0203169298	0.1625354382	0.008478117	0.402307
6	4.0	50	5.236	-0.002379179700	0.000101034	-0.0022781462	0.0119283453	0.0954267628	0.004977618	0.502884

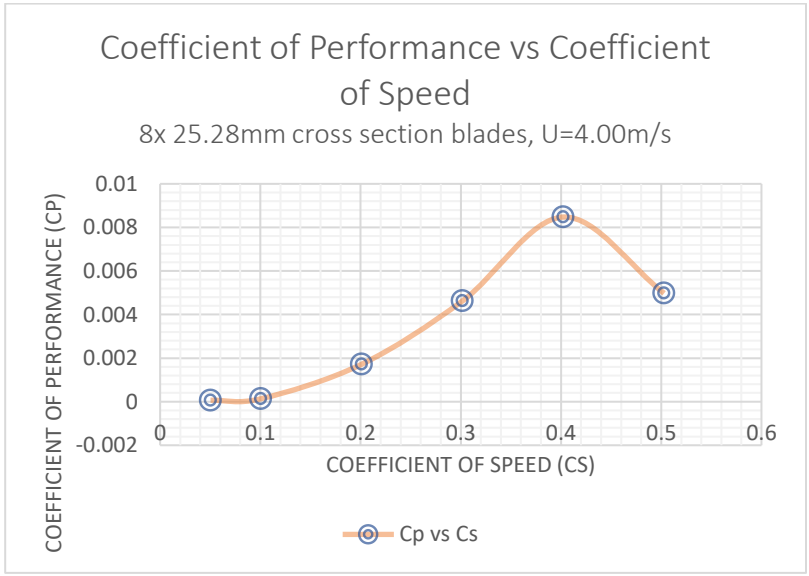

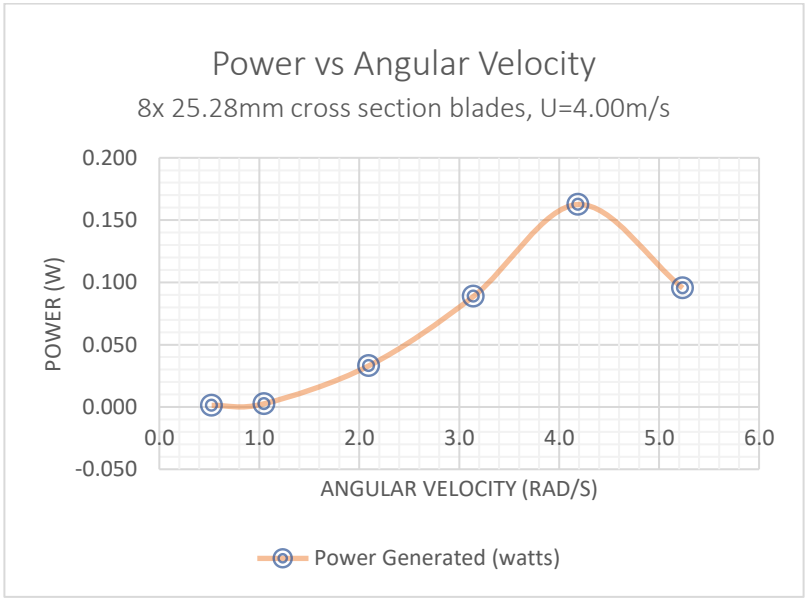

CFD Data for Rotor with Eight 25.28mm Square Blades

U=5.0 m/s

Measured Data							Calculated Data			
Run Number	U_{stream}	ω_{rotor} (RPM)	ω_{rotor} (rad/s)	$\tau_{pressure}$ (N·m)	$\tau_{viscous}$ (N·m)	τ_{rotor} (N·m)	P_{blade} (W)	P_{rotor} (W)	C_p	C_s
1	5.0	5	0.524	-0.000299636950	0.000014711917	-0.0002849250	0.0001491864	0.0011934912	0.0000318743	0.040231
2	5.0	10	1.047	-0.000801527050	0.000027511728	-0.0007740153	0.0008105469	0.0064843756	0.000173177	0.080461
3	5.0	20	2.094	-0.002148701200	0.000051419695	-0.0020972815	0.0043925361	0.0351402889	0.000938483	0.160923
4	5.0	30	3.142	-0.003570382800	0.000076393451	-0.0034939893	0.0109766913	0.0878135302	0.002345215	0.241384
5	5.0	40	4.189	-0.006024552700	0.000103668530	-0.0059208842	0.0248013416	0.1984107329	0.005298909	0.321846
6	5.0	50	5.236	-0.007748241	0.000086353855	-0.0076618871	0.0401175473	0.3209403782	0.00857128	0.402307

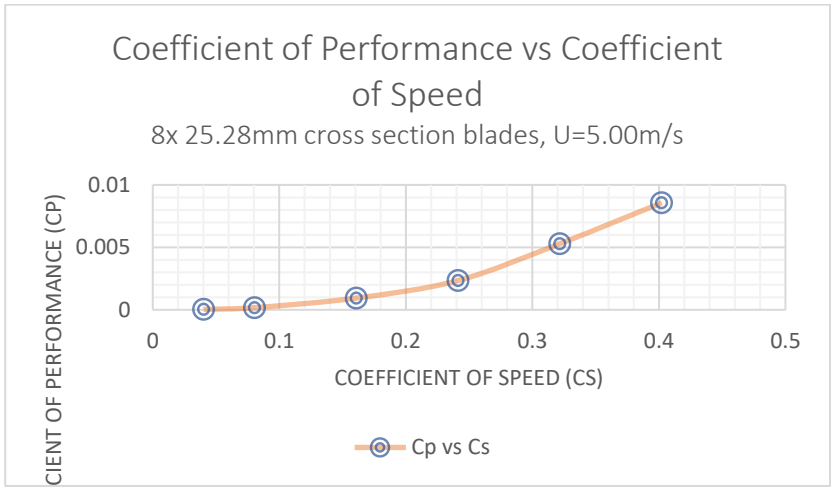

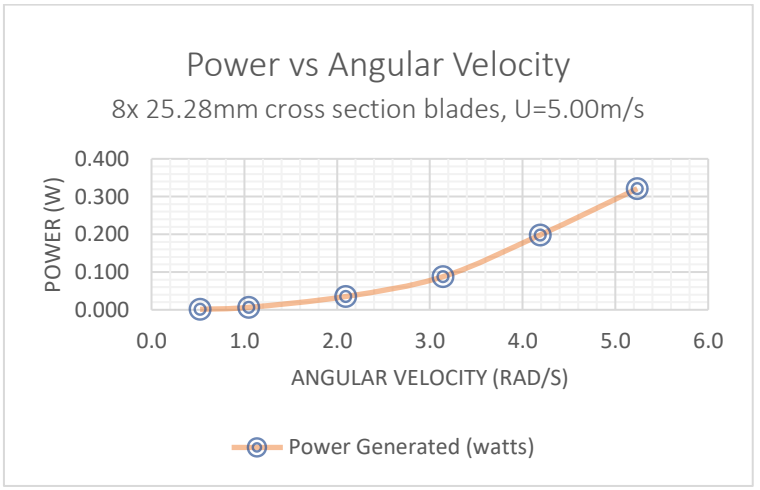

Appendix C – Wind Tunnel Test Data

C1. Rotor with Eight 50.44mm Square Blades

Data for Rotor with Eight 50.44mm Square Blades

U=2.556 m/s

Recorded Data							Calculated Data						Uncertainty					
Run Number	**Windspeed (m/s)**	**Voltage (V)**	**Amperage (A)**	**% Max Current**	**Torque (N·cm)**	**RPM**	**Torque (N·m)**	**ω (rad/s)**	**Power (w)**	**ρ (kg/m^3)**	**Cp**	**Cs**	**$\sigma_{windspeed}$ (± m/s)**	**σ_{Amp} (± A)**	**σω (± rad/s)**	**σT (± N·m)**	**σP (± w)**	**σP (± %)**
1	2.556	0	0.00	0%	0	24.1	0.000	2.524	0.000	1.292	0.0000	0.3793	0.0767	0.0040	0.1060	0.0000062	0.00000000	0.0000
2	2.556	0.17	0.010	3%	0.25	24.1	0.003	2.524	0.006	1.292	0.0013	0.3793	0.0767	0.0042	0.1060	0.0000064	0.00026544	4.2072
3	2.556	0.35	0.020	7%	0.35	23.7	0.004	2.482	0.009	1.292	0.0017	0.3730	0.0767	0.0043	0.1060	0.0000066	0.00037123	4.2736
4	2.556	0.53	0.030	10%	0.4	23.4	0.004	2.450	0.010	1.292	0.0020	0.3683	0.0767	0.0045	0.1059	0.0000069	0.00042411	4.3269
5	2.556	0.74	0.040	14%	0.5	22.9	0.005	2.398	0.012	1.292	0.0024	0.3604	0.0767	0.0046	0.1059	0.0000071	0.00052987	4.4191
6	2.556	0.96	0.050	17%	0.65	22.2	0.007	2.325	0.015	1.292	0.0030	0.3494	0.0767	0.0048	0.1059	0.0000073	0.00068844	4.5559
7	2.556	1.12	0.060	21%	0.8	21.6	0.008	2.262	0.018	1.292	0.0036	0.3400	0.0767	0.0049	0.1059	0.0000075	0.00084698	4.6806
8	2.556	1.35	0.070	24%	1	20.6	0.010	2.157	0.022	1.292	0.0043	0.3242	0.0767	0.0051	0.1058	0.0000078	0.00105812	4.9050
9	2.556	1.56	0.080	28%	1.3	19.8	0.013	2.073	0.027	1.292	0.0054	0.3116	0.0767	0.0052	0.1058	0.0000080	0.00137493	5.1009
10	2.556	1.8	0.090	31%	1.55	18.7	0.016	1.958	0.030	1.292	0.0061	0.2943	0.0767	0.0054	0.1057	0.0000082	0.00163841	5.3979
11	2.556	2.05	0.100	34%	1.85	17.2	0.019	1.801	0.033	1.292	0.0067	0.2707	0.0767	0.0055	0.1056	0.0000085	0.00195404	5.8641
12	2.556	2.22	0.110	38%	2.3	15.9	0.023	1.665	0.038	1.292	0.0077	0.2503	0.0767	0.0057	0.1056	0.0000087	0.00242775	6.3394
13	2.556	2.41	0.120	41%	2.6	14.5	0.026	1.518	0.039	1.292	0.0079	0.2282	0.0767	0.0058	0.1055	0.0000089	0.00274249	6.9466
14	2.556	2.62	0.130	45%	3.05	12.2	0.031	1.278	0.039	1.292	0.0078	0.1920	0.0767	0.0060	0.1054	0.0000092	0.00321346	8.2468
15	2.556	2.81	0.140	48%	3.35	0	0.034	0.000	0.000	1.292	0.0000	0.0000	0.0767	0.0061	0.1047	0.0000094	0.00000000	0.0000

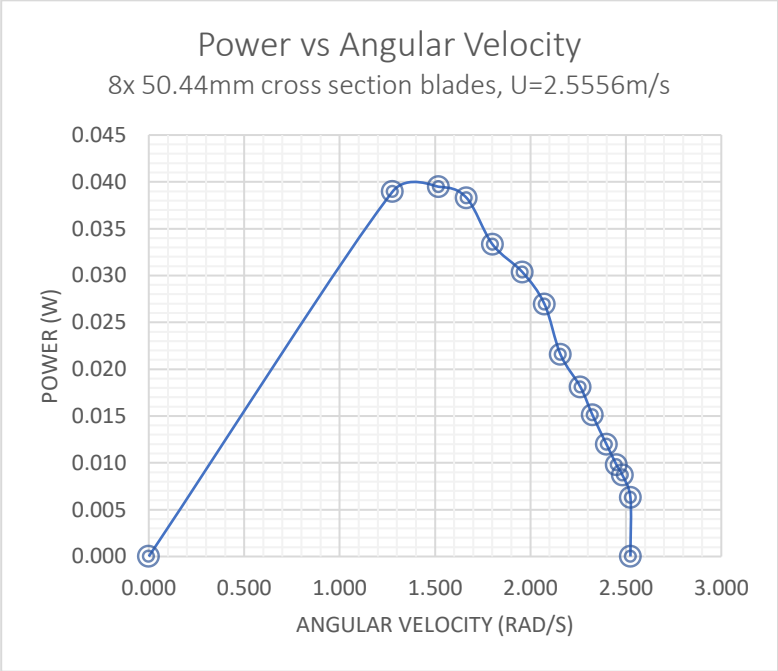
Power vs Angular Velocity
8x 50.44mm cross section blades, U=2.5556m/s
POWER (W)
0.045
0.040
0.035
0.030
0.025
0.020
0.015
0.010
0.005
0.000
0.000
0.500
1.000
1.500
2.000
2.500
3.000
ANGULAR VELOCITY (RAD/S)

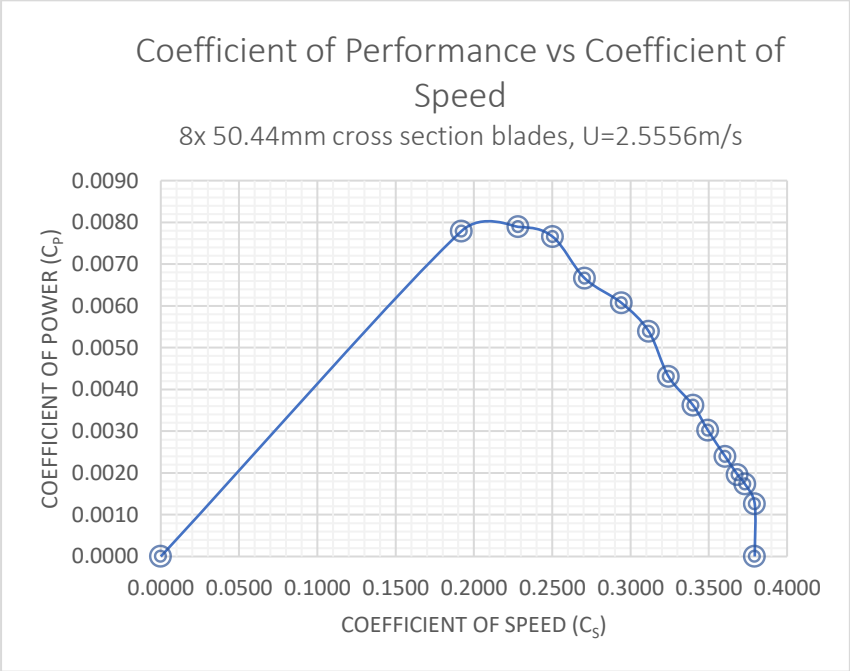
Coefficient of Performance vs Coefficient of Speed
8x 50.44mm cross section blades, U=2.5556m/s
COEFFICIENT OF POWER (C_p)
0.0090
0.0080
0.0070
0.0060
0.0050
0.0040
0.0030
0.0020
0.0010
0.0000
0.0000
0.0500
0.1000
0.1500
0.2000
0.2500
0.3000
0.3500
0.4000
COEFFICIENT OF SPEED (C_S)

Data for Rotor with Eight 50.44mm Square Blades

U=3.106 m/s

Recorded Data							Calculated Data						Uncertainty					
Run Number	**Windspeed (m/s)**	**Voltage (V)**	**Amperage (A)**	**% Max Current**	**Torque (N·cm)**	**RPM**	**Torque (N·m)**	**ω (rad/s)**	**Power (w)**	**ρ (kg/m^3)**	**Cp**	**Cs**	**$\sigma_{windspeed}$ (± m/s)**	**σ_{Amp} (± A)**	**σω (± rad/s)**	**σT (± N·m)**	**σP (± w)**	**σP (± %)**
1	3.106	0	0.00	0%	0	30	0.000	3.142	0.000	1.292	0.0000	0.3886	0.0932	0.0000	0.1063	0.0000000	0.0000000	0.0000
2	3.106	0.17	0.01	3%	0.25	29.7	0.003	3.110	0.008	1.292	0.0009	0.3847	0.0932	0.00415	0.1063	0.0000064	0.0002663	3.4266
3	3.106	0.33	0.02	7%	0.35	29.3	0.004	3.068	0.011	1.292	0.0012	0.3795	0.0932	0.00430	0.1063	0.0000066	0.0003724	3.4681
4	3.106	0.55	0.03	10%	0.4	28.9	0.004	3.026	0.012	1.292	0.0013	0.3743	0.0932	0.00445	0.1062	0.0000069	0.0004254	3.5144
5	3.106	0.81	0.04	14%	0.5	27.9	0.005	2.922	0.015	1.292	0.0016	0.3614	0.0932	0.00460	0.1062	0.0000071	0.0005313	3.6370
6	3.106	0.97	0.05	17%	0.65	27.4	0.007	2.869	0.019	1.292	0.0021	0.3549	0.0932	0.00475	0.1062	0.0000073	0.0006903	3.7013
7	3.106	1.22	0.06	21%	0.8	26.8	0.008	2.806	0.022	1.292	0.0025	0.3471	0.0932	0.00490	0.1061	0.0000075	0.0008492	3.7825
8	3.106	1.35	0.07	24%	1	26.7	0.010	2.796	0.028	1.292	0.0031	0.3458	0.0932	0.00505	0.1061	0.0000078	0.0010614	3.7961
9	3.106	1.58	0.08	28%	1.3	25.8	0.013	2.702	0.035	1.292	0.0039	0.3342	0.0932	0.00520	0.1061	0.0000080	0.0013790	3.9265
10	3.106	1.9	0.09	31%	1.55	24.3	0.016	2.545	0.039	1.292	0.0044	0.3147	0.0932	0.00535	0.1060	0.0000082	0.0016401	4.1656
11	3.106	1.96	0.10	34%	1.85	24.1	0.019	2.524	0.047	1.292	0.0052	0.3122	0.0932	0.00550	0.1060	0.0000085	0.0019607	4.1996
12	3.106	2.2	0.11	38%	2.3	22.8	0.023	2.388	0.055	1.292	0.0061	0.2953	0.0932	0.00565	0.1059	0.0000087	0.0024361	4.4361
13	3.106	2.46	0.12	41%	2.6	21.5	0.026	2.251	0.059	1.292	0.0065	0.2785	0.0932	0.00580	0.1058	0.0000089	0.0027526	4.7013
14	3.106	2.63	0.13	45%	3.05	20.7	0.031	2.168	0.066	1.292	0.0074	0.2681	0.0932	0.00595	0.1058	0.0000092	0.0032270	4.8810
15	3.106	2.84	0.14	48%	3.35	19.2	0.034	2.011	0.067	1.292	0.0075	0.2487	0.0932	0.00610	0.1057	0.0000094	0.0035418	5.2584
16	3.106	3.04	0.15	52%	3.8	17.9	0.038	1.874	0.071	1.292	0.0079	0.2319	0.0932	0.00625	0.1057	0.0000096	0.0040151	5.6366
17	3.106	3.29	0.16	55%	4.2	16.2	0.042	1.696	0.071	1.292	0.0079	0.2098	0.0932	0.00640	0.1056	0.0000099	0.0044338	6.2229
18	3.106	3.46	0.17	59%	4.85	0	0.049	0.000	0.000	1.292	0.0000	0.0000	0.0932	0.00655	0.1047	0.0000101	0.0000000	0.0000

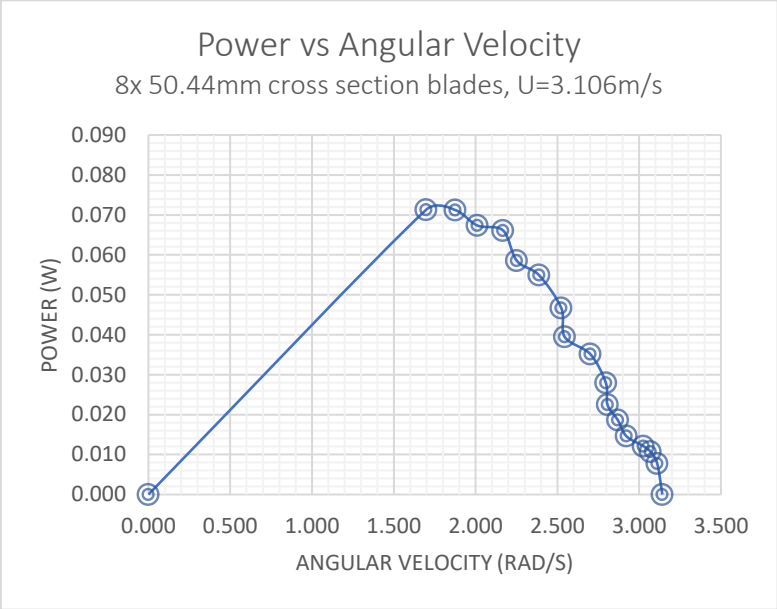
Power vs Angular Velocity
8x 50.44mm cross section blades, U=3.106m/s
POWER (W)
0.090
0.080
0.070
0.060
0.050
0.040
0.030
0.020
0.010
0.000
0.000
0.500
1.000
1.500
2.000
2.500
3.000
3.500
ANGULAR VELOCITY (RAD/S)

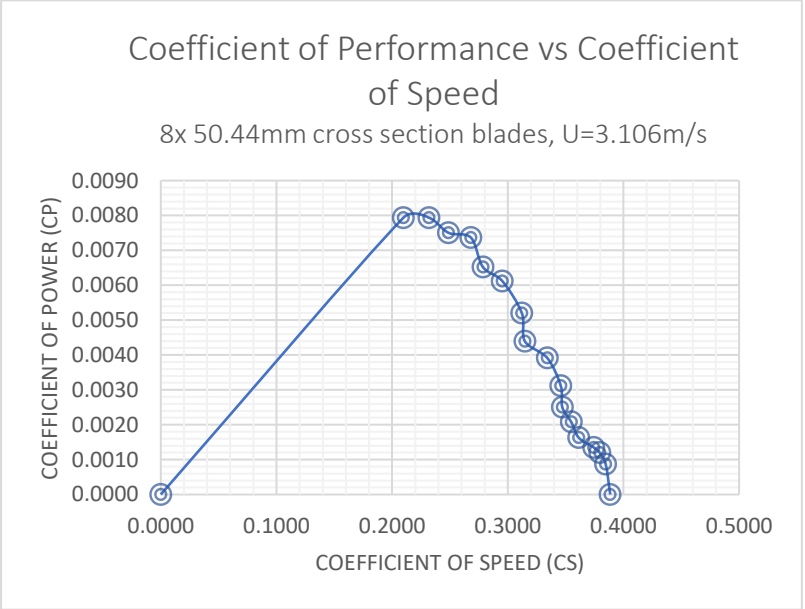
Coefficient of Performance vs Coefficient of Speed
8x 50.44mm cross section blades, U=3.106m/s
COEFFICIENT OF POWER (CP)
0.0090
0.0080
0.0070
0.0060
0.0050
0.0040
0.0030
0.0020
0.0010
0.0000
0.0000
0.1000
0.2000
0.3000
0.4000
0.5000
COEFFICIENT OF SPEED (CS)

Data for Rotor with Eight 50.44mm Square Blades

U=3.440 m/s

Recorded Data							Calculated Data						Uncertainty					
Run Number	**Windspeed (m/s)**	**Voltage (V)**	**Amperage (A)**	**% Max Current**	**Torque (N·cm)**	**RPM**	**Torque (N·m)**	**ω (rad/s)**	**Power (w)**	**ρ (kg/m^3)**	**Cp**	**Cs**	**$\sigma_{windspeed}$ (± m/s)**	**σ Amp (± A)**	**σω (± rad/s)**	**σT (± N·m)**	**σP (± w)**	**σP (± %)**
1	3.44	0	0.00	0%	0	32.6	0.000	3.414	0.000	1.292	0.0000	0.3813	0.1032	0.0000	0.1064	0.0000000	0.0000000	0.0000
2	3.44	0.18	0.01	3%	0.2	32.8	0.002	3.435	0.007	1.292	0.0006	0.3836	0.1032	0.00415	0.1064	0.0000064	0.0002140	3.1152
3	3.44	0.42	0.02	7%	0.4	32.7	0.004	3.424	0.014	1.292	0.0011	0.3824	0.1032	0.00430	0.1064	0.0000066	0.0004263	3.1125
4	3.44	0.61	0.03	10%	0.4	32.1	0.004	3.362	0.013	1.292	0.0011	0.3754	0.1032	0.00445	0.1064	0.0000069	0.0004262	3.1699
5	3.44	0.85	0.04	14%	0.5	31.9	0.005	3.341	0.017	1.292	0.0014	0.3731	0.1032	0.00460	0.1064	0.0000071	0.0005324	3.1879
6	3.44	1.04	0.05	17%	0.6	31.2	0.006	3.267	0.020	1.292	0.0016	0.3649	0.1032	0.00475	0.1064	0.0000073	0.0006385	3.2574
7	3.44	1.18	0.06	21%	0.7	30.9	0.007	3.236	0.023	1.292	0.0019	0.3614	0.1032	0.00490	0.1063	0.0000075	0.0007447	3.2880
8	3.44	1.35	0.07	24%	1	30.2	0.010	3.163	0.032	1.292	0.0026	0.3532	0.1032	0.00505	0.1063	0.0000078	0.0010629	3.3622
9	3.44	1.56	0.08	28%	1.4	29.5	0.014	3.089	0.043	1.292	0.0035	0.3450	0.1032	0.00520	0.1063	0.0000080	0.0014879	3.4403
10	3.44	1.77	0.09	31%	1.6	29.1	0.016	3.047	0.049	1.292	0.0040	0.3403	0.1032	0.00535	0.1062	0.0000082	0.0017008	3.4868
11	3.44	2.04	0.10	34%	1.8	27.7	0.018	2.901	0.052	1.292	0.0043	0.3240	0.1032	0.00550	0.1062	0.0000085	0.0019112	3.6604
12	3.44	2.25	0.11	38%	2.4	26.6	0.024	2.786	0.067	1.292	0.0055	0.3111	0.1032	0.00565	0.1061	0.0000087	0.0025468	3.8096
13	3.44	2.4	0.12	41%	2.6	25.9	0.026	2.712	0.071	1.292	0.0058	0.3029	0.1032	0.00580	0.1061	0.0000089	0.0027580	3.9112
14	3.44	2.67	0.13	45%	3	24.9	0.030	2.608	0.078	1.292	0.0064	0.2912	0.1032	0.00595	0.1060	0.0000092	0.0031808	4.0662
15	3.44	2.89	0.14	48%	3.6	23.7	0.036	2.482	0.089	1.292	0.0073	0.2772	0.1032	0.00610	0.1060	0.0000094	0.0038146	4.2695
16	3.44	3.09	0.15	52%	3.8	22.7	0.038	2.377	0.090	1.292	0.0074	0.2655	0.1032	0.00625	0.1059	0.0000096	0.0040245	4.4554
17	3.44	3.27	0.16	55%	4.3	21.5	0.043	2.251	0.097	1.292	0.0079	0.2514	0.1032	0.00640	0.1058	0.0000099	0.0045514	4.7012
18	3.44	3.47	0.17	59%	4.8	20.7	0.048	2.168	0.104	1.292	0.0085	0.2421	0.1032	0.00655	0.1058	0.0000101	0.0050786	4.8810

19	3.44	3.69	0.18	62%	5.2	18.9	0.052	1.979	0.103	1.292	0.0084	0.2210	0.1032	0.00670	0.1057	0.0000103	0.00549692	5.3410
20	3.44	3.97	0.19	66%	5.9	16.3	0.059	1.707	0.101	1.292	0.0083	0.1906	0.1032	0.00685	0.1056	0.0000105	0.00622885	6.1850
21	3.44	4.16	0.20	69%	6.4	0	0.064	0.000	0.000	1.292	0.0000	0.0000	0.1032	0.00700	0.1047	0.0000108	0.00000000	0.0000

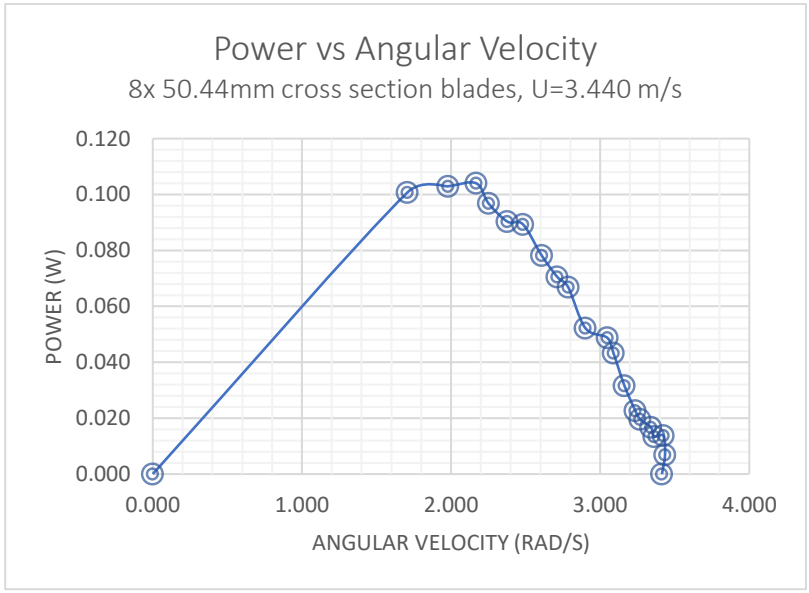

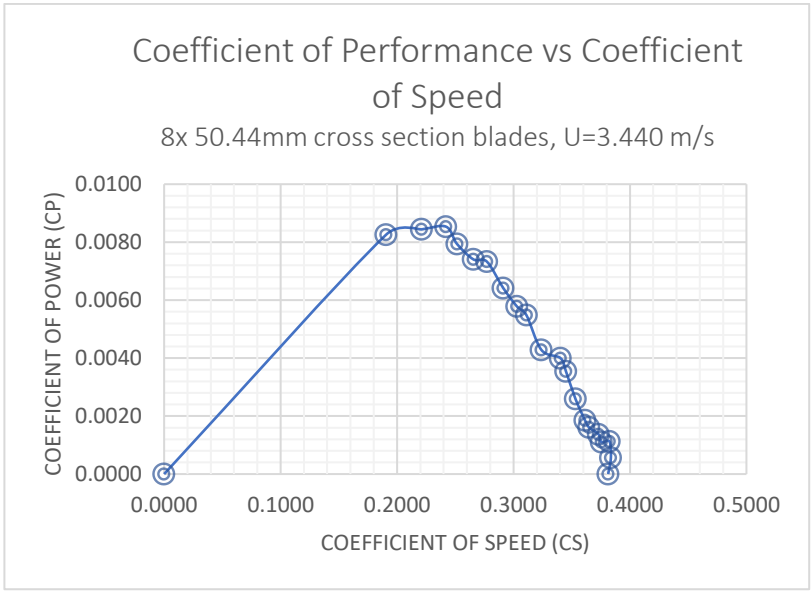

Data for Rotor with Eight 50.44mm Square Blades

U=3.968 m/s

Recorded Data							Calculated Data						Uncertainty					
Run Number	**Windspeed (m/s)**	**Voltage (V)**	**Amperage (A)**	**% Max Current**	**Torque (N·cm)**	**RPM**	**Torque (N·m)**	**ω (rad/s)**	**Power (w)**	**ρ (kg/m^3)**	**Cp**	**Cs**	**$\sigma_{windspeed}$ (± m/s)**	**σ Amp (± A)**	**σω (± rad/s)**	**σT (± N·m)**	**σP (± w)**	**σP (± %)**
1	3.968	0	0.00	0%	0	37.8	0.000	3.958	0.000	1.292	0.0000	0.3832	0.1190	0.0000	0.1067	0.0000000	0.0000000	0.0000
2	3.968	0.21	0.01	3%	0.2	37.8	0.002	3.958	0.008	1.292	0.0004	0.3832	0.1190	0.00415	0.1067	0.0000064	0.0002189	2.7144
3	3.968	0.44	0.02	7%	0.4	37.6	0.004	3.937	0.016	1.292	0.0008	0.3812	0.1190	0.00430	0.1067	0.0000066	0.0004275	2.7146
4	3.968	0.58	0.03	10%	0.4	37.6	0.004	3.937	0.016	1.292	0.0008	0.3812	0.1190	0.00445	0.1067	0.0000069	0.0004276	2.7150
5	3.968	0.78	0.04	14%	0.5	37.1	0.005	3.885	0.019	1.292	0.0010	0.3761	0.1190	0.00460	0.1067	0.0000071	0.0005340	2.7491
6	3.968	0.95	0.05	17%	0.6	36.8	0.006	3.854	0.023	1.292	0.0012	0.3731	0.1190	0.00475	0.1066	0.0000073	0.0006405	2.7701
7	3.968	1.21	0.06	21%	0.7	36.2	0.007	3.791	0.027	1.292	0.0014	0.3670	0.1190	0.00490	0.1066	0.0000075	0.0007468	2.8145
8	3.968	1.35	0.07	24%	1	35.7	0.010	3.738	0.037	1.292	0.0020	0.3620	0.1190	0.00505	0.1066	0.0000078	0.0010662	2.8522
9	3.968	1.56	0.08	28%	1.4	34.7	0.014	3.634	0.051	1.292	0.0027	0.3518	0.1190	0.00520	0.1065	0.0000080	0.0014918	2.9324
10	3.968	1.76	0.09	31%	1.6	34.3	0.016	3.592	0.057	1.292	0.0031	0.3478	0.1190	0.00535	0.1065	0.0000082	0.0017045	2.9659
11	3.968	2	0.10	34%	1.8	33.2	0.018	3.477	0.063	1.292	0.0033	0.3366	0.1190	0.00550	0.1065	0.0000085	0.0019164	3.0624
12	3.968	2.28	0.11	38%	2.4	32.4	0.024	3.393	0.081	1.292	0.0044	0.3285	0.1190	0.00565	0.1064	0.0000087	0.0025541	3.1366
13	3.968	2.4	0.12	41%	2.6	31.8	0.026	3.330	0.087	1.292	0.0046	0.3224	0.1190	0.00580	0.1064	0.0000089	0.0027661	3.1948
14	3.968	2.61	0.13	45%	3	30.8	0.030	3.225	0.097	1.292	0.0052	0.3123	0.1190	0.00595	0.1063	0.0000092	0.0031901	3.2969
15	3.968	2.8	0.14	48%	3.6	30.1	0.036	3.152	0.113	1.292	0.0061	0.3052	0.1190	0.00610	0.1063	0.0000094	0.0038276	3.3724
16	3.968	3.02	0.15	52%	3.8	29.2	0.038	3.058	0.116	1.292	0.0062	0.2961	0.1190	0.00625	0.1062	0.0000096	0.0040375	3.4747
17	3.968	3.26	0.16	55%	4.3	28.3	0.043	2.964	0.127	1.292	0.0068	0.2869	0.1190	0.00640	0.1062	0.0000099	0.0045676	3.5836
18	3.968	3.43	0.17	59%	4.8	27.4	0.048	2.869	0.138	1.292	0.0074	0.2778	0.1190	0.00655	0.1062	0.0000101	0.0050954	3.6997

19	3.968	3.66	0.18	62%	5.2	25.9	0.052	2.712	0.141	1.292	0.0075	0.2626	0.1190	0.00670	0.1061	0.0000103	0.00551602	3.9111
20	3.968	3.88	0.19	66%	5.9	25.1	0.059	2.628	0.155	1.292	0.0083	0.2545	0.1190	0.00685	0.1060	0.0000105	0.00625607	4.0341
21	3.968	4.09	0.20	69%	6.4	23.7	0.064	2.482	0.159	1.292	0.0085	0.2403	0.1190	0.00700	0.1060	0.0000108	0.00678154	4.2694
22	3.968	4.3	0.21	72%	6.8	22.3	0.068	2.335	0.159	1.292	0.0085	0.2261	0.1190	0.00715	0.1059	0.0000110	0.00720039	4.5343
23	3.968	4.56	0.22	76%	7.5	20.6	0.075	2.157	0.162	1.292	0.0086	0.2089	0.1190	0.00730	0.1058	0.0000112	0.00793491	4.9044
24	3.968	4.74	0.23	79%	7.9	17.4	0.079	1.822	0.144	1.292	0.0077	0.1764	0.1190	0.00745	0.1056	0.0000115	0.00834486	5.7971
25	3.968	4.94	0.24	83%	8.4	0	0.084	0.000	0.000	1.292	0.0000	0.0000	0.1190	0.00760	0.1047	0.0000117	0.00000000	0.0000

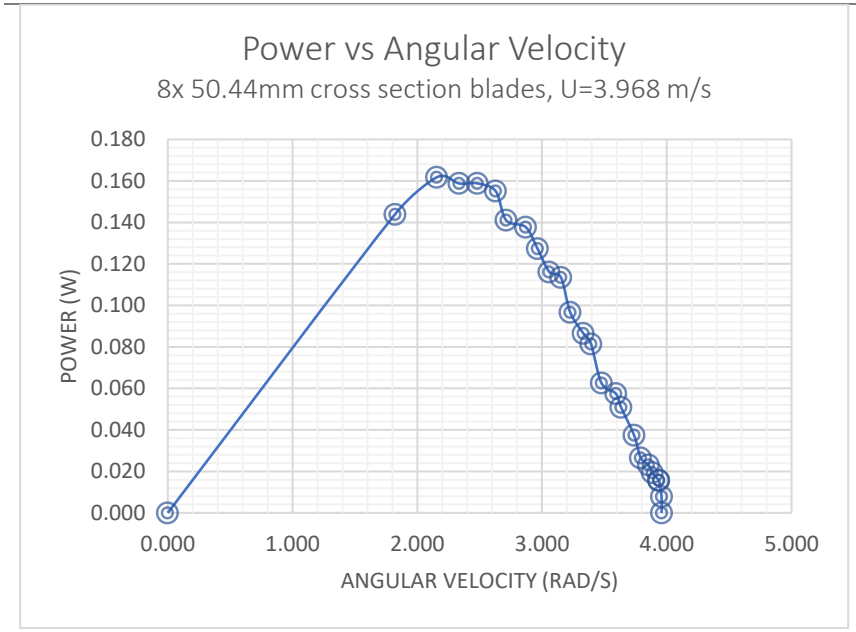

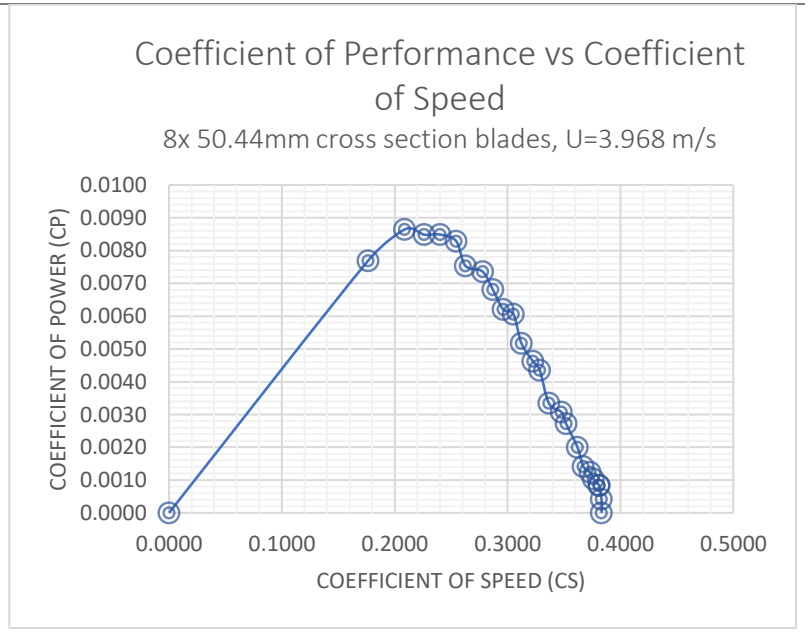

Data for Rotor with Eight 50.44mm Square Blades

U=4.456 m/s

Recorded Data							Calculated Data						Uncertainty					
Run Number	**Windspeed (m/s)**	**Voltage (V)**	**Amperage (A)**	**% Max Current**	**Torque (N·cm)**	**RPM**	**Torque (N·m)**	**ω (rad/s)**	**Power (w)**	**ρ (kg/m^3)**	**Cp**	**Cs**	**$\sigma_{windspeed}$ (± m/s)**	**σ_{Amp} (± A)**	**σω (± rad/s)**	**σT (± N·m)**	**σP (± w)**	**σP (± %)**
1	4.456	0	0.00	0%	0	43.2	0.000	4.524	0.000	1.292	0.0000	0.3900	0.1337	0.0000	0.1070	0.0000000	0.00000000	0.0000
2	4.456	0.12	0.01	3%	0.25	42.5	0.003	4.451	0.011	1.292	0.0004	0.3837	0.1337	0.00415	0.1069	0.0000064	0.00026887	2.4165
3	4.456	0.39	0.02	7%	0.35	42.4	0.004	4.440	0.016	1.292	0.0006	0.3828	0.1337	0.00430	0.1069	0.0000066	0.00037544	2.4159
4	4.456	0.63	0.03	10%	0.4	42.4	0.004	4.440	0.018	1.292	0.0007	0.3828	0.1337	0.00445	0.1069	0.0000069	0.00042884	2.4146
5	4.456	0.75	0.04	14%	0.5	42.1	0.005	4.409	0.022	1.292	0.0008	0.3801	0.1337	0.00460	0.1069	0.0000071	0.00053553	2.4294
6	4.456	0.95	0.05	17%	0.65	41.8	0.007	4.377	0.028	1.292	0.0011	0.3774	0.1337	0.00475	0.1069	0.0000073	0.00069564	2.4449
7	4.456	1.16	0.06	21%	0.8	41.5	0.008	4.346	0.035	1.292	0.0013	0.3747	0.1337	0.00490	0.1069	0.0000075	0.00085577	2.4614
8	4.456	1.37	0.07	24%	1	40.5	0.010	4.241	0.042	1.292	0.0016	0.3657	0.1337	0.00505	0.1068	0.0000078	0.00106891	2.5203
9	4.456	1.56	0.08	28%	1.3	39.8	0.013	4.168	0.054	1.292	0.0020	0.3593	0.1337	0.00520	0.1068	0.0000080	0.00138885	2.5633
10	4.456	1.82	0.09	31%	1.55	39.2	0.016	4.105	0.064	1.292	0.0024	0.3539	0.1337	0.00535	0.1068	0.0000082	0.00165532	2.6016
11	4.456	2.01	0.10	34%	1.85	38.9	0.019	4.074	0.075	1.292	0.0028	0.3512	0.1337	0.00550	0.1068	0.0000085	0.00197530	2.6211
12	4.456	2.28	0.11	38%	2.3	37.8	0.023	3.958	0.091	1.292	0.0034	0.3413	0.1337	0.00565	0.1067	0.0000087	0.00245432	2.6958
13	4.456	2.49	0.12	41%	2.6	37.4	0.026	3.917	0.102	1.292	0.0038	0.3377	0.1337	0.00580	0.1067	0.0000089	0.00277385	2.7240
14	4.456	2.68	0.13	45%	3.05	36.4	0.031	3.812	0.116	1.292	0.0044	0.3286	0.1337	0.00595	0.1066	0.0000092	0.00325227	2.7974
15	4.456	2.87	0.14	48%	3.35	35.9	0.034	3.759	0.126	1.292	0.0048	0.3241	0.1337	0.00610	0.1066	0.0000094	0.00357126	2.8357
16	4.456	3.08	0.15	52%	3.8	35	0.038	3.665	0.139	1.292	0.0053	0.3160	0.1337	0.00625	0.1066	0.0000096	0.00404914	2.9073
17	4.456	3.33	0.16	55%	4.2	33.3	0.042	3.487	0.146	1.292	0.0055	0.3006	0.1337	0.00640	0.1065	0.0000099	0.00447159	3.0531
18	4.456	3.52	0.17	59%	4.85	32.8	0.049	3.435	0.167	1.292	0.0063	0.2961	0.1337	0.00655	0.1064	0.0000101	0.00516232	3.0989
19	4.456	3.7	0.18	62%	5.3	32.4	0.053	3.393	0.180	1.292	0.0068	0.2925	0.1337	0.00670	0.1064	0.0000103	0.00564017	3.1365
20	4.456	3.91	0.19	66%	5.85	31.6	0.059	3.309	0.194	1.292	0.0073	0.2853	0.1337	0.00685	0.1064	0.0000105	0.00622300	3.2146

21	4.456	4.09	0.20	69%	6.3	30.3	0.063	3.173	0.200	1.292	0.0075	0.2736	0.1337	0.00700	0.1063	0.0000108	0.00669738	3.3504
22	4.456	4.36	0.21	72%	6.8	29.2	0.068	3.058	0.208	1.292	0.0078	0.2636	0.1337	0.00715	0.1062	0.0000110	0.00722499	3.4747
23	4.456	4.55	0.22	76%	7.45	28.2	0.075	2.953	0.220	1.292	0.0083	0.2546	0.1337	0.00730	0.1062	0.0000112	0.00791169	3.5961
24	4.456	4.74	0.23	79%	7.85	27.6	0.079	2.890	0.227	1.292	0.0086	0.2492	0.1337	0.00745	0.1062	0.0000115	0.00833401	3.6732
25	4.456	4.92	0.24	83%	8.45	26.7	0.085	2.796	0.236	1.292	0.0089	0.2411	0.1337	0.00760	0.1061	0.0000117	0.00896701	3.7953
26	4.456	5.17	0.25	86%	9	25.3	0.090	2.649	0.238	1.292	0.0090	0.2284	0.1337	0.00775	0.1060	0.0000119	0.00954405	4.0026
27	4.456	5.41	0.26	90%	9.5	24.3	0.095	2.545	0.242	1.292	0.0091	0.2194	0.1337	0.00790	0.1060	0.0000122	0.01006930	4.1652
28	4.456	5.63	0.27	93%	10	22	0.100	2.304	0.230	1.292	0.0087	0.1986	0.1337	0.00805	0.1059	0.0000124	0.01058721	4.5955
29	4.456	5.86	0.28	97%	10.7	0	0.107	0.000	0.000	1.292	0.0000	0.0000	0.1337	0.00820	0.1047	0.0000126	0.00000000	0.0000

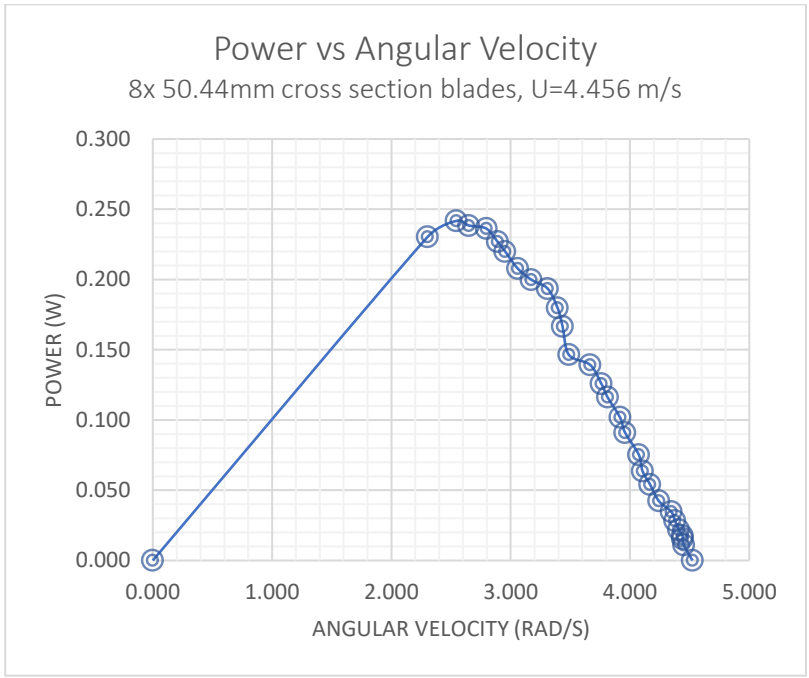
Power vs Angular Velocity
8x 50.44mm cross section blades, U=4.456 m/s
POWER (W)
0.300
0.250
0.200
0.150
0.100
0.050
0.000
0.000
1.000
2.000
3.000
4.000
5.000
ANGULAR VELOCITY (RAD/S)

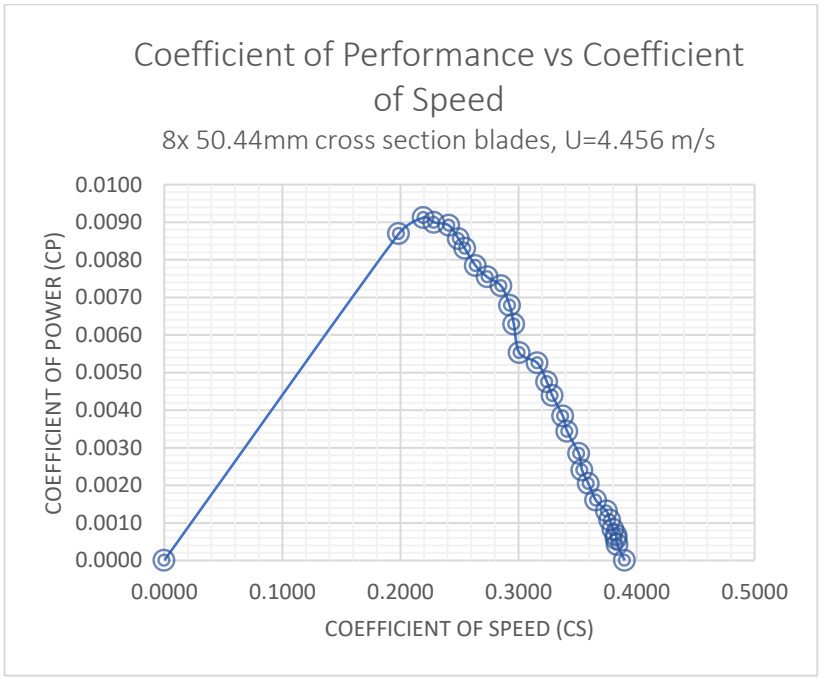
Coefficient of Performance vs Coefficient of Speed
8x 50.44mm cross section blades, U=4.456 m/s
COEFFICIENT OF POWER (CP)
0.0100
0.0090
0.0080
0.0070
0.0060
0.0050
0.0040
0.0030
0.0020
0.0010
0.0000
0.0000
0.1000
0.2000
0.3000
0.4000
0.5000
COEFFICIENT OF SPEED (CS)

Data for Rotor with Eight 50.44mm Square Blades

U=5.002 m/s

Recorded Data							Calculated Data						Uncertainty					
Run Number	**Windspeed (m/s)**	**Voltage (V)**	**Amperage (A)**	**% Max Current**	**Torque (N·cm)**	**RPM**	**Torque (N·m)**	**ω (rad/s)**	**Power (w)**	**ρ (kg/m^3)**	**Cp**	**Cs**	**$\sigma_{windspeed}$ (± m/s)**	**σ_{Amp} (± A)**	**σω (± rad/s)**	**σT (± N·m)**	**σP (± w)**	**σP (± %)**
1	5.002	0	0.00	0%	0	48.6	0.000	5.089	0.000	1.292	0.00000	0.39309	0.1501	0.00000	0.1073	0.0000000	0.0000	0.0000
2	5.002	0.14	0.01	3%	0.25	48.6	0.003	5.089	0.013	1.292	0.00003	0.39309	0.1501	0.00415	0.1073	0.0000064	0.0002701	2.1231
3	5.002	0.41	0.02	7%	0.35	48.4	0.004	5.068	0.018	1.292	0.00005	0.38933	0.1501	0.00430	0.1073	0.0000066	0.0003768	2.1246
4	5.002	0.65	0.03	10%	0.4	48.1	0.004	5.037	0.020	1.292	0.00005	0.38669	0.1501	0.00445	0.1072	0.0000069	0.0004303	2.1359
5	5.002	0.83	0.04	14%	0.5	47.6	0.005	4.985	0.025	1.292	0.00007	0.38228	0.1501	0.00460	0.1072	0.0000071	0.0005372	2.1555
6	5.002	0.95	0.05	17%	0.65	47.9	0.007	5.016	0.033	1.292	0.00009	0.38553	0.1501	0.00475	0.1072	0.0000073	0.0006979	2.1406
7	5.002	1.11	0.06	21%	0.8	47.2	0.008	4.943	0.040	1.292	0.00011	0.37996	0.1501	0.00490	0.1072	0.0000075	0.0008584	2.1707
8	5.002	1.35	0.07	24%	1	47.3	0.010	4.953	0.050	1.292	0.00013	0.38004	0.1501	0.00505	0.1072	0.0000078	0.0010726	2.1656
9	5.002	1.57	0.08	28%	1.3	46.4	0.013	4.859	0.063	1.292	0.00017	0.37332	0.1501	0.00520	0.1071	0.0000080	0.0013948	2.2060
10	5.002	1.77	0.09	31%	1.55	45.8	0.016	4.796	0.074	1.292	0.00020	0.36884	0.1501	0.00535	0.1071	0.0000082	0.0016608	2.2340
11	5.002	1.99	0.10	34%	1.85	45.2	0.019	4.733	0.088	1.292	0.00023	0.36335	0.1501	0.00550	0.1071	0.0000085	0.0019815	2.2629
12	5.002	2.22	0.11	38%	2.3	43.9	0.023	4.597	0.106	1.292	0.00028	0.35131	0.1501	0.00565	0.1070	0.0000087	0.0024617	2.3282
13	5.002	2.53	0.12	41%	2.6	43.1	0.026	4.513	0.117	1.292	0.00031	0.34667	0.1501	0.00580	0.1070	0.0000089	0.0027816	2.3704
14	5.002	2.61	0.13	45%	3.05	43.4	0.031	4.545	0.139	1.292	0.00037	0.34991	0.1501	0.00595	0.1070	0.0000092	0.0032635	2.3543
15	5.002	2.91	0.14	48%	3.35	41.7	0.034	4.367	0.146	1.292	0.00039	0.33554	0.1501	0.00610	0.1069	0.0000094	0.0035814	2.4482
16	5.002	3.03	0.15	52%	3.8	41.6	0.038	4.356	0.166	1.292	0.00044	0.33446	0.1501	0.00625	0.1069	0.0000096	0.0040623	2.4540
17	5.002	3.22	0.16	55%	4.2	41.1	0.042	4.304	0.181	1.292	0.00048	0.33061	0.1501	0.00640	0.1069	0.0000099	0.0044888	2.4832
18	5.002	3.47	0.17	59%	4.85	40.1	0.049	4.199	0.204	1.292	0.00054	0.32225	0.1501	0.00655	0.1068	0.0000101	0.0051809	2.5439

19	5.002	3.68	0.18	62%	5.3	39.2	0.053	4.105	0.218	1.292	0.0058	0.3153	0.1501	0.00670	0.1068	0.0000103	0.00565909	2.6011
20	5.002	3.9	0.19	66%	5.85	38.2	0.059	4.000	0.234	1.292	0.0062	0.3072	0.1501	0.00685	0.1067	0.0000105	0.00624326	2.6679
21	5.002	4.13	0.20	69%	6.3	37.3	0.063	3.906	0.246	1.292	0.0066	0.3000	0.1501	0.00700	0.1067	0.0000108	0.00672052	2.7310
22	5.002	4.27	0.21	72%	6.8	36.6	0.068	3.833	0.261	1.292	0.0070	0.2944	0.1501	0.00715	0.1066	0.0000110	0.00725138	2.7823
23	5.002	4.52	0.22	76%	7.45	35.9	0.075	3.759	0.280	1.292	0.0075	0.2887	0.1501	0.00730	0.1066	0.0000112	0.00794177	2.8356
24	5.002	4.76	0.23	79%	7.85	34.6	0.079	3.623	0.284	1.292	0.0076	0.2783	0.1501	0.00745	0.1065	0.0000115	0.00836282	2.9402
25	5.002	5.01	0.24	83%	8.45	33.6	0.085	3.519	0.297	1.292	0.0079	0.2702	0.1501	0.00760	0.1065	0.0000117	0.00899757	3.0262
26	5.002	5.26	0.25	86%	9	32.8	0.090	3.435	0.309	1.292	0.0082	0.2638	0.1501	0.00775	0.1064	0.0000119	0.00957943	3.0988
27	5.002	5.44	0.26	90%	9.5	32	0.095	3.351	0.318	1.292	0.0085	0.2574	0.1501	0.00790	0.1064	0.0000122	0.01010763	3.1750
28	5.002	5.64	0.27	93%	10	31.5	0.100	3.299	0.330	1.292	0.0088	0.2534	0.1501	0.00805	0.1064	0.0000124	0.01063699	3.2246
29	5.002	6.8	0.28	97%	10.7	30	0.107	3.142	0.336	1.292	0.0090	0.2413	0.1501	0.00820	0.1063	0.0000126	0.01137316	3.3834
30	5.002	6.12	0.29	100%	11	29.2	0.110	3.058	0.336	1.292	0.0090	0.2349	0.1501	0.00835	0.1062	0.0000129	0.01168742	3.4747

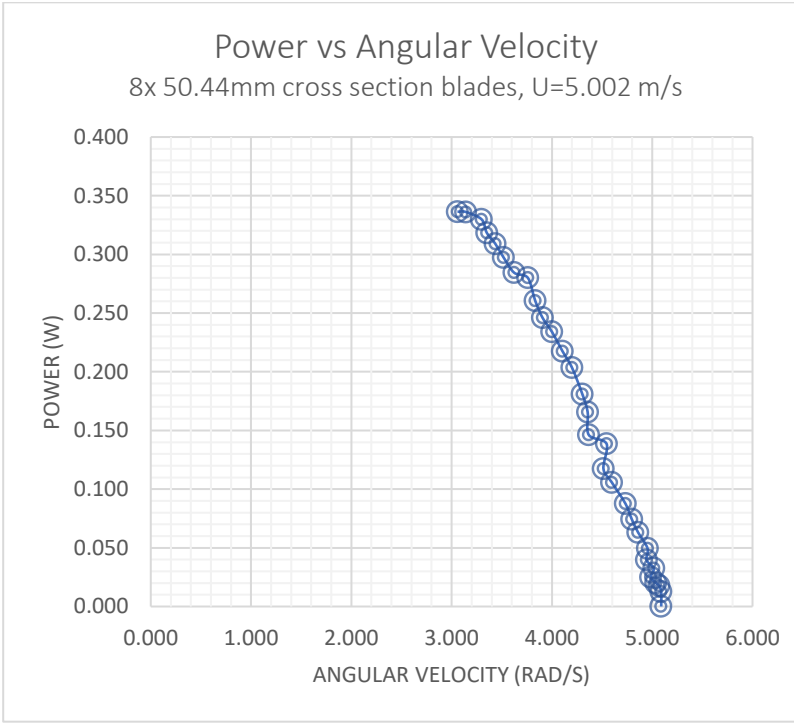
Power vs Angular Velocity
8x 50.44mm cross section blades, U=5.002 m/s
POWER (W)
0.400
0.350
0.300
0.250
0.200
0.150
0.100
0.050
0.000
0.000
1.000
2.000
3.000
4.000
5.000
6.000
ANGULAR VELOCITY (RAD/S)

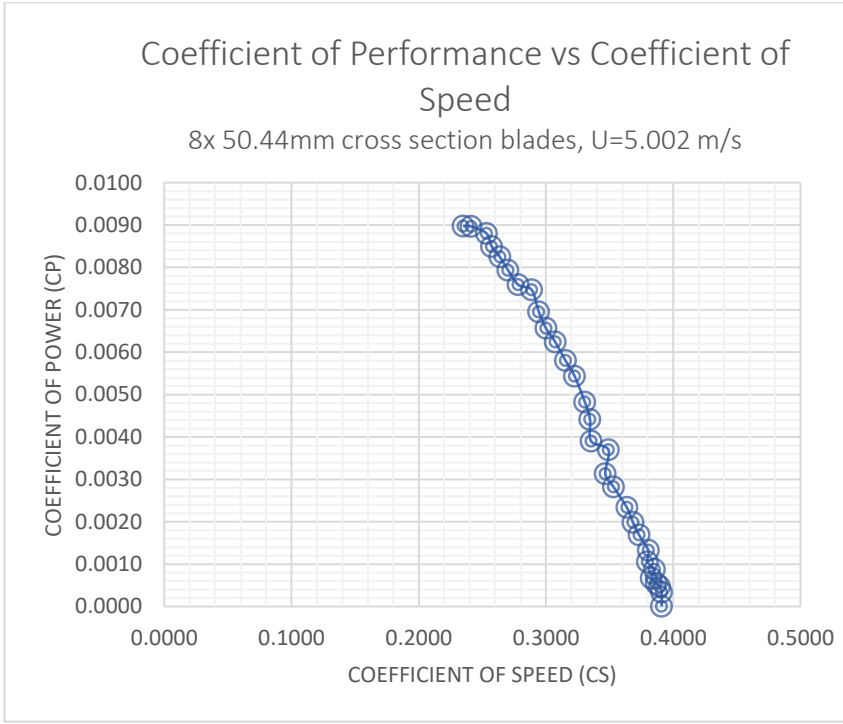
Coefficient of Performance vs Coefficient of Speed
8x 50.44mm cross section blades, U=5.002 m/s
COEFFICIENT OF POWER (CP)
0.0100
0.0090
0.0080
0.0070
0.0060
0.0050
0.0040
0.0030
0.0020
0.0010
0.0000
0.0000
0.1000
0.2000
0.3000
0.4000
0.5000
COEFFICIENT OF SPEED (CS)

C2. Rotor with Eight 25.28mm Square Blades

Data for Rotor with Eight 25.28mm Square Blades

U=3.036 m/s

Recorded Data							Calculated Data						Uncertainty					
Run Number	**Windspeed (m/s)**	**Voltage (V)**	**Amperage (A)**	**% Max Current**	**Torque (N·cm)**	**RPM**	**Torque (N·m)**	**ω (rad/s)**	**Power (w)**	**ρ (kg/m^3)**	**Cp**	**Cs**	**$\sigma_{windspeed}$ (± m/s)**	**σ_{Amp} (± A)**	**σω (± rad/s)**	**σT (± N·m)**	**σP (± w)**	**σP (± %)**
1	3.036	0	0.00	0%	0	36.1	0.000	3.780	0.000	1.292	0.0000	0.4784	0.0911	0.0000	0.1066	0.0000000	0.0000	0.0000
2	3.036	0.17	0.01	3%	0.25	36	0.003	3.770	0.009	1.292	0.0011	0.4770	0.0911	0.00415	0.1066	0.0000064	0.0002676	2.8393
3	3.036	0.42	0.02	7%	0.35	35.6	0.004	3.728	0.013	1.292	0.0016	0.4717	0.0911	0.00430	0.1066	0.0000066	0.0003736	2.8652
4	3.036	0.64	0.03	10%	0.4	34.9	0.004	3.655	0.015	1.292	0.0017	0.4625	0.0911	0.00445	0.1065	0.0000069	0.0004269	2.9204
5	3.036	0.73	0.04	14%	0.5	34.5	0.005	3.613	0.018	1.292	0.0022	0.4572	0.0911	0.00460	0.1065	0.0000071	0.0005332	2.9520
6	3.036	0.95	0.05	17%	0.65	33.8	0.007	3.540	0.023	1.292	0.0027	0.4479	0.0911	0.00475	0.1065	0.0000073	0.0006927	3.0107
7	3.036	1.17	0.06	21%	0.8	32.7	0.008	3.424	0.027	1.292	0.0033	0.4333	0.0911	0.00490	0.1064	0.0000075	0.0008518	3.1095
8	3.036	1.42	0.07	24%	1	31.5	0.010	3.299	0.033	1.292	0.0039	0.4174	0.0911	0.00505	0.1064	0.0000078	0.0010640	3.2255
9	3.036	1.64	0.08	28%	1.3	30.1	0.013	3.152	0.041	1.292	0.0049	0.3989	0.0911	0.00520	0.1063	0.0000080	0.0013820	3.3728
10	3.036	1.76	0.09	31%	1.55	29	0.016	3.037	0.047	1.292	0.0056	0.3843	0.0911	0.00535	0.1062	0.0000082	0.0016468	3.4987
11	3.036	2	0.10	34%	1.85	26.6	0.019	2.786	0.052	1.292	0.0061	0.3525	0.0911	0.00550	0.1061	0.0000085	0.0019632	3.8097
12	3.036	2.23	0.11	38%	2.3	0	0.023	0.000	0.000	1.292	0.0000	0.0000	0.0911	0.00565	0.1047	0.0000087	0.0000000	0.0000

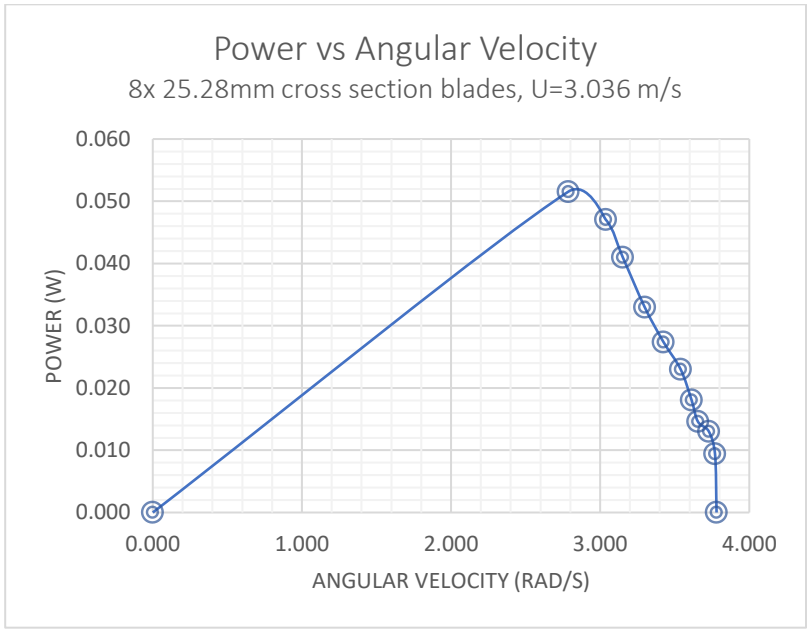
Power vs Angular Velocity
8x 25.28mm cross section blades, U=3.036 m/s
POWER (W)
0.060
0.050
0.040
0.030
0.020
0.010
0.000
0.000
1.000
2.000
3.000
4.000
ANGULAR VELOCITY (RAD/S)

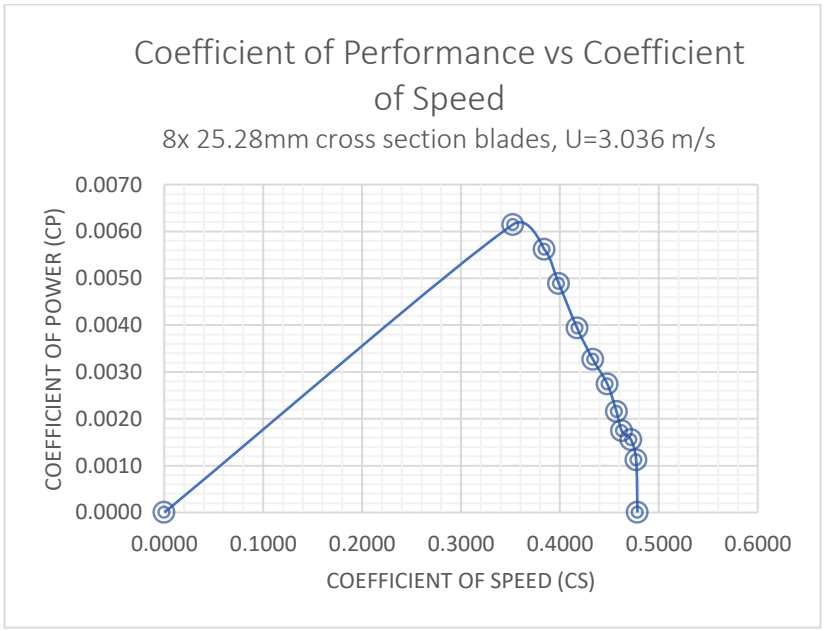
Coefficient of Performance vs Coefficient of Speed
8x 25.28mm cross section blades, U=3.036 m/s
COEFFICIENT OF POWER (CP)
0.0070
0.0060
0.0050
0.0040
0.0030
0.0020
0.0010
0.0000
0.0000
0.1000
0.2000
0.3000
0.4000
0.5000
0.6000
COEFFICIENT OF SPEED (CS)

Data for Rotor with Eight 25.28mm Square Blades

U=3.476 m/s

Recorded Data							Calculated Data						Uncertainty					
Run Number	**Windspeed (m/s)**	**Voltage (V)**	**Amperage (A)**	**% Max Current**	**Torque (N·cm)**	**RPM**	**Torque (N·m)**	**ω (rad/s)**	**Power (w)**	**ρ (kg/m^3)**	**Cp**	**Cs**	**$\sigma_{windspeed}$ (± m/s)**	**σ_{Amp} (± A)**	**σω (± rad/s)**	**σT (± N·m)**	**σP (± w)**	**σP (± %)**
1	3.476	0	0.00	0%	0	42.2	0.000	4.419	0.000	1.292	0.0000	0.4884	0.1043	0.0000	0.1069	0.0000000	0.0000	0.0000
2	3.476	0.18	0.01	3%	0.25	42	0.003	4.398	0.011	1.292	0.0009	0.4861	0.1043	0.00415	0.1069	0.0000064	0.0002677	2.4444
3	3.476	0.39	0.02	7%	0.35	41.8	0.004	4.377	0.015	1.292	0.0012	0.4838	0.1043	0.00430	0.1069	0.0000066	0.0003753	2.4497
4	3.476	0.54	0.03	10%	0.4	41.5	0.004	4.346	0.017	1.292	0.0014	0.4803	0.1043	0.00445	0.1069	0.0000069	0.0004281	2.4656
5	3.476	0.72	0.04	14%	0.5	40.9	0.005	4.283	0.021	1.292	0.0017	0.4734	0.1043	0.00460	0.1069	0.0000071	0.0005351	2.4990
6	3.476	0.94	0.05	17%	0.65	40	0.007	4.189	0.027	1.292	0.0022	0.4630	0.1043	0.00475	0.1068	0.0000073	0.0006949	2.5525
7	3.476	1.15	0.06	21%	0.8	39.4	0.008	4.126	0.033	1.292	0.0026	0.4560	0.1043	0.00490	0.1068	0.0000075	0.0008543	2.5898
8	3.476	1.37	0.07	24%	1	38.4	0.010	4.021	0.040	1.292	0.0032	0.4444	0.1043	0.00505	0.1067	0.0000078	0.0010676	2.6553
9	3.476	1.56	0.08	28%	1.3	37.3	0.013	3.906	0.051	1.292	0.0040	0.4317	0.1043	0.00520	0.1067	0.0000080	0.0013871	2.7317
10	3.476	1.84	0.09	31%	1.55	35.7	0.016	3.738	0.058	1.292	0.0046	0.4132	0.1043	0.00535	0.1066	0.0000082	0.0016524	2.8516
11	3.476	2.02	0.10	34%	1.85	34.6	0.019	3.623	0.067	1.292	0.0053	0.4005	0.1043	0.00550	0.1065	0.0000085	0.0019710	2.9405
12	3.476	2.19	0.11	38%	2.3	33.5	0.023	3.508	0.081	1.292	0.0064	0.3877	0.1043	0.00565	0.1065	0.0000087	0.0024490	3.0353
13	3.476	2.4	0.12	41%	2.6	31.3	0.026	3.278	0.085	1.292	0.0068	0.3623	0.1043	0.00580	0.1064	0.0000089	0.0027654	3.2451
14	3.476	2.58	0.13	45%	3.05	0	0.031	0.000	0.000	1.292	0.0000	0.0000	0.1043	0.00595	0.1047	0.0000092	0.0000000	0.0000

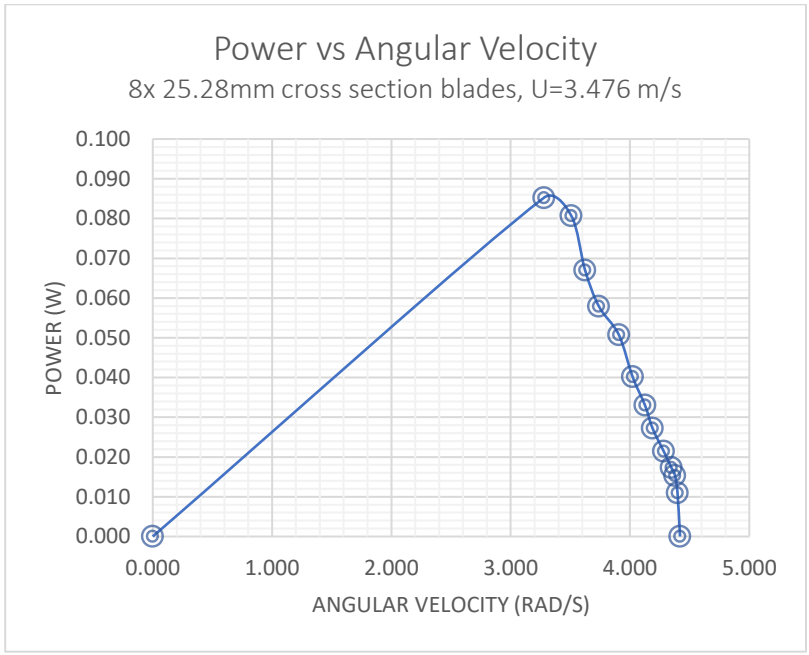
Power vs Angular Velocity
8x 25.28mm cross section blades, U=3.476 m/s
POWER (W)
0.100
0.090
0.080
0.070
0.060
0.050
0.040
0.030
0.020
0.010
0.000
0.000
1.000
2.000
3.000
4.000
5.000
ANGULAR VELOCITY (RAD/S)

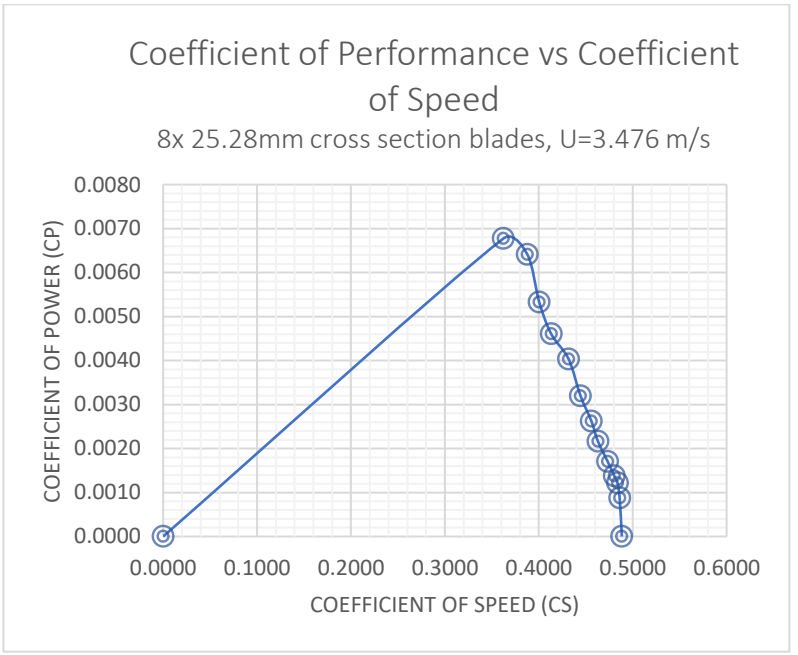
Coefficient of Performance vs Coefficient of Speed
8x 25.28mm cross section blades, U=3.476 m/s
COEFFICIENT OF POWER (CP)
0.0080
0.0070
0.0060
0.0050
0.0040
0.0030
0.0020
0.0010
0.0000
0.0000
0.1000
0.2000
0.3000
0.4000
0.5000
0.6000
COEFFICIENT OF SPEED (CS)

Data for Rotor with Eight 25.28mm Square Blades

U=3.958 m/s

Recorded Data							Calculated Data						Uncertainty					
Run Number	**Windspeed (m/s)**	**Voltage (V)**	**Amperage (A)**	**% Max Current**	**Torque (N·cm)**	**RPM**	**Torque (N·m)**	**ω (rad/s)**	**Power (w)**	**ρ (kg/m^3)**	**Cp**	**Cs**	**$\sigma_{windspeed}$ (± m/s)**	**σ_{Amp} (± A)**	**σω (± rad/s)**	**σT (± N·m)**	**σP (± w)**	**σP (± %)**
1	3.958	0	0.00	0%	0	48.5	0.000	5.079	0.000	1.292	0.0000	0.4930	0.1187	0.0000	0.1073	0.0000000	0.0000	0.0000
2	3.958	0.14	0.01	3%	0.25	48.2	0.003	5.047	0.013	1.292	0.0007	0.4899	0.1187	0.00415	0.1072	0.0000064	0.0002704	2.1400
3	3.958	0.35	0.02	7%	0.35	48.1	0.004	5.037	0.018	1.292	0.0009	0.4889	0.1187	0.00430	0.1072	0.0000066	0.0003768	2.1374
4	3.958	0.62	0.03	10%	0.4	47.8	0.004	5.006	0.020	1.292	0.0011	0.4859	0.1187	0.00445	0.1072	0.0000069	0.0004302	2.1489
5	3.958	0.72	0.04	14%	0.5	47.6	0.005	4.985	0.025	1.292	0.0013	0.4838	0.1187	0.00460	0.1072	0.0000071	0.0005372	2.1555
6	3.958	0.93	0.05	17%	0.65	46.8	0.007	4.901	0.032	1.292	0.0017	0.4757	0.1187	0.00475	0.1072	0.0000073	0.0006953	2.1896
7	3.958	1.27	0.06	21%	0.8	45.6	0.008	4.775	0.038	1.292	0.0021	0.4635	0.1187	0.00490	0.1071	0.0000075	0.0008562	2.2450
8	3.958	1.44	0.07	24%	1	45	0.010	4.712	0.047	1.292	0.0025	0.4574	0.1187	0.00505	0.1071	0.0000078	0.0010713	2.2736
9	3.958	1.59	0.08	28%	1.3	44.2	0.013	4.629	0.060	1.292	0.0032	0.4493	0.1187	0.00520	0.1070	0.0000080	0.0013919	2.3133
10	3.958	1.73	0.09	31%	1.55	43.4	0.016	4.545	0.070	1.292	0.0038	0.4411	0.1187	0.00535	0.1070	0.0000082	0.0016580	2.3547
11	3.958	1.97	0.10	34%	1.85	42.3	0.019	4.430	0.082	1.292	0.0044	0.4300	0.1187	0.00550	0.1069	0.0000085	0.0019765	2.4145
12	3.958	2.2	0.11	38%	2.3	40.7	0.023	4.262	0.098	1.292	0.0053	0.4137	0.1187	0.00565	0.1069	0.0000087	0.0024585	2.5073
13	3.958	2.39	0.12	41%	2.6	39.2	0.026	4.105	0.107	1.292	0.0057	0.3984	0.1187	0.00580	0.1068	0.0000089	0.0027732	2.6012
14	3.958	2.61	0.13	45%	3.05	38.1	0.031	3.990	0.122	1.292	0.0066	0.3873	0.1187	0.00595	0.1067	0.0000092	0.0032550	2.6748
15	3.958	2.83	0.14	48%	3.35	36	0.034	3.770	0.126	1.292	0.0068	0.3659	0.1187	0.00610	0.1066	0.0000094	0.0035714	2.8279
16	3.958	3.04	0.15	52%	3.8	33.8	0.038	3.540	0.135	1.292	0.0072	0.3436	0.1187	0.00625	0.1065	0.0000096	0.0040467	3.0087
17	3.958	3.25	0.16	55%	4.2	0	0.042	0.000	0.000	1.292	0.0000	0.0000	0.1187	0.00640	0.1047	0.0000099	0.0000	0.0000

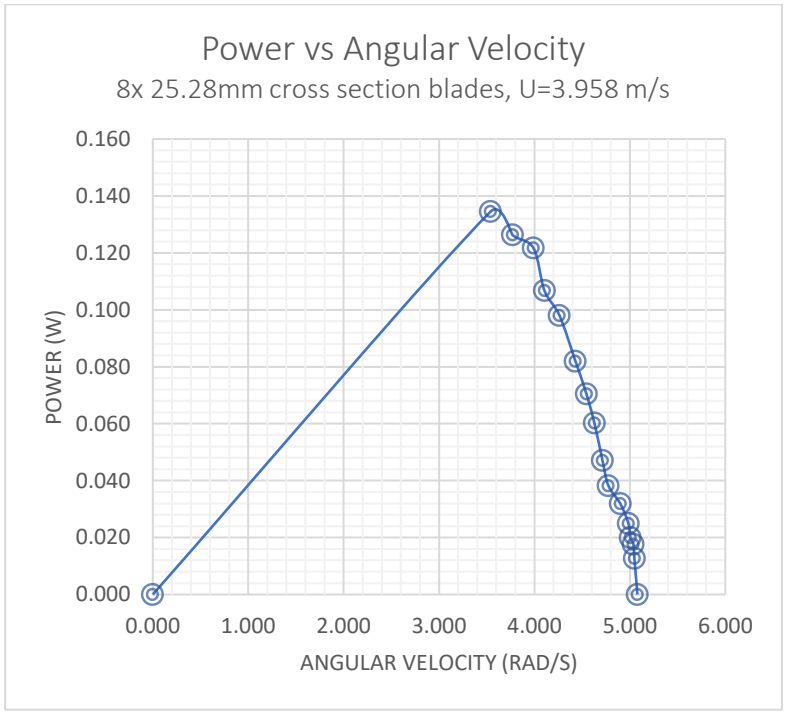
Power vs Angular Velocity
8x 25.28mm cross section blades, U=3.958 m/s
POWER (W)
0.160
0.140
0.120
0.100
0.080
0.060
0.040
0.020
0.000
0.000
1.000
2.000
3.000
4.000
5.000
6.000
ANGULAR VELOCITY (RAD/S)

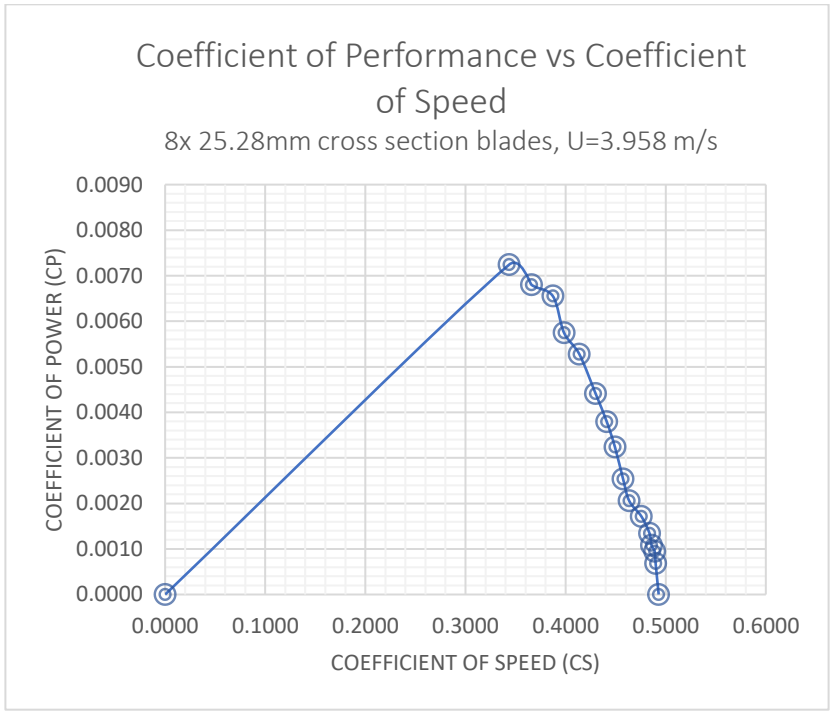
Coefficient of Performance vs Coefficient of Speed
8x 25.28mm cross section blades, U=3.958 m/s
COEFFICIENT OF POWER (CP)
0.0090
0.0080
0.0070
0.0060
0.0050
0.0040
0.0030
0.0020
0.0010
0.0000
0.0000
0.1000
0.2000
0.3000
0.4000
0.5000
0.6000
COEFFICIENT OF SPEED (CS)

Data for Rotor with Eight 25.28mm Square Blades

U=4.432 m/s

Recorded Data							Calculated Data						Uncertainty					
Run Number	**Windspeed (m/s)**	**Voltage (V)**	**Amperage (A)**	**% Max Current**	**Torque (N·cm)**	**RPM**	**Torque (N·m)**	**ω (rad/s)**	**Power (w)**	**ρ (kg/m^3)**	**Cp**	**Cs**	**$\sigma_{windspeed}$ (± m/s)**	**σ Amp (± A)**	**σω (± rad/s)**	**σT (± N·m)**	**σP (± w)**	**σP (± %)**
1	4.432	0	0.00	0%	0	55.6	0.000	5.822	0.000	1.292	0.0000	0.5047	0.1330	0.0000	0.1076	0.0000000	0.0000	0.0000
2	4.432	0.21	0.01	3%	0.25	55.2	0.003	5.781	0.014	1.292	0.0006	0.5011	0.1330	0.00415	0.1076	0.0000064	0.0002715	1.8791
3	4.432	0.41	0.02	7%	0.35	54.6	0.004	5.718	0.020	1.292	0.0008	0.4956	0.1330	0.00430	0.1076	0.0000066	0.0003784	1.8910
4	4.432	0.63	0.03	10%	0.4	54.3	0.004	5.686	0.023	1.292	0.0009	0.4929	0.1330	0.00445	0.1076	0.0000069	0.0004321	1.8994
5	4.432	0.77	0.04	14%	0.5	54	0.005	5.655	0.028	1.292	0.0011	0.4902	0.1330	0.00460	0.1075	0.0000071	0.0005392	1.9071
6	4.432	0.95	0.05	17%	0.65	53.2	0.007	5.571	0.036	1.292	0.0014	0.4829	0.1330	0.00475	0.1075	0.0000073	0.0006997	1.9330
7	4.432	1.17	0.06	21%	0.8	52.6	0.008	5.508	0.044	1.292	0.0017	0.4775	0.1330	0.00490	0.1075	0.0000075	0.0008680	1.9534
8	4.432	1.35	0.07	24%	1	52.1	0.010	5.456	0.055	1.292	0.0021	0.4729	0.1330	0.00505	0.1074	0.0000078	0.0010753	1.9709
9	4.432	1.54	0.08	28%	1.3	51.3	0.013	5.372	0.070	1.292	0.0027	0.4657	0.1330	0.00520	0.1074	0.0000080	0.0013969	2.0003
10	4.432	1.76	0.09	31%	1.55	50.2	0.016	5.257	0.081	1.292	0.0031	0.4557	0.1330	0.00535	0.1073	0.0000082	0.0016646	2.0427
11	4.432	1.98	0.10	34%	1.85	49.2	0.019	5.152	0.095	1.292	0.0037	0.4466	0.1330	0.00550	0.1073	0.0000085	0.0019845	2.0830
12	4.432	2.18	0.11	38%	2.3	48.1	0.023	5.037	0.116	1.292	0.0044	0.4366	0.1330	0.00565	0.1072	0.0000087	0.0024668	2.1293
13	4.432	2.38	0.12	41%	2.6	47.1	0.026	4.932	0.128	1.292	0.0049	0.4275	0.1330	0.00580	0.1072	0.0000089	0.0027871	2.1734
14	4.432	2.59	0.13	45%	3.05	45.7	0.031	4.786	0.146	1.292	0.0056	0.4148	0.1330	0.00595	0.1071	0.0000092	0.0032723	2.2384
15	4.432	2.86	0.14	48%	3.35	43.9	0.034	4.597	0.154	1.292	0.0059	0.3985	0.1330	0.00610	0.1070	0.0000094	0.0035853	2.3281
16	4.432	3.07	0.15	52%	3.8	42.5	0.038	4.451	0.169	1.292	0.0065	0.3858	0.1330	0.00625	0.1069	0.0000096	0.0040641	2.4031
17	4.432	3.35	0.16	55%	4.2	39.8	0.042	4.168	0.175	1.292	0.0067	0.3613	0.1330	0.00640	0.1068	0.0000099	0.0044859	2.5627
18	4.432	3.57	0.17	59%	4.85	36.6	0.049	3.833	0.186	1.292	0.0071	0.3322	0.1330	0.00655	0.1066	0.0000101	0.0051720	2.7823

19	4.432	3.76	0.18	62%	5.3	0	0.053	0.000	0.00 0	1.292	0.00 00	0.00 00	0.133 0	0.006 70	0.10 47	0.00001 03	0.0000	0.00 00

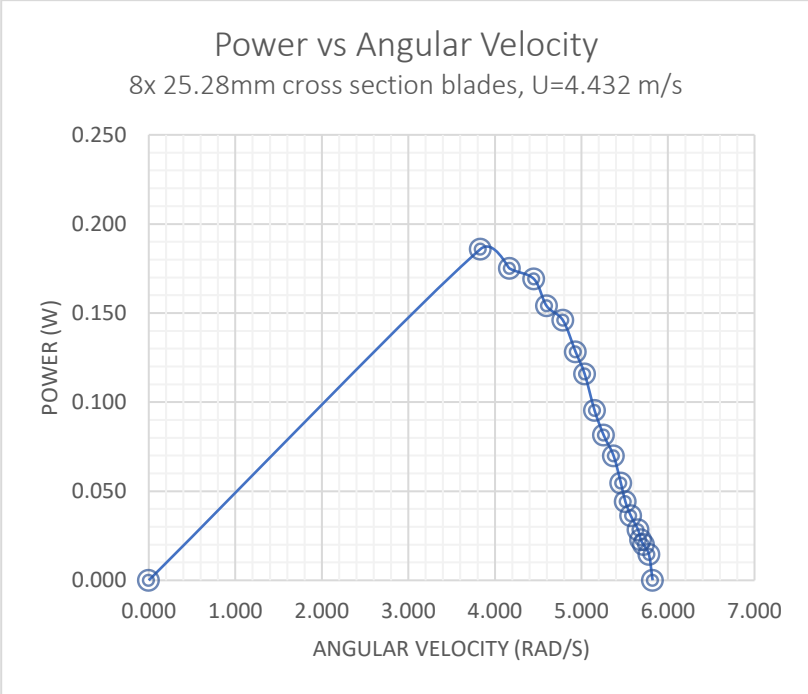

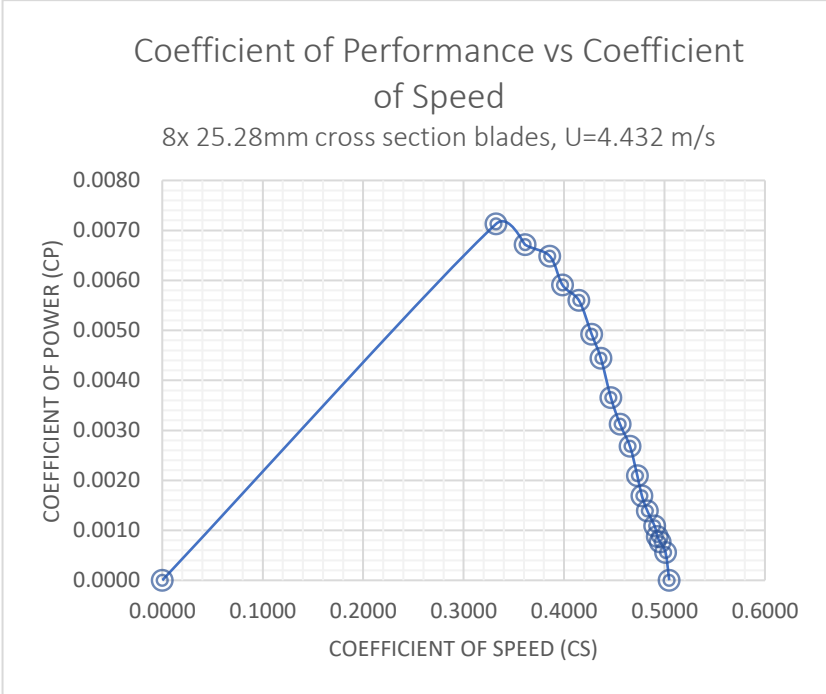

Data for Rotor with Eight 25.28mm Square Blades

U=4.992 m/s

Recorded Data							Calculated Data						Uncertainty					
Run Number	**Windspeed (m/s)**	**Voltage (V)**	**Amperage (A)**	**% Max Current**	**Torque (N·cm)**	**RPM**	**Torque (N·m)**	**ω (rad/s)**	**Power (w)**	**ρ (kg/m^3)**	**Cp**	**Cs**	**$\sigma_{windspeed}$ (± m/s)**	**σ_{Amp} (± A)**	**σω (± rad/s)**	**σT (± N·m)**	**σP (± w)**	**σP (± %)**
1	4.992	0	0.00	0%	0	62.8	0.000	6.576	0.000	1.292	0.0000	0.5061	0.1498	0.0000	0.1080	0.000000	0.0000	0.0000
2	4.992	0.16	0.01	3%	0.25	62.6	0.003	6.555	0.016	1.292	0.0004	0.5045	0.1498	0.00415	0.1080	0.000006	0.000273	1.6672
3	4.992	0.38	0.02	7%	0.35	62.6	0.004	6.555	0.023	1.292	0.0006	0.5045	0.1498	0.00430	0.1080	0.000006	0.000380	1.6583
4	4.992	0.61	0.03	10%	0.4	61.9	0.004	6.482	0.026	1.292	0.0007	0.4989	0.1498	0.00445	0.1080	0.000006	0.000434	1.6743
5	4.992	0.71	0.04	14%	0.5	61.7	0.005	6.461	0.032	1.292	0.0009	0.4972	0.1498	0.00460	0.1080	0.000007	0.000541	1.6767
6	4.992	0.92	0.05	17%	0.65	61.5	0.007	6.440	0.042	1.292	0.0011	0.4956	0.1498	0.00475	0.1079	0.000007	0.000703	1.6798
7	4.992	1.1	0.06	21%	0.8	60.9	0.008	6.377	0.051	1.292	0.0014	0.4908	0.1498	0.00490	0.1079	0.000007	0.000864	1.6947
8	4.992	1.44	0.07	24%	1	59.6	0.010	6.241	0.062	1.292	0.0017	0.4803	0.1498	0.00505	0.1078	0.000007	0.001079	1.7296
9	4.992	1.62	0.08	28%	1.3	59.4	0.013	6.220	0.081	1.292	0.0022	0.4787	0.1498	0.00520	0.1078	0.000008	0.001402	1.7346
10	4.992	1.81	0.09	31%	1.55	58.5	0.016	6.126	0.095	1.292	0.0025	0.4715	0.1498	0.00535	0.1078	0.000008	0.001671	1.7602
11	4.992	1.98	0.10	34%	1.85	57.9	0.019	6.063	0.112	1.292	0.0030	0.4666	0.1498	0.00550	0.1078	0.000008	0.001994	1.7777
12	4.992	2.21	0.11	38%	2.3	56.8	0.023	5.948	0.137	1.292	0.0037	0.4578	0.1498	0.00565	0.1077	0.000008	0.002477	1.8110
13	4.992	2.35	0.12	41%	2.6	55.8	0.026	5.843	0.152	1.292	0.0041	0.4497	0.1498	0.00580	0.1076	0.000008	0.002799	1.8424
14	4.992	2.57	0.13	45%	3.05	55.2	0.031	5.781	0.176	1.292	0.0047	0.4449	0.1498	0.00595	0.1076	0.000009	0.003282	1.8618
15	4.992	2.86	0.14	48%	3.35	53.4	0.034	5.592	0.187	1.292	0.0050	0.4304	0.1498	0.00610	0.1075	0.000009	0.003602	1.9229
16	4.992	3.05	0.15	52%	3.8	52.6	0.038	5.508	0.209	1.292	0.0056	0.4239	0.1498	0.00625	0.1075	0.000009	0.004084	1.9513
17	4.992	3.23	0.16	55%	4.2	51.4	0.042	5.383	0.226	1.292	0.0061	0.4142	0.1498	0.00640	0.1074	0.000009	0.004511	1.9957
18	4.992	3.44	0.17	59%	4.85	50.3	0.049	5.267	0.255	1.292	0.0069	0.4054	0.1498	0.00655	0.1074	0.000010	0.005206	2.0382

19	4.992	3.67	0.18	62%	5.3	48.6	0.053	5.089	0.270	1.292	0.0072	0.3917	0.1498	0.00670	0.1073	0.0000103	0.00568526	2.1077
20	4.992	3.88	0.19	66%	5.85	46.9	0.059	4.911	0.287	1.292	0.0077	0.3780	0.1498	0.00685	0.1072	0.0000105	0.00626998	2.1823
21	4.992	4.08	0.20	69%	6.3	45.3	0.063	4.744	0.299	1.292	0.0080	0.3651	0.1498	0.00700	0.1071	0.0000108	0.00674697	2.2576
22	4.992	4.28	0.21	72%	6.8	43	0.068	4.503	0.306	1.292	0.0082	0.3465	0.1498	0.00715	0.1070	0.0000110	0.00727421	2.3756
23	4.992	4.52	0.22	76%	7.45	0	0.075	0.000	0.000	1.292	0.0000	0.0000	0.1498	0.00730	0.1047	0.0000112	0.0000	0.0000

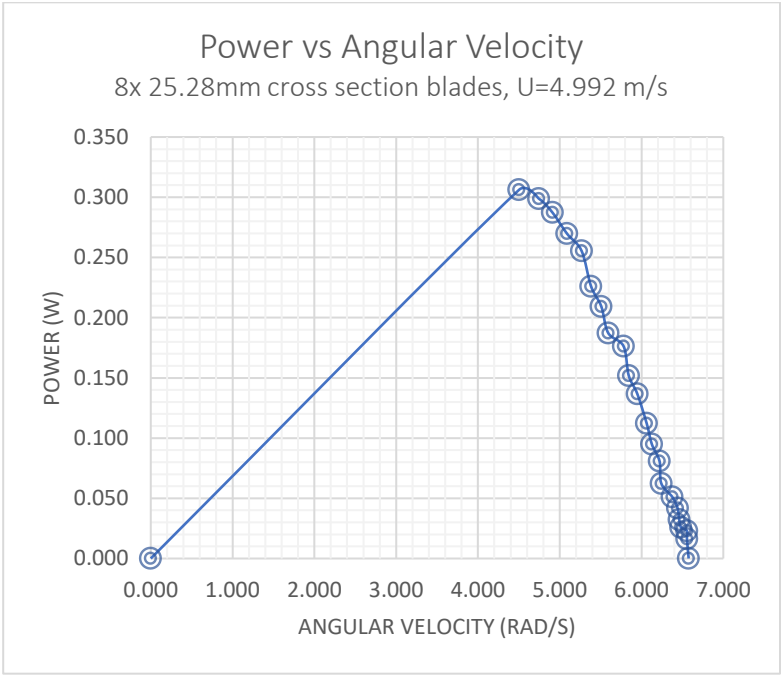
Power vs Angular Velocity
8x 25.28mm cross section blades, U=4.992 m/s
POWER (W)
0.350
0.300
0.250
0.200
0.150
0.100
0.050
0.000
0.000
1.000
2.000
3.000
4.000
5.000
6.000
7.000
ANGULAR VELOCITY (RAD/S)

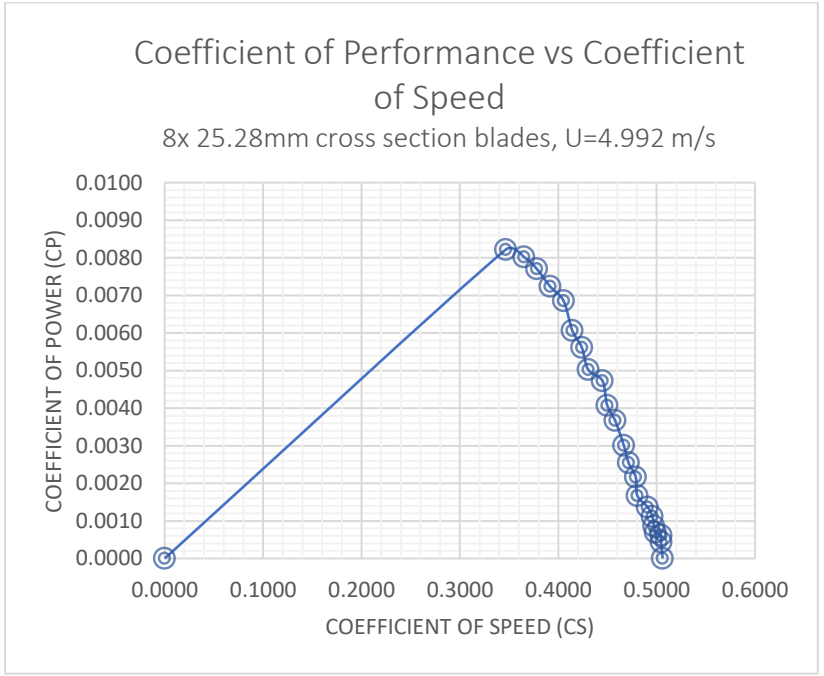
Coefficient of Performance vs Coefficient of Speed
8x 25.28mm cross section blades, U=4.992 m/s
COEFFICIENT OF POWER (CP)
0.0100
0.0090
0.0080
0.0070
0.0060
0.0050
0.0040
0.0030
0.0020
0.0010
0.0000
0.0000
0.1000
0.2000
0.3000
0.4000
0.5000
0.6000
COEFFICIENT OF SPEED (CS)

Data for Rotor with Eight 25.28mm Square Blades

U=5.482 m/s

Recorded Data							Calculated Data						Uncertainty					
Run Number	**Windspeed (m/s)**	**Voltage (V)**	**Amperage (A)**	**% Max Current**	**Torque (N·cm)**	**RPM**	**Torque (N·m)**	**ω (rad/s)**	**Power (w)**	**ρ (kg/m^3)**	**Cp**	**Cs**	**$\sigma_{windspeed}$ (± m/s)**	**σ_{Amp} (± A)**	**σω (± rad/s)**	**σT (± N·m)**	**σP (± w)**	**σP (± %)**
1	5.482	0	0.00	0%	0	69.1	0.000	7.236	0.000	1.292	0.0000	0.5071	0.1645	0.0000	0.1083	0.000000	0.0000	0.0000
2	5.482	0.16	0.01	3%	0.25	68.5	0.003	7.173	0.018	1.292	0.0004	0.5027	0.1645	0.00415	0.1083	0.000006	0.000274	1.5313
3	5.482	0.43	0.02	7%	0.35	68.3	0.004	7.152	0.025	1.292	0.0005	0.5012	0.1645	0.00430	0.1083	0.000006	0.000381	1.5259
4	5.482	0.65	0.03	10%	0.4	68.1	0.004	7.131	0.029	1.292	0.0006	0.4998	0.1645	0.00445	0.1083	0.000006	0.000435	1.5281
5	5.482	0.76	0.04	14%	0.5	67.5	0.005	7.069	0.035	1.292	0.0007	0.4954	0.1645	0.00460	0.1083	0.000007	0.000543	1.5380
6	5.482	0.93	0.05	17%	0.65	67.2	0.007	7.037	0.046	1.292	0.0009	0.4932	0.1645	0.00475	0.1082	0.000007	0.000705	1.5422
7	5.482	1.24	0.06	21%	0.8	66.3	0.008	6.943	0.056	1.292	0.0011	0.4866	0.1645	0.00490	0.1082	0.000007	0.000867	1.5611
8	5.482	1.42	0.07	24%	1	66.3	0.010	6.943	0.069	1.292	0.0014	0.4866	0.1645	0.00505	0.1082	0.000007	0.001083	1.5602
9	5.482	1.66	0.08	28%	1.3	65.2	0.013	6.828	0.089	1.292	0.0018	0.4785	0.1645	0.00520	0.1081	0.000008	0.001406	1.5849
10	5.482	1.89	0.09	31%	1.55	64.1	0.016	6.713	0.104	1.292	0.0021	0.4704	0.1645	0.00535	0.1081	0.000008	0.001676	1.6109
11	5.482	2.09	0.10	34%	1.85	63.5	0.019	6.650	0.123	1.292	0.0025	0.4660	0.1645	0.00550	0.1080	0.000008	0.001999	1.6254
12	5.482	2.28	0.11	38%	2.3	62.4	0.023	6.535	0.150	1.292	0.0030	0.4579	0.1645	0.00565	0.1080	0.000008	0.002484	1.6530
13	5.482	2.4	0.12	41%	2.6	62.3	0.026	6.524	0.170	1.292	0.0034	0.4572	0.1645	0.00580	0.1080	0.000008	0.002808	1.6555
14	5.482	2.62	0.13	45%	3.05	61.6	0.031	6.451	0.197	1.292	0.0040	0.4521	0.1645	0.00595	0.1079	0.000009	0.003292	1.6736
15	5.482	2.82	0.14	48%	3.35	60.6	0.034	6.346	0.213	1.292	0.0043	0.4447	0.1645	0.00610	0.1079	0.000009	0.003614	1.7004
16	5.482	3.06	0.15	52%	3.8	59.1	0.038	6.189	0.235	1.292	0.0048	0.4337	0.1645	0.00625	0.1078	0.000009	0.004097	1.7422
17	5.482	3.26	0.16	55%	4.2	57.4	0.042	6.011	0.252	1.292	0.0051	0.4212	0.1645	0.00640	0.1077	0.000009	0.004524	1.7923
18	5.482	3.42	0.17	59%	4.85	57.2	0.049	5.990	0.291	1.292	0.0059	0.4198	0.1645	0.00655	0.1077	0.000010	0.005224	1.7984

19	5.482	3.67	0.18	62%	5.3	55.7	0.053	5.833	0.309	1.292	0.0063	0.4088	0.1645	0.00670	0.1076	0.0000103	0.00570504	1.8454
20	5.482	3.84	0.19	66%	5.85	54.5	0.059	5.707	0.334	1.292	0.0068	0.4000	0.1645	0.00685	0.1076	0.0000105	0.00629333	1.8849
21	5.482	4.07	0.20	69%	6.3	52.9	0.063	5.540	0.349	1.292	0.0071	0.3882	0.1645	0.00700	0.1075	0.0000108	0.00677211	1.9404
22	5.482	4.3	0.21	72%	6.8	51.5	0.068	5.393	0.367	1.292	0.0074	0.3779	0.1645	0.00715	0.1074	0.0000110	0.00730455	1.9918
23	5.482	4.56	0.22	76%	7.45	49.5	0.075	5.184	0.386	1.292	0.0078	0.3633	0.1645	0.00730	0.1073	0.0000112	0.00799492	2.0703
24	5.482	4.77	0.23	79%	7.85	46.8	0.079	4.901	0.385	1.292	0.0078	0.3435	0.1645	0.00745	0.1072	0.0000115	0.00841305	2.1868
25	5.482	4.96	0.24	83%	8.45	0	0.085	0.000	0.000	1.292	0.0000	0.0000	0.1645	0.00760	0.1047	0.0000117	0.0000	0.0000

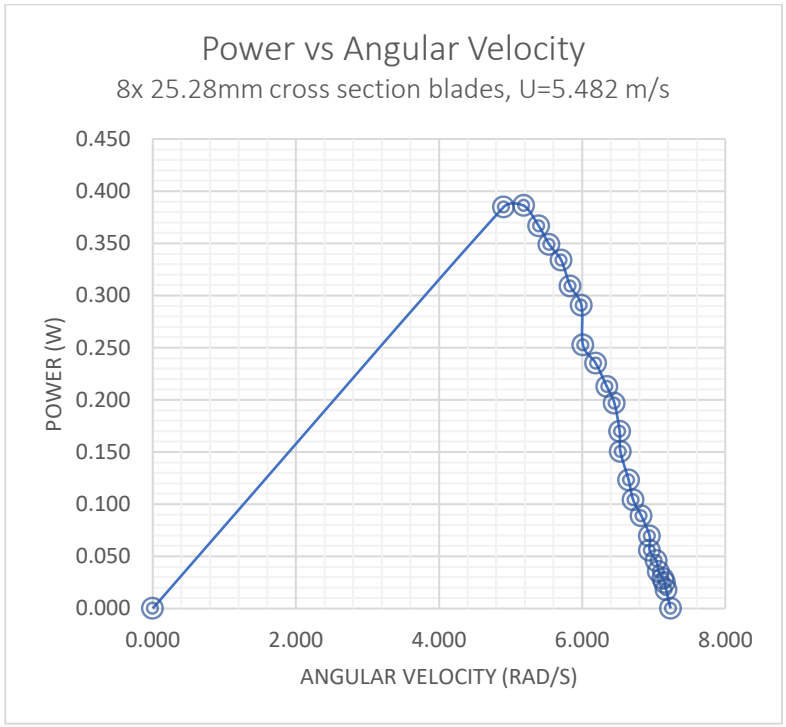
Power vs Angular Velocity
8x 25.28mm cross section blades, U=5.482 m/s
POWER (W)
0.450
0.400
0.350
0.300
0.250
0.200
0.150
0.100
0.050
0.000
0.000
2.000
4.000
6.000
8.000
ANGULAR VELOCITY (RAD/S)

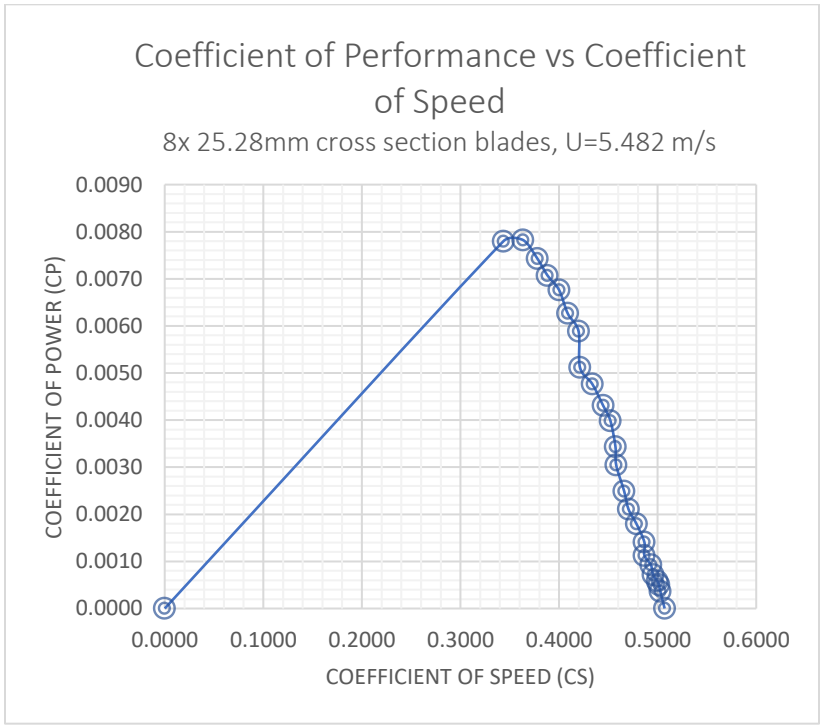
Coefficient of Performance vs Coefficient of Speed
8x 25.28mm cross section blades, U=5.482 m/s
COEFFICIENT OF POWER (CP)
0.0090
0.0080
0.0070
0.0060
0.0050
0.0040
0.0030
0.0020
0.0010
0.0000
0.0000
0.1000
0.2000
0.3000
0.4000
0.5000
0.6000
COEFFICIENT OF SPEED (CS)

Data for Rotor with Eight 25.28mm Square Blades

U=5.870 m/s

Recorded Data							Calculated Data						Uncertainty					
Run Number	**Windspeed (m/s)**	**Voltage (V)**	**Amperage (A)**	**% Max Current**	**Torque (N·cm)**	**RPM**	**Torque (N·m)**	**ω (rad/s)**	**Power (w)**	**ρ (kg/m^3)**	**Cp**	**Cs**	**$\sigma_{windspeed}$ (± m/s)**	**σ_{Amp} (± A)**	**σω (± rad/s)**	**σT (± N·m)**	**σP (± w)**	**σP (± %)**
1	5.87	0	0.00	0%	0	74.8	0.000	7.833	0.000	1.292	0.0000	0.5127	0.1761	0.0000	0.1086	0.0000000	0.0000	0.0000
2	5.87	0.17	0.01	3%	0.25	74.1	0.003	7.760	0.019	1.292	0.0003	0.5079	0.1761	0.00415	0.1086	0.0000064	0.0002759	1.4227
3	5.87	0.4	0.02	7%	0.35	73.9	0.004	7.739	0.027	1.292	0.0004	0.5065	0.1761	0.00430	0.1086	0.0000066	0.0003835	1.4159
4	5.87	0.62	0.03	10%	0.4	73.4	0.004	7.686	0.031	1.292	0.0005	0.5031	0.1761	0.00445	0.1086	0.0000069	0.0004373	1.4228
5	5.87	0.83	0.04	14%	0.5	73.2	0.005	7.665	0.038	1.292	0.0006	0.5017	0.1761	0.00460	0.1086	0.0000071	0.0005457	1.4232
6	5.87	0.96	0.05	17%	0.65	73.2	0.007	7.665	0.050	1.292	0.0008	0.5017	0.1761	0.00475	0.1086	0.0000073	0.0007082	1.4206
7	5.87	1.17	0.06	21%	0.8	72.7	0.008	7.613	0.061	1.292	0.0010	0.4983	0.1761	0.00490	0.1085	0.0000075	0.0008711	1.4286
8	5.87	1.38	0.07	24%	1	72	0.010	7.540	0.075	1.292	0.0012	0.4935	0.1761	0.00505	0.1085	0.0000078	0.0010864	1.4410
9	5.87	1.62	0.08	28%	1.3	71.4	0.013	7.477	0.097	1.292	0.0016	0.4893	0.1761	0.00520	0.1085	0.0000080	0.0014112	1.4519
10	5.87	1.78	0.09	31%	1.55	70.1	0.016	7.341	0.114	1.292	0.0019	0.4804	0.1761	0.00535	0.1084	0.0000082	0.0016814	1.4775
11	5.87	1.97	0.10	34%	1.85	69.7	0.019	7.299	0.135	1.292	0.0022	0.4777	0.1761	0.00550	0.1084	0.0000085	0.0020057	1.4854
12	5.87	2.18	0.11	38%	2.3	68.6	0.023	7.184	0.165	1.292	0.0027	0.4702	0.1761	0.00565	0.1083	0.0000087	0.0024919	1.5082
13	5.87	2.42	0.12	41%	2.6	67.7	0.026	7.090	0.184	1.292	0.0030	0.4640	0.1761	0.00580	0.1083	0.0000089	0.0028159	1.5275
14	5.87	2.67	0.13	45%	3.05	66.8	0.031	6.995	0.213	1.292	0.0035	0.4578	0.1761	0.00595	0.1082	0.0000092	0.0033012	1.5473
15	5.87	2.85	0.14	48%	3.35	66.1	0.034	6.922	0.232	1.292	0.0038	0.4530	0.1761	0.00610	0.1082	0.0000094	0.0036264	1.5631
16	5.87	3.07	0.15	52%	3.8	65.1	0.038	6.817	0.259	1.292	0.0043	0.4462	0.1761	0.00625	0.1081	0.0000096	0.0041094	1.5863
17	5.87	3.26	0.16	55%	4.2	63.9	0.042	6.692	0.281	1.292	0.0046	0.4379	0.1761	0.00640	0.1081	0.0000099	0.0045392	1.6151
18	5.87	3.5	0.17	59%	4.85	62.8	0.049	6.576	0.319	1.292	0.0053	0.4304	0.1761	0.00655	0.1080	0.0000101	0.0052381	1.6425

19	5.87	3.68	0.18	62%	5.3	61.5	0.053	6.440	0.341	1.292	0.0056	0.4215	0.1761	0.00670	0.1079	0.0000103	0.00572120	1.6761
20	5.87	3.87	0.19	66%	5.85	60.8	0.059	6.367	0.372	1.292	0.0061	0.4167	0.1761	0.00685	0.1079	0.0000105	0.00631270	1.6948
21	5.87	4.08	0.20	69%	6.3	60	0.063	6.283	0.396	1.292	0.0065	0.4112	0.1761	0.00700	0.1079	0.0000108	0.00679560	1.7168
22	5.87	4.28	0.21	72%	6.8	58.5	0.068	6.126	0.417	1.292	0.0069	0.4009	0.1761	0.00715	0.1078	0.0000110	0.00732954	1.7595
23	5.87	4.48	0.22	76%	7.45	57.2	0.075	5.990	0.446	1.292	0.0074	0.3920	0.1761	0.00730	0.1077	0.0000112	0.00802503	1.7983
24	5.87	4.7	0.23	79%	7.85	55.8	0.079	5.843	0.459	1.292	0.0076	0.3824	0.1761	0.00745	0.1076	0.0000115	0.00845012	1.8422
25	5.87	4.96	0.24	83%	8.45	53.9	0.085	5.644	0.477	1.292	0.0079	0.3694	0.1761	0.00760	0.1075	0.0000117	0.00908754	1.9053
26	5.87	5.29	0.25	86%	9	50.8	0.090	5.320	0.479	1.292	0.0079	0.3482	0.1761	0.00775	0.1074	0.0000119	0.00966438	2.0185
27	5.87	5.49	0.26	90%	9.5	0	0.095	0.000	0.000	1.292	0.0000	0.0000	0.1761	0.00790	0.1047	0.0000122	0.0000	0.0000

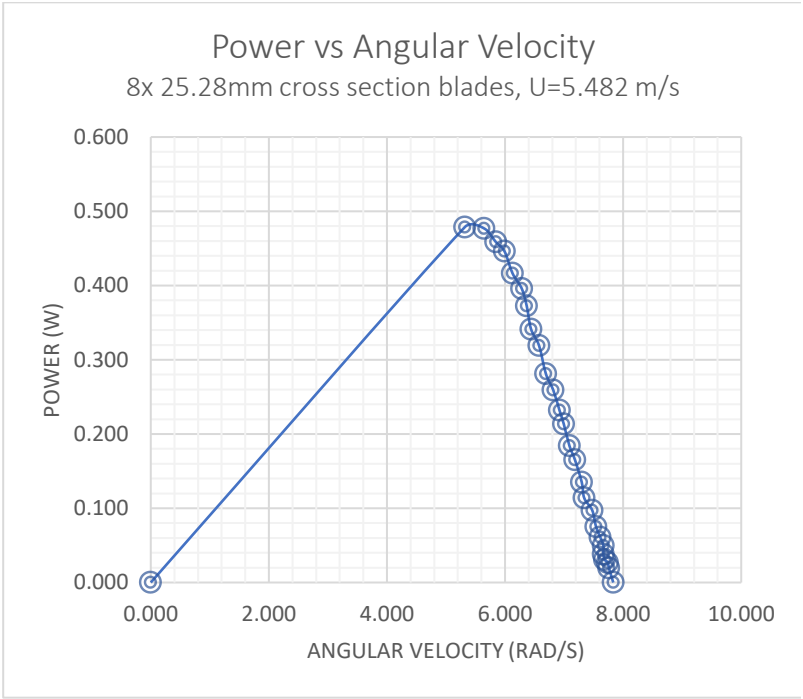
Power vs Angular Velocity
8x 25.28mm cross section blades, U=5.482 m/s
POWER (W)
0.600
0.500
0.400
0.300
0.200
0.100
0.000
0.000
2.000
4.000
6.000
8.000
10.000
ANGULAR VELOCITY (RAD/S)

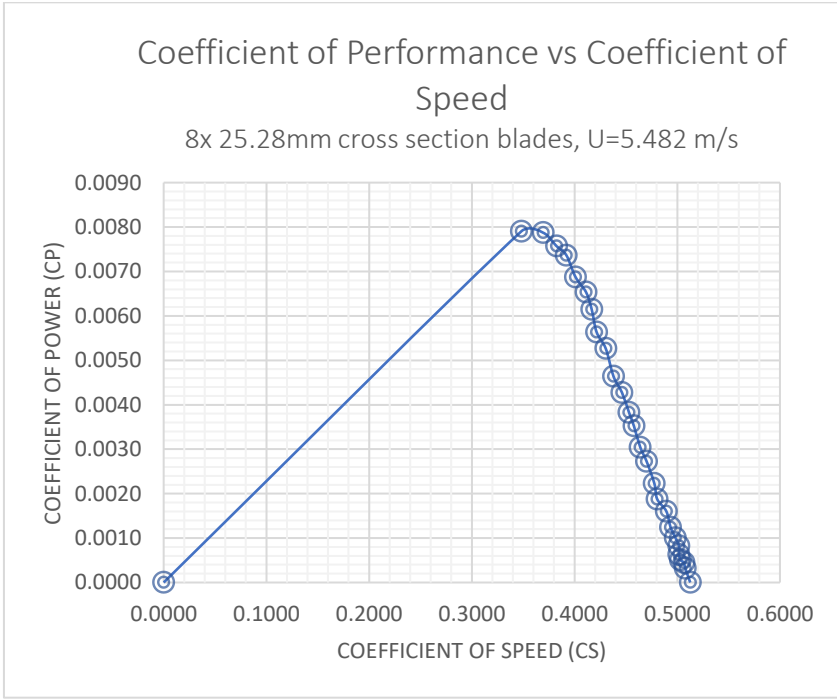
Coefficient of Performance vs Coefficient of Speed
8x 25.28mm cross section blades, U=5.482 m/s
COEFFICIENT OF POWER (CP)
0.0090
0.0080
0.0070
0.0060
0.0050
0.0040
0.0030
0.0020
0.0010
0.0000
0.0000
0.1000
0.2000
0.3000
0.4000
0.5000
0.6000
COEFFICIENT OF SPEED (CS)

C3. Rotor with Four 50.44mm Square Blades

Data for Rotor with Four 50.44mm Square Blades

U=5.990 m/s

Recorded Data							Calculated Data						Uncertainty					
Run Number	**Windspeed (m/s)**	**Voltage (V)**	**Amperage (A)**	**% Max Current**	**Torque (N·cm)**	**RPM**	**Torque (N·m)**	**ω (rad/s)**	**Power (w)**	**ρ (kg/m^3)**	**Cp**	**Cs**	**$\sigma_{windspeed}$ (± m/s)**	**σ_{Amp} (± A)**	**σω (± rad/s)**	**σT (± N·m)**	**σP (± w)**	**σP (± %)**
1	5.99	0	0.00	0%	0	67.8	0.000	7.100	0.000	1.292	0.0000	0.4554	0.1797	0.0000	0.1083	0.0000000	0.0000	0.0000
2	5.99	0.16	0.01	3%	0.25	67.5	0.003	7.069	0.018	1.292	0.0003	0.4534	0.1797	0.00415	0.1083	0.0000064	0.0002743	1.5527
3	5.99	0.39	0.02	7%	0.35	65.8	0.004	6.891	0.024	1.292	0.0004	0.4419	0.1797	0.00430	0.1082	0.0000066	0.0003813	1.5811
4	5.99	0.6	0.03	10%	0.4	65.2	0.004	6.828	0.027	1.292	0.0004	0.4379	0.1797	0.00445	0.1081	0.0000069	0.0004350	1.5930
5	5.99	0.75	0.04	14%	0.5	64.7	0.005	6.775	0.034	1.292	0.0005	0.4345	0.1797	0.00460	0.1081	0.0000071	0.0005426	1.6019
6	5.99	1.01	0.05	17%	0.65	63.3	0.007	6.629	0.043	1.292	0.0007	0.4251	0.1797	0.00475	0.1080	0.0000073	0.0007038	1.6337
7	5.99	1.21	0.06	21%	0.8	61.9	0.008	6.482	0.052	1.292	0.0008	0.4157	0.1797	0.00490	0.1080	0.0000075	0.0008650	1.6682
8	5.99	1.41	0.07	24%	1	58.4	0.010	6.116	0.061	1.292	0.0009	0.3922	0.1797	0.00505	0.1078	0.0000078	0.0010782	1.7640
9	5.99	1.56	0.08	28%	1.3	57.5	0.013	6.021	0.078	1.292	0.0012	0.3862	0.1797	0.00520	0.1077	0.0000080	0.0014013	1.7902
10	5.99	1.73	0.09	31%	1.55	56.8	0.016	5.948	0.092	1.292	0.0014	0.3815	0.1797	0.00535	0.1077	0.0000082	0.0016697	1.8113
11	5.99	1.99	0.10	34%	1.85	51.5	0.019	5.393	0.100	1.292	0.0015	0.3459	0.1797	0.00550	0.1074	0.0000085	0.0019873	1.9923
12	5.99	2.14	0.11	38%	2.3	47.8	0.023	5.006	0.115	1.292	0.0018	0.3210	0.1797	0.00565	0.1072	0.0000087	0.0024665	2.1424
13	5.99	2.39	0.12	41%	2.6	44.5	0.026	4.660	0.121	1.292	0.0019	0.2989	0.1797	0.00580	0.1070	0.0000089	0.0027836	2.2974
14	5.99	2.6	0.13	45%	3.05	0	0.031	0.000	0.000	1.292	0.0000	0.0000	0.1797	0.00595	0.1047	0.0000092	0.0000	0.0000

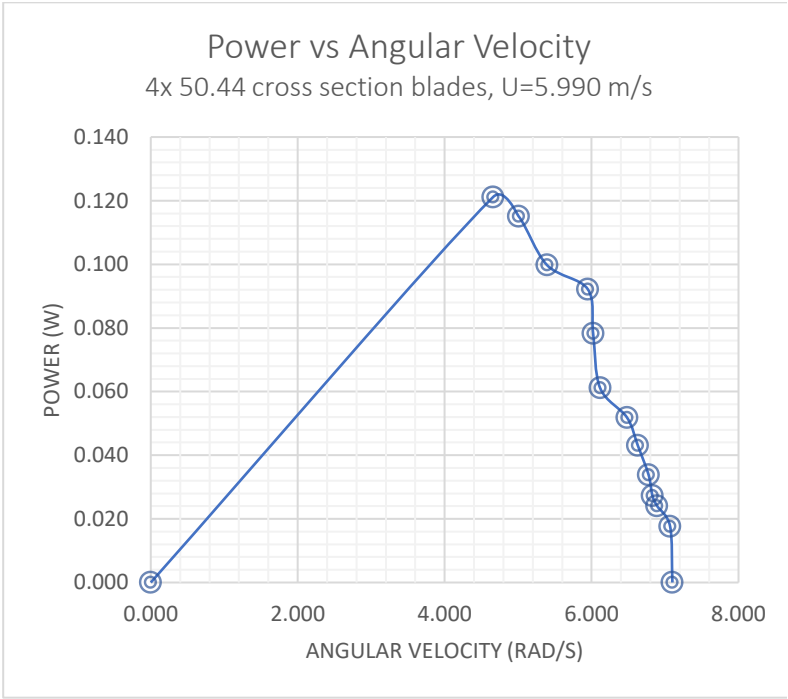
Power vs Angular Velocity
4x 50.44 cross section blades, U=5.990 m/s
POWER (W)
0.140
0.120
0.100
0.080
0.060
0.040
0.020
0.000
0.000
2.000
4.000
6.000
8.000
ANGULAR VELOCITY (RAD/S)

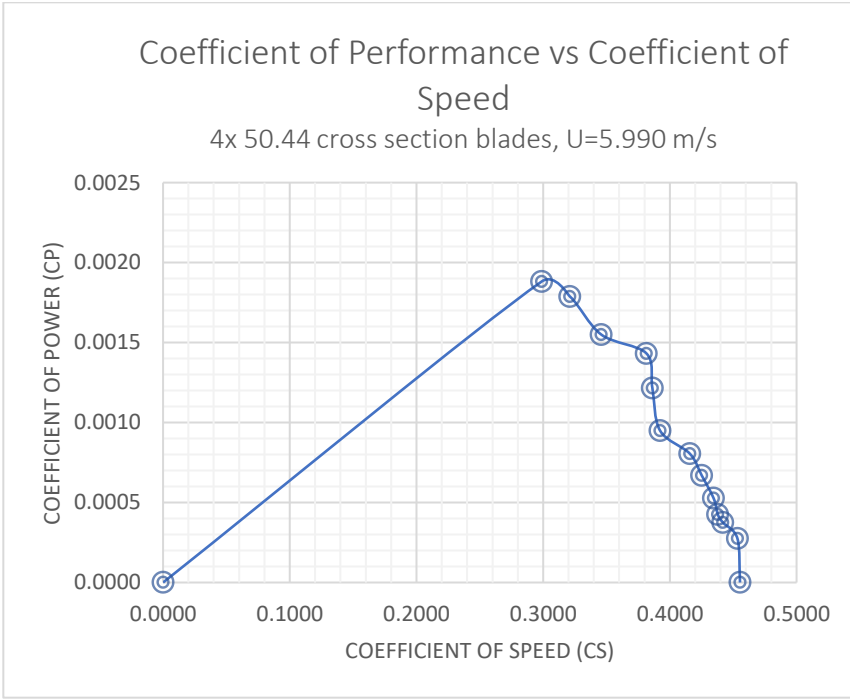
Coefficient of Performance vs Coefficient of Speed
4x 50.44 cross section blades, U=5.990 m/s
COEFFICIENT OF POWER (CP)
0.0025
0.0020
0.0015
0.0010
0.0005
0.0000
0.0000
0.1000
0.2000
0.3000
0.4000
0.5000
COEFFICIENT OF SPEED (CS)

Data for Rotor with Four 50.44mm Square Blades

U=6.614 m/s

Recorded Data							Calculated Data						Uncertainty					
Run Number	**Windspeed (m/s)**	**Voltage (V)**	**Amperage (A)**	**% Max Current**	**Torque (N·cm)**	**RPM**	**Torque (N·m)**	**ω (rad/s)**	**Power (w)**	**ρ (kg/m^3)**	**Cp**	**Cs**	**$\sigma_{windspeed}$ (± m/s)**	**σ Amp (± A)**	**σω (± rad/s)**	**σT (± N·m)**	**σP (± w)**	**σP (± %)**
1	6.614	0	0.00	0%	0	76.2	0.000	7.980	0.000	1.292	0.0000	0.4635	0.1984	0.0000	0.1087	0.0000000	0.0000	0.0000
2	6.614	0.25	0.01	3%	0.25	75.4	0.003	7.896	0.020	1.292	0.0002	0.4586	0.1984	0.00415	0.1087	0.0000064	0.0002763	1.3998
3	6.614	0.52	0.02	7%	0.35	74.9	0.004	7.844	0.027	1.292	0.0003	0.4556	0.1984	0.00430	0.1086	0.0000066	0.0003837	1.3980
4	6.614	0.73	0.03	10%	0.4	74.5	0.004	7.802	0.031	1.292	0.0004	0.4532	0.1984	0.00445	0.1086	0.0000069	0.0004376	1.4028
5	6.614	0.83	0.04	14%	0.5	73.9	0.005	7.739	0.039	1.292	0.0004	0.4495	0.1984	0.00460	0.1086	0.0000071	0.0005457	1.4103
6	6.614	1.11	0.05	17%	0.65	72.7	0.007	7.613	0.049	1.292	0.0006	0.4422	0.1984	0.00475	0.1085	0.0000073	0.0007076	1.4300
7	6.614	1.23	0.06	21%	0.8	71.6	0.008	7.498	0.060	1.292	0.0007	0.4355	0.1984	0.00490	0.1085	0.0000075	0.0008695	1.4497
8	6.614	1.58	0.07	24%	1	68.2	0.010	7.142	0.071	1.292	0.0008	0.4148	0.1984	0.00505	0.1083	0.0000078	0.0010843	1.5183
9	6.614	1.68	0.08	28%	1.3	67.6	0.013	7.079	0.092	1.292	0.0011	0.4112	0.1984	0.00520	0.1083	0.0000080	0.0014085	1.5305
10	6.614	2.01	0.09	31%	1.55	65.2	0.016	6.828	0.106	1.292	0.0012	0.3966	0.1984	0.00535	0.1081	0.0000082	0.0016770	1.5846
11	6.614	2.2	0.10	34%	1.85	63.3	0.019	6.629	0.123	1.292	0.0014	0.3850	0.1984	0.00550	0.1080	0.0000085	0.0019994	1.6304
12	6.614	2.26	0.11	38%	2.3	60.2	0.023	6.304	0.145	1.292	0.0017	0.3662	0.1984	0.00565	0.1079	0.0000087	0.0024816	1.7115
13	6.614	2.31	0.12	41%	2.6	57.1	0.026	5.979	0.155	1.292	0.0018	0.3473	0.1984	0.00580	0.1077	0.0000089	0.0028009	1.8016
14	6.614	2.56	0.13	45%	3.05	55.5	0.031	5.812	0.177	1.292	0.0020	0.3376	0.1984	0.00595	0.1076	0.0000092	0.0032830	1.8520
15	6.614	2.81	0.14	48%	3.35	45.2	0.034	4.733	0.159	1.292	0.0018	0.2749	0.1984	0.00610	0.1071	0.0000094	0.0035867	2.2626
16	6.614	3.01	0.15	52%	3.8	0	0.038	0.000	0.000	1.292	0.0000	0.0000	0.1984	0.00625	0.1047	0.0000096	0.0000	0.0000

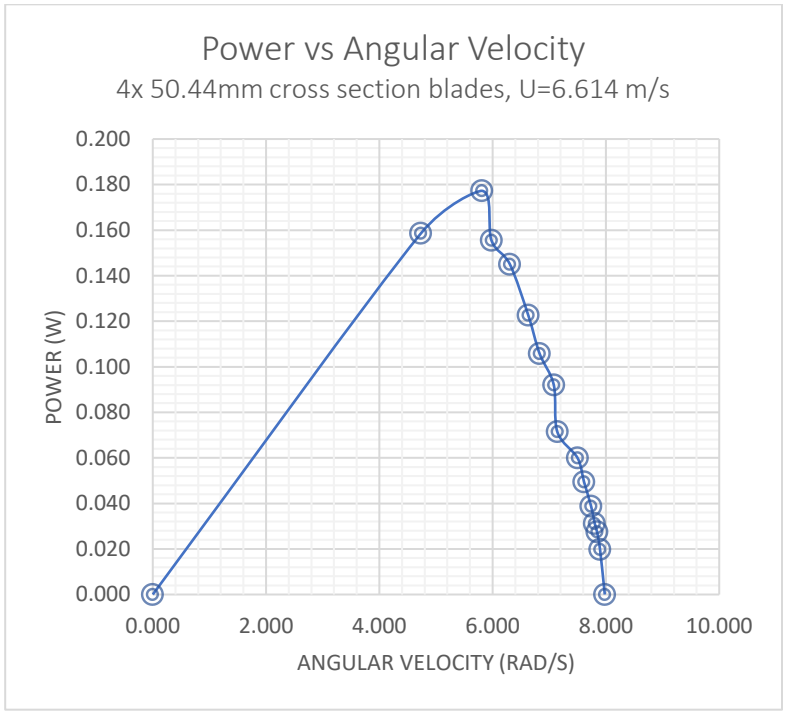
Power vs Angular Velocity
4x 50.44mm cross section blades, U=6.614 m/s
POWER (W)
0.200
0.180
0.160
0.140
0.120
0.100
0.080
0.060
0.040
0.020
0.000
0.000
2.000
4.000
6.000
8.000
10.000
ANGULAR VELOCITY (RAD/S)

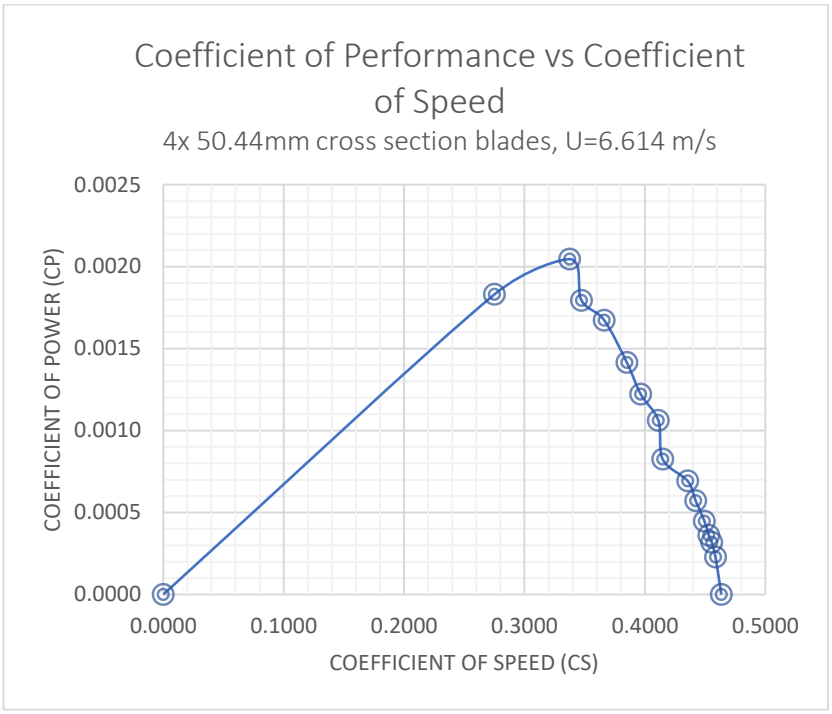
Coefficient of Performance vs Coefficient of Speed
4x 50.44mm cross section blades, U=6.614 m/s
COEFFICIENT OF POWER (CP)
0.0025
0.0020
0.0015
0.0010
0.0005
0.0000
0.0000
0.1000
0.2000
0.3000
0.4000
0.5000
COEFFICIENT OF SPEED (CS)

C4. Rotor with Four 25.28mm Square Blades

Data for Rotor with Four 25.28mm Square Blades

U=6.082 m/s

Recorded Data							Calculated Data						Uncertainty					
Run Number	**Windspeed (m/s)**	**Voltage (V)**	**Amperage (A)**	**% Max Current**	**Torque (N·cm)**	**RPM**	**Torque (N·m)**	**ω (rad/s)**	**Power (w)**	**ρ (kg/m^3)**	**Cp**	**Cs**	**$\sigma_{windspeed}$ (± m/s)**	**σ_{Amp} (± A)**	**σω (± rad/s)**	**σT (± N·m)**	**σP (± w)**	**σP (± %)**
1	6.082	0	0.00	0%	0	75.2	0.000	7.875	0.000	1.292	0.0000	0.4974	0.1825	0.0000	0.1087	0.0000000	0.0000	0.0000
2	6.082	0.16	0.01	3%	0.25	74.3	0.003	7.781	0.019	1.292	0.0003	0.4915	0.1825	0.00415	0.1086	0.0000064	0.00027604	1.4191
3	6.082	0.3	0.02	7%	0.35	74	0.004	7.749	0.027	1.292	0.0004	0.4895	0.1825	0.00430	0.1086	0.0000066	0.00038353	1.4141
4	6.082	0.5	0.03	10%	0.4	73.7	0.004	7.718	0.031	1.292	0.0005	0.4875	0.1825	0.00445	0.1086	0.0000069	0.00043752	1.4172
5	6.082	0.7	0.04	14%	0.5	71.7	0.005	7.508	0.038	1.292	0.0006	0.4743	0.1825	0.00460	0.1085	0.0000071	0.00054497	1.4516
6	6.082	0.89	0.05	17%	0.65	70.8	0.007	7.414	0.048	1.292	0.0007	0.4683	0.1825	0.00475	0.1084	0.0000073	0.00070686	1.4668
7	6.082	1.09	0.06	21%	0.8	69.7	0.008	7.299	0.058	1.292	0.0009	0.4610	0.1825	0.00490	0.1084	0.0000075	0.00086870	1.4877
8	6.082	1.42	0.07	24%	1	65.5	0.010	6.859	0.069	1.292	0.0010	0.4333	0.1825	0.00505	0.1081	0.0000078	0.00108281	1.5786
9	6.082	1.55	0.08	28%	1.3	63	0.013	6.597	0.086	1.292	0.0013	0.4167	0.1825	0.00520	0.1080	0.0000080	0.00140523	1.6385
10	6.082	1.68	0.09	31%	1.55	60.2	0.016	6.304	0.098	1.292	0.0015	0.3982	0.1825	0.00535	0.1079	0.0000082	0.00167282	1.7120
11	6.082	1.9	0.10	34%	1.85	0	0.019	0.000	0.000	1.292	0.0000	0.0000	0.1825	0.00550	0.1047	0.0000085	0.0000	0.0000

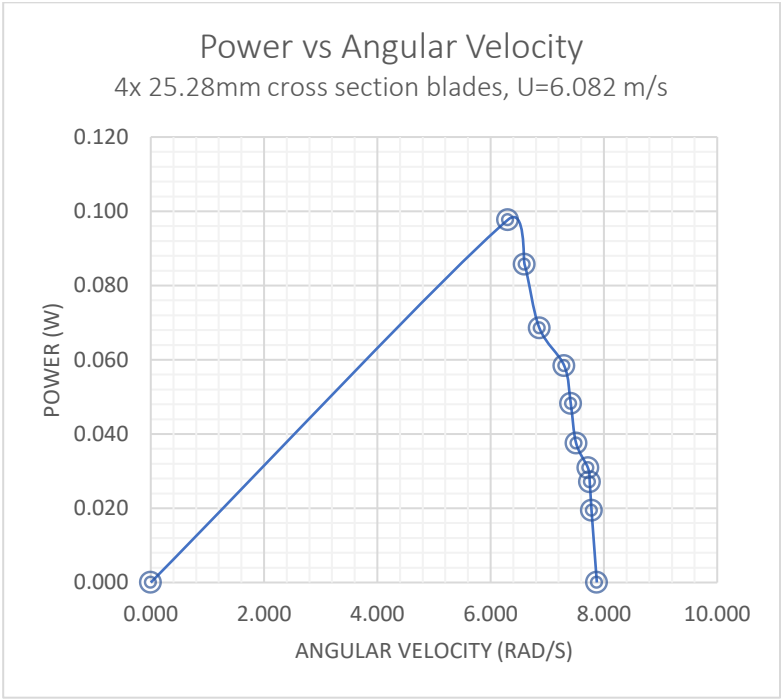
Power vs Angular Velocity
4x 25.28mm cross section blades, U=6.082 m/s
POWER (W)
0.120
0.100
0.080
0.060
0.040
0.020
0.000
0.000
2.000
4.000
6.000
8.000
10.000
ANGULAR VELOCITY (RAD/S)

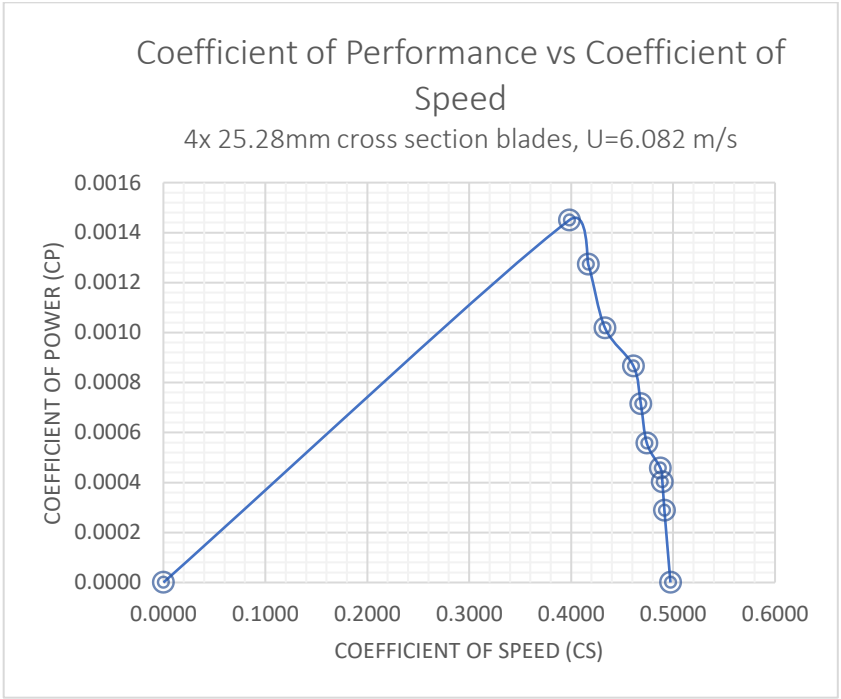
Coefficient of Performance vs Coefficient of Speed
4x 25.28mm cross section blades, U=6.082 m/s
COEFFICIENT OF POWER (CP)
0.0016
0.0014
0.0012
0.0010
0.0008
0.0006
0.0004
0.0002
0.0000
0.0000
0.1000
0.2000
0.3000
0.4000
0.5000
0.6000
COEFFICIENT OF SPEED (CS)

Data for Rotor with Four 25.28mm Square Blades

U=6.440 m/s

Recorded Data							Calculated Data						Uncertainty					
Run Number	**Windspeed (m/s)**	**Voltage (V)**	**Amperage (A)**	**% Max Current**	**Torque (N·cm)**	**RPM**	**Torque (N·m)**	**ω (rad/s)**	**Power (w)**	**ρ (kg/m^3)**	**Cp**	**Cs**	**$\sigma_{windspeed}$ (± m/s)**	**σ_{Amp} (± A)**	**σω (± rad/s)**	**σT (± N·m)**	**σP (± w)**	**σP (± %)**
1	6.44	0	0.00	0%	0	79.5	0.000	8.325	0.000	1.292	0.0000	0.4966	0.1932	0.0000	0.1089	0.0000000	0.0000000	0.0000
2	6.44	0.15	0.01	3%	0.25	78.9	0.003	8.262	0.021	1.292	0.0003	0.4929	0.1932	0.00415	0.1089	0.0000064	0.0002772	1.3420
3	6.44	0.34	0.02	7%	0.35	78.5	0.004	8.221	0.029	1.292	0.0004	0.4904	0.1932	0.00430	0.1088	0.0000066	0.0003847	1.3373
4	6.44	0.55	0.03	10%	0.4	78.1	0.004	8.179	0.033	1.292	0.0004	0.4879	0.1932	0.00445	0.1088	0.0000069	0.0004383	1.3414
5	6.44	0.71	0.04	14%	0.5	77.1	0.005	8.074	0.040	1.292	0.0005	0.4816	0.1932	0.00460	0.1088	0.0000071	0.0005467	1.3544
6	6.44	0.93	0.05	17%	0.65	75.7	0.007	7.927	0.052	1.292	0.0006	0.4729	0.1932	0.00475	0.1087	0.0000073	0.0007082	1.3756
7	6.44	1.11	0.06	21%	0.8	74.2	0.008	7.770	0.062	1.292	0.0008	0.4635	0.1932	0.00490	0.1086	0.0000075	0.0008702	1.4009
8	6.44	1.36	0.07	24%	1	70.8	0.010	7.414	0.074	1.292	0.0009	0.4423	0.1932	0.00505	0.1084	0.0000078	0.0010858	1.4645
9	6.44	1.61	0.08	28%	1.3	68	0.013	7.121	0.093	1.292	0.0012	0.4248	0.1932	0.00520	0.1083	0.0000080	0.0014088	1.5218
10	6.44	1.77	0.09	31%	1.55	65.1	0.016	6.817	0.106	1.292	0.0013	0.4067	0.1932	0.00535	0.1081	0.0000082	0.0016769	1.5870
11	6.44	1.99	0.10	34%	1.85	0	0.019	0.000	0.000	1.292	0.0000	0.0000	0.1932	0.00550	0.1047	0.0000085	0.0000000	0.0000

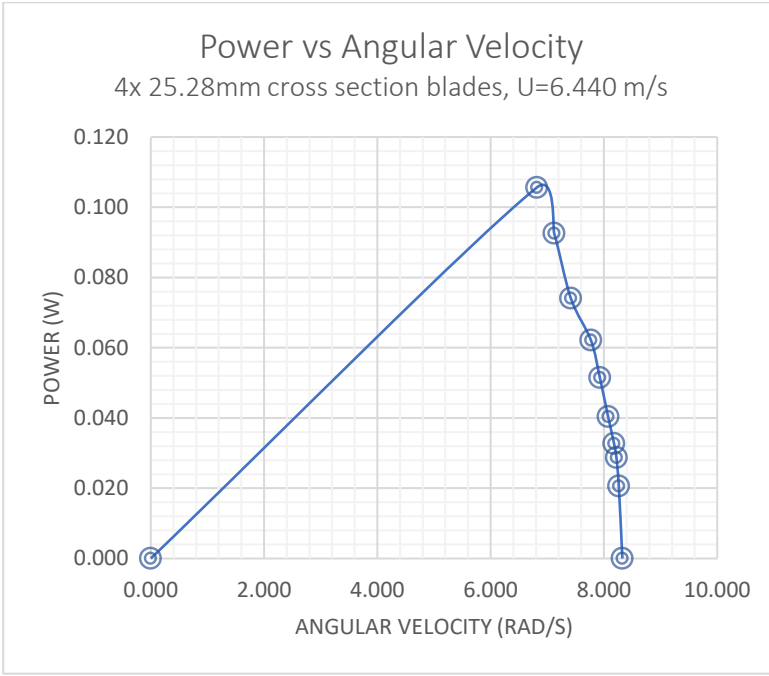
Power vs Angular Velocity
4x 25.28mm cross section blades, U=6.440 m/s
POWER (W)
0.120
0.100
0.080
0.060
0.040
0.020
0.000
0.000
2.000
4.000
6.000
8.000
10.000
ANGULAR VELOCITY (RAD/S)

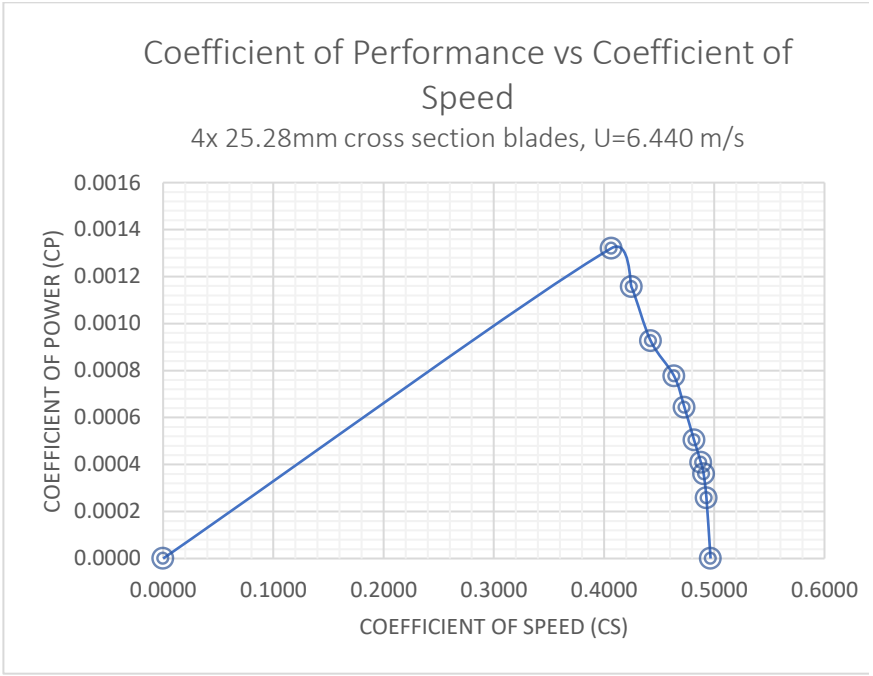
Coefficient of Performance vs Coefficient of Speed
4x 25.28mm cross section blades, U=6.440 m/s
COEFFICIENT OF POWER (CP)
0.0016
0.0014
0.0012
0.0010
0.0008
0.0006
0.0004
0.0002
0.0000
0.0000
0.1000
0.2000
0.3000
0.4000
0.5000
0.6000
COEFFICIENT OF SPEED (CS)

C5. Rotor with Two 50.44mm Square Blades

Data for Rotor with Two 50.44mm Square Blades

U=6.588 m/s

Recorded Data							Calculated Data						Uncertainty					
Run Number	**Windspeed (m/s)**	**Voltage (V)**	**Amperage (A)**	**% Max Current**	**Torque (N·cm)**	**RPM**	**Torque (N·m)**	**ω (rad/s)**	**Power (w)**	**ρ (kg/m^3)**	**Cp**	**Cs**	**$\sigma_{windspeed}$ (± m/s)**	**σ_{Amp} (± A)**	**σω (± rad/s)**	**σT (± N·m)**	**σP (± w)**	**σP (± %)**
1	6.588	0	0.00	0%	0	74.2	0.000	7.770	0.000	1.292	0.0000	0.4531	0.1976	0.0000	0.1086	0.0000000	0.0000	0.0000
2	6.588	0.2	0.01	3%	0.25	73.7	0.003	7.718	0.019	1.292	0.0002	0.4501	0.1976	0.00415	0.1086	0.0000064	0.0002758	1.4299
3	6.588	0.4	0.02	7%	0.35	71.9	0.004	7.529	0.026	1.292	0.0003	0.4391	0.1976	0.00430	0.1085	0.0000066	0.0003829	1.4532
4	6.588	0.6	0.03	10%	0.4	70.8	0.004	7.414	0.030	1.292	0.0003	0.4324	0.1976	0.00445	0.1084	0.0000069	0.0004367	1.4724
5	6.588	0.7	0.04	14%	0.5	69.9	0.005	7.320	0.037	1.292	0.0004	0.4269	0.1976	0.00460	0.1084	0.0000071	0.0005443	1.4874
6	6.588	0.9	0.05	17%	0.65	67.3	0.007	7.048	0.046	1.292	0.0005	0.4110	0.1976	0.00475	0.1082	0.0000073	0.0007054	1.5400
7	6.588	1.1	0.06	21%	0.8	64.8	0.008	6.786	0.054	1.292	0.0006	0.3957	0.1976	0.00490	0.1081	0.0000075	0.0008664	1.5960
8	6.588	1.3	0.07	24%	1	61.5	0.010	6.440	0.064	1.292	0.0008	0.3756	0.1976	0.00505	0.1079	0.0000078	0.0010805	1.6778
9	6.588	1.5	0.08	28%	1.3	58.1	0.013	6.084	0.079	1.292	0.0009	0.3548	0.1976	0.00520	0.1078	0.0000080	0.0014017	1.7722
10	6.588	1.7	0.09	31%	1.55	53.1	0.016	5.561	0.086	1.292	0.0010	0.3243	0.1976	0.00535	0.1075	0.0000082	0.0016668	1.9340
11	6.588	1.9	0.10	34%	1.85	0	0.019	0.000	0.000	1.292	0.0000	0.0000	0.1976	0.00550	0.1047	0.0000085	0.0000	0.0000

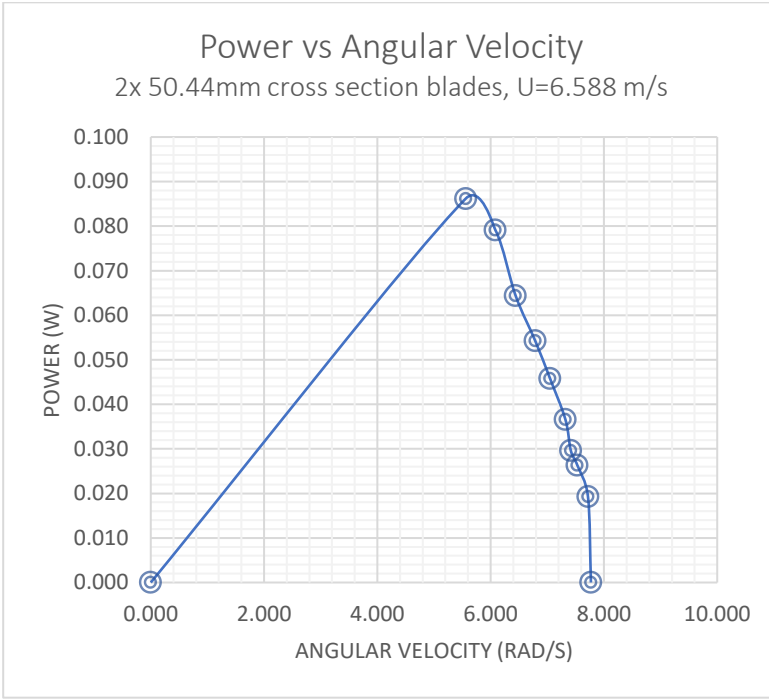
Power vs Angular Velocity
2x 50.44mm cross section blades, U=6.588 m/s
POWER (W)
0.100
0.090
0.080
0.070
0.060
0.050
0.040
0.030
0.020
0.010
0.000
0.000
2.000
4.000
6.000
8.000
10.000
ANGULAR VELOCITY (RAD/S)

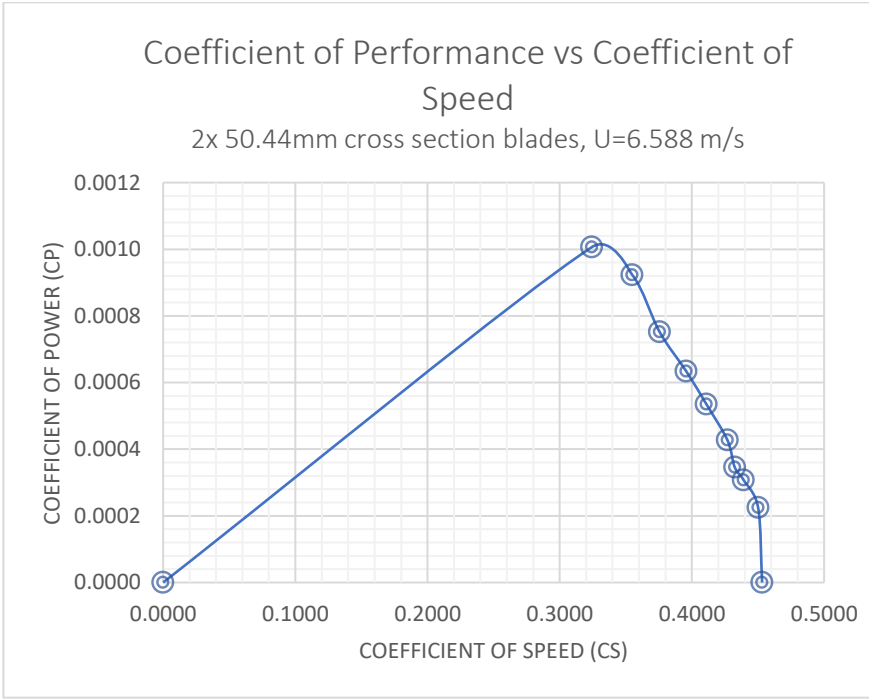
Coefficient of Performance vs Coefficient of Speed
2x 50.44mm cross section blades, U=6.588 m/s
COEFFICIENT OF POWER (CP)
0.0012
0.0010
0.0008
0.0006
0.0004
0.0002
0.0000
0.0000
0.1000
0.2000
0.3000
0.4000
0.5000
COEFFICIENT OF SPEED (CS)